

# POPULATION STUDIES. XIII. A NEW ANALYSIS OF THE BIDELMAN-MACCONNELL “WEAK-METAL” STARS – CONFIRMATION OF METAL-POOR STARS IN THE THICK DISK OF THE GALAXY

TIMOTHY C. BEERS<sup>1,2</sup>, JOHN E. NORRIS<sup>3</sup>, VINICIUS M. PLACCO<sup>4</sup>, YOUNG SUN LEE<sup>5</sup>,  
 SILVIA ROSSI<sup>6</sup>, DANIELA CAROLLO<sup>7</sup>, THOMAS MASSERON<sup>8</sup>

*Draft version October 21, 2018*

## ABSTRACT

A new set of very high signal-to-noise ( $S/N > 100/1$ ), medium-resolution ( $R \sim 3000$ ) optical spectra have been obtained for 302 of the candidate “weak-metal” stars selected by Bidelman & MacConnell. We use these data to calibrate the recently developed generalization of the SEGUE Stellar Parameter Pipeline, and obtain estimates of the atmospheric parameters ( $T_{\text{eff}}$ ,  $\log g$ , and  $[\text{Fe}/\text{H}]$ ) for these non-SDSS/SEGUE data; we also obtain estimates of  $[\text{C}/\text{Fe}]$ . The new abundance measurements are shown to be consistent with available high-resolution spectroscopic determinations, and represent a substantial improvement over the accuracies obtained from the previous photometric estimates reported in Paper I of this series. The apparent offset in the photometric abundances of the giants in this sample noted by several authors is confirmed by our new spectroscopy; no such effect is found for the dwarfs. The presence of a metal-weak thick-disk (MWTD) population is clearly supported by these new abundance data. Some 25% of the stars with metallicities  $-1.8 < [\text{Fe}/\text{H}] \leq -0.8$  exhibit orbital eccentricities  $e < 0.4$ , yet are clearly separated from members of the inner-halo population with similar metallicities by their location in a Lindblad energy vs. angular momentum diagram. A comparison is made with recent results for a similar-size sample of RAVE stars from Ruchti et al. We conclude, based on both of these samples, that the MWTD is real, and must be accounted for in discussions of the formation and evolution of the disk system of the Milky Way.

*Keywords:* stars: abundances – stars: Population II – Galaxy: kinematics and dynamics – Galaxy: stellar content – Galaxy: structure

## 1. INTRODUCTION

### 1.1. Historical Overview

In the first paper of this series, Norris et al. (1985, NBP, Paper I) presented DDO photometric estimates of metallicity, spectroscopic measurements of radial velocities, and photometric classifications for a sample of 309 non-kinematically selected stars taken from the list of “weak-metal” candidates originally identified by Bidelman & MacConnell (1973). Based on these data, and supplemented with proper motions that were available at the time, NBP obtained space motions and estimates of orbital eccentricities for a subset of this sample. Inspection of this distribution led these authors to conclude that there exists a substantial number of low-metallicity stars on low-eccentricity orbits ( $e < 0.4$ ), which they found difficult to reconcile with the classical rapid col-

lapse model for the formation of the Galaxy put forward by Eggen et al. (1962). NBP suggested instead that the low-metallicity, low-eccentricity stars belong to a population that is “(i) ... intermediate in its motion perpendicular to the Galactic plane between that of the thin disk and that of metal-deficient objects of extreme eccentricity, and (ii) that the velocity dispersion of this group of stars is consistent with its belonging to the thick-disk population described by Gilmore (1984).” This suggested population has become known as the metal-weak thick disk (MWTD - e.g. Morrison et al. 1990; Beers & Sommer-Larsen 1995).

Attempts to confirm or refute the existence of a MWTD population have led to numerous (and ever more-detailed) studies over the past two decades. Morrison et al. (1990) provided additional support for the MWTD, based on a (slightly revised) DDO photometric abundance scale, and the kinematics of a low-latitude sample of giants selected to test for a separation of halo-like and disk-like objects. However, the conclusions of both of these efforts were called into question by subsequent work. In the case of NBP, Anthony-Twarog & Twarog (1994) obtained an improved calibration of the DDO abundance estimates for their sample giants, and concluded that there existed an offset of about 0.5 dex for giants of intermediate metallicity (around  $[\text{Fe}/\text{H}] = -1.2$ ). As a result, these authors suggested that the numbers of stars with disk-like motions and metallicities  $[\text{Fe}/\text{H}] < -1.0$  in the work of NBP had been substantially overestimated, compromising the claim for a MWTD population. Ryan & Lambert (1995) sought to resolve these discrepancies by obtaining high-resolution spectroscopic abundance determinations of some 30 giants in

<sup>1</sup> National Optical Astronomy Observatory, Tucson, AZ 85719, USA. [beers@noao.edu](mailto:beers@noao.edu)

<sup>2</sup> JINA: Joint Institute for Nuclear Astrophysics.

<sup>3</sup> Research School of Astronomy and Astrophysics, The Australian National University, Mount Stromlo Observatory, Cotter Road, Weston, ACT 2611, Australia. [jen@mso.anu.edu.au](mailto:jen@mso.anu.edu.au)

<sup>4</sup> Gemini Observatory - Northern Operations Center, Hilo, HI 96720, USA. [vplacco@gemini.edu](mailto:vplacco@gemini.edu)

<sup>5</sup> Department of Astronomy, New Mexico State University, Las Cruces, NM 88003, USA. [yslee@nmsu.edu](mailto:yslee@nmsu.edu)

<sup>6</sup> Instituto de Astronomia, Geofísica e Ciências Atmosféricas, Departamento de Astronomia, Universidade de São Paulo, Rua do Matão 1226, 05508-900 São Paulo, Brazil. [rossi@astro.iag.usp.br](mailto:rossi@astro.iag.usp.br)

<sup>7</sup> Department of Physics and Astronomy - Astronomy, Astrophysics and Astrophotonic Research Center - Macquarie University - North Ryde, 2019, NSW, Australia. [daniela.carollo@mq.edu.au](mailto:daniela.carollo@mq.edu.au)

<sup>8</sup> Institute of Astronomy, University of Cambridge, Madingley Road, Cambridge CB3 0HA, UK. [tpm40@ast.cam.ac.uk](mailto:tpm40@ast.cam.ac.uk)

these two samples with claimed photometric abundance estimates  $[\text{Fe}/\text{H}] < -1.0$ . The results of their study indicated that many, but not all, of the giants in the NBP and the Morrison et al. (1990) sample possessed higher metallicities than had been inferred from the DDO photometry. As a consequence, they argued that, although a MWTD may indeed exist, its contribution to the populations of stars within 1 kpc of the Galactic disk had likely been overestimated by previous work.

Other observational efforts have addressed the problem of the existence of a MWTD component in the Galaxy. For instance, Beers & Sommer-Larsen (1995) argued from their sample of non-kinematically selected stars that a surprisingly large fraction of the metal-poor stars ( $> 30\%$  of stars with  $[\text{Fe}/\text{H}] < -1.5$ , rising to  $60\%$  for stars with  $-1.6 \leq [\text{Fe}/\text{H}] \leq -1.0$ ) in the Solar Neighborhood might be associated with a MWTD component. Chiba & Yoshii (1998) used high-quality proper motions from the Hipparcos satellite for a much smaller sample of red giants and RR Lyraes to argue that, while a MWTD appeared present, the fractions of stars at low metallicity associated with it were substantially smaller, roughly 10% for stars in the interval  $-1.6 \leq [\text{Fe}/\text{H}] \leq -1.0$ . Martin & Morrison (1998) considered the space motions of nearby RR Lyrae stars with well-determined kinematics, and concluded that a MWTD existed in their sample (including stars with metallicities as low as  $[\text{Fe}/\text{H}] \sim -2.0$ ), similar to previous results for the sample of RR Lyrae examined by Layden (1995).

Chiba & Beers (2000) performed a detailed analysis of a large sample of non-kinematically selected stars with available (medium-resolution) spectroscopic abundances, radial velocities, and (for roughly half of their sample) proper motions from the assembly of Beers et al. (2000). These authors concluded that the fraction of likely MWTD stars in the Solar Neighborhood with  $-1.7 < [\text{Fe}/\text{H}] \leq -1.0$  was on the order of 30%, falling to on the order of 10% for stars with  $-2.2 < [\text{Fe}/\text{H}] \leq -1.7$ . Beers et al. (2002) analyzed a sample of candidate low-metallicity giants located close to the Galactic plane from the LSE survey of Drilling & Bergeron (1995). Their Monte-Carlo experiments on the distribution of orbital eccentricities of this sample suggested that the fraction of MWTD stars with  $[\text{Fe}/\text{H}] < -1.0$  might actually be as high as 40%, and that it may remain as high as 30% for stars with  $[\text{Fe}/\text{H}] < -1.6$ . Beers et al. reasoned that the origin of this discrepancy with respect to the work of Chiba & Beers (2000) came from the selection criteria employed by most surveys for low-metallicity stars, which understandably concentrated on regions of the Galaxy with latitudes above  $|b| = 30^\circ$ .

Arifyanto et al. (2005) re-analyzed the kinematically selected sample of Carney et al. (1994), using Hipparcos-based parallaxes and (where available) Hipparcos and Tycho-2 proper motions, and applying corrections to the Carney et al. photometric distance estimates based on the overlap of the two samples. Their analysis also indicated the presence of a MWTD component, with a local stellar fraction smaller than that claimed by Chiba & Beers (2000) in the metallicity interval  $-1.7 < [\text{Fe}/\text{H}] \leq -1.0$  (18% vs. 30%). They interpreted the origin of the MWTD in terms of the debris of a “shredded satellite”, similar to the argument of Gilmore et al. (2002). It is notable that Gilmore et al. (2002) concluded, based

on an analysis of their spectroscopic survey of some 2000 F/G stars located 0.5–5 kpc above the Galactic plane, that the stars they proposed to originate in a shredded satellite exhibited a large rotational velocity lag with respect to the thin/thick disk, on the order of  $100 \text{ km s}^{-1}$ . Previous analyses for potential MWTD stars generally did not consider stars with such a large lag as likely candidate disk-like stars. Large lags for accreted MWTD stars may in fact be expected, as argued by Villalobos & Helmi (2009). Clearly, care must be exercised in the selection of potential MWTD stars before attempting to discern their kinematic and chemical properties.

## 1.2. The Nature and Role of the MWTD in the Context of the Milky Way

The preponderance of evidence acquired prior to 2009 suggested that a MWTD component exists, although doubts remained as to its level of contribution to the numbers of metal-poor stars in the Solar Neighborhood, as well as regarding its detailed kinematical behavior and relationship to the canonical thick-disk component, and to the halo. In the period since 2009, a substantial volume of work has been carried out, making use of large samples of stars with medium-resolution ( $R \sim 2000$ ) spectroscopy obtained from a variety of surveys, in particular the Sloan Digital Sky Survey (SDSS; York et al. 2000), and its Galactic extensions, the Sloan Extension for Galactic Exploration and Understanding (SEGUE-1; Yanny et al. 2009) and SEGUE-2 (C. Rockosi et al., in preparation), as well as higher-resolution ( $R \sim 7500$ ) data from the Radial Velocity Experiment(RAVE; Steinmetz et al. 2006), and other sources. A partial list of these works includes: Carollo et al. (2010), Ruchti et al. (2010, 2011), Kordopatis et al. (2011, 2013a,b), Lee et al. (2011), Bovy et al. (2012a,c,b), Carrell et al. (2012), Cheng et al. (2012a,b), Pasetto et. al (2012), Adibekyan et al. (2013), Boeche et. al (2013a,b), Haywood et al. (2013), Jayaraman et al. (2013), Bensby et al. (2014), and Minchev et. al (2014).

During this period, our appreciation of the complexity of the halo has also increased. Carollo et al. (2007), Carollo et al. (2010), and Beers et al. (2012) have presented the case that this system is well-described in terms of an inner-halo and outer-halo population – terms that we shall use in what follows<sup>9</sup>. Additional evidence supporting the existence of (at least) a dual halo has come from recognition that the frequency of carbon-enhanced metal-poor (CEMP) stars that can be kinematically associated with the outer-halo component is roughly twice that of the inner-halo component (Carollo et. al 2012), analysis of the metallicity distribution function (MDF), in combination with the motions, of local halo stars by An et. al (2014), the apparent preference for stars of the CEMP-s sub-class (those exhibiting *s*-process-element over-abundances) to be associated with the inner-halo component, while stars of the CEMP-no sub-class (those exhibiting no neutron-capture over-abundances) are more likely associated with the outer-halo component (Carollo et. al 2014), and analysis of the in-situ change of the halo system MDF with distance for a large sample of F-turnoff stars from SDSS Allende Pri-

<sup>9</sup> We note for completeness that an alternative view has been expressed by Schönrich et al. (2011).

eto et. al (2014).

Furthermore, Morrison et al. (2009) have used a sample of some 250 stars with very well-determined kinematical properties to argue for the presence of a new component of the local halo, with an axial ratio  $c/a \sim 0.2$  (similar in flattening to the thick disk) and populated by stars with  $-1.5 < [\text{Fe}/\text{H}] < -1.0$ , which is, however, *not* rotationally supported. The potential confusion of such stars with MWTD candidates is obvious, due to their proximity to the Galactic plane.

These works have raised new and interesting questions concerning the nature of the formation and evolution of both the disk and halo systems. In the discussion of the MWTD, there seems to be no consensus yet as to what the inter-relationships are between it, the canonical thick disk, and the thin disk. Are they independent and discrete sub-systems? What have been the roles (if any) of major mergers, the formation of the thin disk from an early thick disk, the heating of a pre-existing thin stellar disk by minor mergers, and/or efficient radial migration of stars in the plane of the disk? We call the reader's attention to the inciteful discussion by Haywood et al. (2013) of the apparently disparate results concerning the nature of the thick/thin disks arising from several recent studies. The issues being considered are clearly complex, even in the face of high-quality data, and subtleties of the approaches used and conclusions reached ensure that we have not yet arrived at a widely accepted view.

### 1.3. Scope of Present Investigation

The focus of this paper is considerably narrower. Here, we re-investigate the original sample of Bidelman & MacConnell (1973) discussed by NBP, in order to resolve whether or not it includes substantial numbers of stars that could be considered members of the MWTD population. New high signal-to-noise medium-resolution ( $R \sim 3000$ ) spectroscopy has been obtained for some 300 stars of the NBP sample. Roughly one-third of this sample now has available high-resolution spectroscopic determinations of  $[\text{Fe}/\text{H}]$  (and other physical parameters) from the literature, which we employ to carry out a calibration of the physical parameter estimates obtained by a “non-SEGUE” version of the SEGUE Stellar Parameter Pipeline (SSPP; originally described by Lee et al. 2008a), and referred to as the n-SSPP. We also report estimates of “carbonicity,”  $[\text{C}/\text{Fe}]$ , calibrated with respect to some 50 of the NBP stars with previous high-resolution spectroscopic determinations of this ratio reported in the literature, supplemented by a number of additional stars with available high-resolution determinations. The results of this calibration effort will be used in a number of future investigations based on non-SEGUE spectroscopic data. We then combine available radial velocities, accurate proper motions from the Hipparcos and Tycho-II catalogs, and the newly refined spectroscopic estimates of  $[\text{Fe}/\text{H}]$  to consider the presence of a MWTD in this sample. The resulting determinations of kinematic estimates represent a substantial improvement in the space velocities derived by NBP, sharpening the picture of the stellar populations obtained from these data, and confirming the suggestion of NBP that the ELS paradigm is an oversimplification of the manner in which the Milky Way formed.

This paper is outlined as follows. Our new observa-

tions are described in Section 2, where we also discuss the determination of radial velocities and spectroscopic line-strength indices for the program stars. Section 3 describes the techniques used to obtain estimates of the stellar atmospheric parameters ( $T_{\text{eff}}$ ,  $\log g$ ,  $[\text{Fe}/\text{H}]$ ), as well as  $[\text{C}/\text{Fe}]$ , for these stars. A comparison of the newly derived metallicity estimates with available high-resolution abundance results drawn from the recent literature and with the original DDO photometry-based estimates of NBP is presented in this section as well. We then make use of these comparisons to carry out a calibration of the n-SSPP. Distance estimates and proper motions for our sample stars are described in Section 4. In Section 5, we use these data to perform a new kinematic analysis of the NBP sample, and compare with the kinematics derived from a similar sample of RAVE stars described by Ruchti et al. (2011). A brief discussion of the implications of our new results is presented in Section 6.

## 2. SPECTROSCOPIC OBSERVATIONS, AVAILABLE PHOTOMETRIC MEASUREMENTS, AND DERIVATION OF RADIAL VELOCITIES AND LINE INDICES

### 2.1. Details of Spectroscopic Observations

During several observing runs conducted in January 1996, December 1996, and June 1997, optical spectra for a total of 302 stars from the subsample of 309 Bidelman & Maconnell weak-metal candidates studied by NBP (hereafter referred to as the B&M sample) were obtained with the Siding Spring Observatory 2.3m telescope, using the Double Beam Spectrograph. These spectra covered the wavelength interval  $3800 \text{ \AA} \leq \lambda \leq 4500 \text{ \AA}$ , with a resolving power of  $R \sim 3000$ , similar to that obtained during the course of previous work on follow-up spectroscopy by Norris et al. (1999) of metal-poor candidates selected from the HK survey of Beers et al. (1985, 1992). However, because the stars in the current program are, in general, quite bright ( $6.7 < V < 11.0$ ), high-quality spectra (with  $S/N > 100$  per resolution element) could be obtained in reasonably short integration times. A total of 383 spectra were obtained, including a number of stars with repeated measurements. These spectra were reduced using standard procedures for flat-fielding, extraction, and wavelength calibration (based on arc-lamp exposures taken immediately before or after each science spectrum), using the FIGARO software (Shortridge 1993) and ancillary FORTRAN routines. No attempt to spectro-photometrically calibrate the spectra was made.

Figure 1 provides examples of the medium-resolution spectra obtained. Also shown on the plots are the stellar atmospheric parameters, determined using the methods described below (Section 3). The left column of panels shows two examples of stars classified as dwarfs by NBP (using taxonomy based on DDO photometry), as well as by our own spectroscopic analysis. The upper-left panel is the spectrum of a metal-poor dwarf (BM-060 = CD-48:1741), while the lower-left panel is the spectrum of a dwarf with solar metallicity (BM-047 = BD-13:959). The right column of panels provides examples of spectra for stars classified as giants (by both NBP and the present work). The upper-right panel is the spectrum of a metal-poor giant (BM-120 = HD 84903), while the lower-right panel is the spectrum for a giant with metallicity slightly above solar (BM-072 = HD 40361).

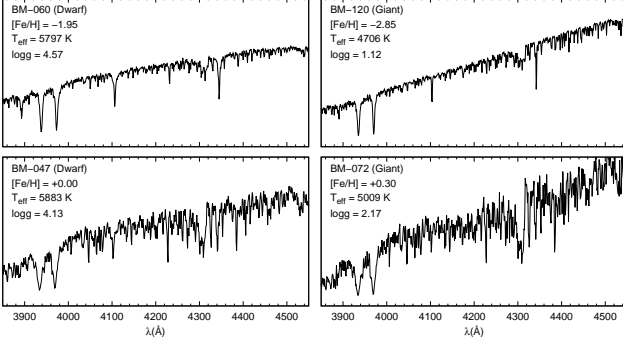


**Figure 1.** Example medium-resolution ( $R = 3000$ ) spectra for four of our program stars obtained with the SSO 2.3m telescope. The left-hand column of panels are main-sequence dwarfs, while the right-hand columns are giants (and are classified as such by both the taxonomy of NBP and the present analysis). The stellar atmospheric parameters from our analysis are indicated in the legend of each spectrum.

## 2.2. Broadband Photometry and Reddening Estimation

The NBP study provided broadband  $V$  magnitudes and  $B - V$  colors for the majority of our program objects. We have checked the SIMBAD database for consistency with other measurements, and in a few cases replaced the values listed by NBP with what we judged to be an improved set of information. In some cases, photometry was not available from NBP. For these stars, we adopted values provided in the SIMBAD database. The results are listed in Table 1. In this table, column (1) lists the star names used by NBP, in the format BM-XXX, while column (2) lists a more commonly used name for the star (e.g., BD, CD, HD, etc.). Columns (3) and (4) are the Galactic longitude and latitude in decimal degrees, respectively. Columns (5) and (6) list the adopted  $V$  magnitude and  $B - V$  colors, respectively. Near-IR  $JHK$  photometry is available for the bulk of our sample, based on results from the 2MASS catalog (Skrutskie et al. 2006). The  $J$  magnitude and  $J - K$  colors reported by 2MASS for stars without flags indicating potential problems in the listed values are given in columns (7) and (8), respectively.

In order to obtain absorption- and reddening-corrected estimates of the magnitudes and colors, respectively, we initially adopt the Schlegel et al. (1998) estimates of reddening, listed in column (9) of Table 1. We have applied corrections to these estimates for objects with reddening greater than  $E(B - V)_S = 0.10$ , as described by Beers et al. (2002). The corrected reddening estimates,  $E(B - V)_A$ , are listed in column (10) of Table 1. The final reddening estimates must be obtained in conjunction with the distance estimates, obtained as described below, in order to properly account for the amount of foreground reddening suffered by each star. The final estimated redshifts,  $E(B - V)_F$ , are listed in column (11). Note that about 20% of our sample stars are located at low Galactic latitudes,  $|b| < 10^\circ$ , for which the reddening estimate along the line of sight to a star is unreliable. For these stars we simply set the reddening estimate to zero for the initial parameter analysis<sup>10</sup>.

<sup>10</sup> The n-SSPP employs multiple approaches, some of which use spectroscopic-only input information, which provides robustness in the parameter estimates in spite of spurious reddening estimates.

## 2.3. Measurement of Radial Velocities and Line Indices

Our program stars, and the number of medium-resolution spectra obtained for each star, are listed in the first two columns of Table 1. Radial velocities were measured for our program objects using the line-by-line and cross-correlation techniques described in detail by Beers et al. (1999), and references therein. The spectral resolution is similar to that obtained for the majority of the HK survey follow-up, so we expect that the measured radial velocities should be precise to the same level (or better, given the higher signal-to-noise of our present spectra), on the order of 7–10 km s<sup>-1</sup> (one sigma). Heliocentric radial velocities obtained from the medium-resolution spectra for our program stars,  $RV_M$ , are listed in column (3) of Table 1.

Roughly one-third of our program objects have had radial velocities determined from high-resolution spectroscopic studies (available results are provided in column (4) of Table 1,  $RV_H$ ). The upper two panels of Figure 2 compare  $RV_M$  with those obtained from the independent high-resolution observations. As can be appreciated from inspection of this figure, there is generally excellent agreement. A maximum likelihood fit to the residuals in radial velocity, as shown in the lower panel of Figure 2, indicates that the rms scatter is only on the order of 5.5 km s<sup>-1</sup>. Assuming that the (combined) high-resolution radial velocities from the literature have a precision on the order of 2.0 km s<sup>-1</sup>, the external errors in our medium-resolution radial-velocity determinations appear to be no worse than about 5 km s<sup>-1</sup>, slightly better than expected. This represents a factor of two improvement in the precision of the radial velocities reported by NBP.

Although we do not employ them for obtaining stellar metallicity estimates in the present paper, we have measured a set of spectral indices that have been used for this and other purposes in previous papers (e.g., alternative schemes for estimation of de-reddened colors based on Balmer-line strengths, [C/Fe] estimates based on the CH  $G$ -band line index, etc.). Since these may prove useful in the future, and are very well-measured in our high-S/N medium-resolution spectra, we describe their determination below.

For each star, the measured (geocentric) radial velocities were used to place a set of fixed bands for the derivation of line-strength indices, which are pseudo-equivalent widths of prominent spectral features. We employ a subset of the bands listed in Table 1 of Beers et al. (1999)<sup>11</sup>.

Line indices for prominent spectral features for each of our program stars are reported in columns (5)–(8) of Table 1. A number of our program stars had more than one spectrum obtained during the course of the follow-up observations. From a comparison of the stars with repeated measurements, we estimate that errors in the line indices on the order of 0.1 Å are achieved. In order for a line-index measurement to be considered a detection, we require that the derived indices be above a minimum value of 0.25 Å. Indices that failed to reach this minimum

<sup>11</sup> The indices KP, HP2, GP, and HG2 measure the strength of the Ca II K line, hydrogen H $\delta$ , the CH  $G$ -band, and hydrogen H $\gamma$ , respectively. A complete discussion of the choice of bands and the “band-switching” scheme used to determine the indices are provided in this reference as well.

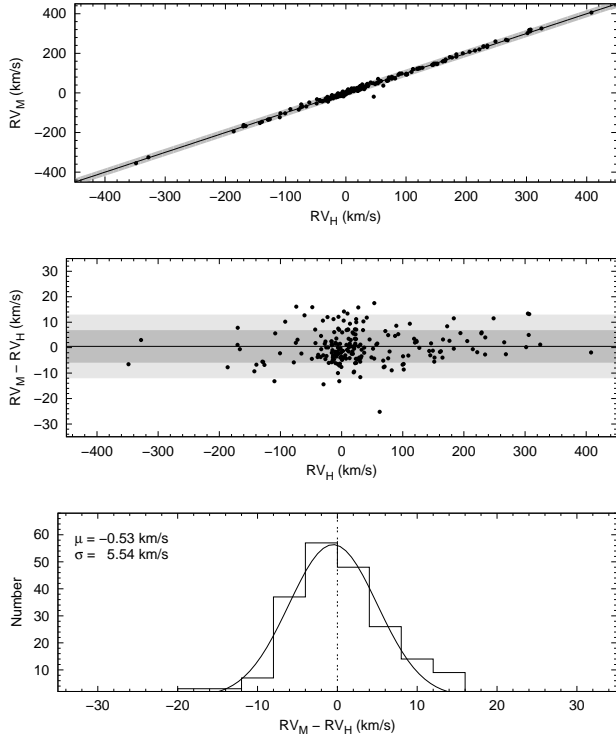


**Figure 2.** Upper panel: Comparison between the radial velocities of our program stars, determined from the medium-resolution spectra using the techniques described by Beers et al. (1999), and those reported in the literature from analyses of high-resolution spectra. The solid line is the one-to-one line, and the shaded area represents a 3- $\sigma$  interval around this line (where  $\sigma$  represents the scatter in the residuals shown in the lower panel,  $5.5 \text{ km s}^{-1}$ ). Middle panel: Residuals between the medium-resolution and high-resolution radial velocities, as a function of the high-resolution values. The horizontal solid line is the average of the residuals, while the darker and lighter shaded areas represent the 1- $\sigma$  and 2- $\sigma$  regions, respectively. Lower panel: Histogram of the residuals in the radial-velocity determinations. The values of the mean offset and scatter are the parameters from the Gaussian fit shown.

value are indicated in the Table 1 as missing data.

In addition to the line-strength indices, we have measured an autocorrelation function index for each star, as described in detail in Beers et al. (1999), and references therein. We actually make use of the base-10 logarithm of this index, hence it is referred to as LACF (listed in column (9) of Table 1). The LACF index quantifies the strength of the multitude of weak metallic lines that are present in each spectrum, and provides an additional indicator of the overall abundance. This index is of particular use for cooler and/or metal-rich stars, where the KP-index technique for inference of stellar metallicity approaches saturation.

### 3. STELLAR ATMOSPHERIC PARAMETERS AND CARBON ABUNDANCE RATIOS

Stellar atmospheric parameters for our program stars were determined using the n-SSPP, a modified version of the SEGUE Stellar Parameter Pipeline (SSPP; see Lee et al. 2008a,b; Allende Prieto et al. 2008; Lee et al. 2011; Smolinski et al. 2011, for a detailed description of the procedures used). The n-SSPP is a collection of routines for the analysis of non-SDSS/SEGUE data that employs both spectroscopic and photometric ( $V_0$ ,  $(B-V)_0$ ,  $J_0$  and  $(J-K)_0$ ) information as inputs, in order to make

a series of estimates for each stellar parameter<sup>12</sup>. Then, using  $\chi^2$  minimization matching techniques within dense grids of synthetic spectra, and averaging with other techniques as available (depending on the wavelength range of the input spectra; see Table 5 of Lee et al. 2008a), the best set of values is adopted. For the SSPP, internal errors for the stellar parameters are: 125 K for  $T_{\text{eff}}$ , 0.25 dex for  $\log g$ , and 0.20 dex for [Fe/H]; external errors are of a similar size. We might expect the external errors in n-SSPP determinations to be somewhat larger, owing to the generally more limited wavelength coverage and (in the present application) lack of available *ugriz* photometry. An empirical determination of these errors for the n-SSPP is obtained below.

The spectra for our program stars do not reach as far redward as SDSS/SEGUE spectra (hence we cannot use as many of the independent methods as the SSPP provides), and they are of slightly higher resolving power. Thus, during the execution of the n-SSPP, our spectra were first rebinned in order to match the resolving power of SDSS/SEGUE spectra (i.e., to 1 Å linear pixels). The n-SSPP stellar atmospheric parameter estimates are listed in columns (10)-(12) of Table 1 as  $\text{Teff}_S$ ,  $\log g_S$ , and  $[\text{Fe}/\text{H}]_S$ , respectively.

The n-SSPP has been modified recently in order to estimate carbon-to-iron abundance ratios (carbonicity, [C/Fe]), based on spectral matching against a dense grid of synthetic spectra. Lee et al. (2013) describes in detail the procedures adopted to estimate [C/Fe] for SDSS/SEGUE spectra; these techniques, with different input photometric information, also apply to the n-SSPP. Note that we have recently expanded the carbon grid to reach as low as [C/Fe] = -1.5, rather than the limit of [C/Fe] = -0.5 employed by Lee et al. (2013). As shown by Lee et al. (2013), the precision of the carbonicity estimates are better than 0.35 dex for the parameter space and (generally lower) S/N ratios explored by SDSS/SEGUE spectra. We expect similar (or improved) results for application of the n-SSPP to our program spectra, which is checked empirically below. Table 1 lists the medium-resolution estimates of carbonicity,  $[\text{C}/\text{Fe}]_S$ , in column (2). Column (3) indicates whether the listed measurement is considered a detection, DETECT = “D”, lower limit “L”, or upper limit “U”, and Column (4) provides the correlation coefficient, CC, obtained between the observed spectrum and the best-matching [C/Fe] from the model grids. For an acceptable measurement of carbonicity, we demand DETECT = “D” and  $\text{CC} \geq 0.7$ . See Lee et al. (2013) for further discussion of these quantities. There are two stars listed in Table 1 (BM-083 and BM-284) which have CC less than this value; they are marked with a “:” in the DETECT column.

#### 3.1. Comparison to High-Resolution Spectroscopic Analyses

External measurements of atmospheric parameters and carbon abundances were obtained from various sources in the literature, including the compilations of Cayrel

<sup>12</sup> If both sets of  $V, B - V$  and  $J, J - K$  photometry are available, they are used, but the n-SSPP can operate well with one or the other. Even if no photometric measurements are available, the n-SSPP can, in most cases, produce viable stellar parameter estimates (but not distance estimates, which require an input apparent magnitude).

de Strobel et al. (2001), Suda et al. (2008), and Frebel (2010), as well as the references listed in SIMBAD<sup>13</sup> and in the PASTEL catalogue (Soubiran et al. 2010)<sup>14</sup>. In total, we found 170 measurements of  $T_{\text{eff}}$ , 111 of  $\log g$ , 114 of  $[\text{Fe}/\text{H}]$ , and 50 for  $[\text{C}/\text{Fe}]$ . Note that we have only made use of estimates based on studies published since 1990. A straight average of all available estimates for these parameters was taken (excepting a few instances where it appeared that a given high-resolution estimate was clearly highly discrepant); the results are listed in columns (13)-(15) of Table 1 as  $T_{\text{eff}}_H$ ,  $\log g_H$ , and  $[\text{Fe}/\text{H}]_H$ , respectively. Column (4) of Table 1 lists the high-resolution estimates of carbonicity,  $[\text{C}/\text{Fe}]_H$ , for our program stars, where available. Since the range in carbonicity for our program stars with available high-resolution determinations is relatively limited, and does not include many stars with  $[\text{Fe}/\text{H}] < -2.0$ , we have supplemented the comparison sample by obtaining n-SSPP estimates of  $[\text{C}/\text{Fe}]_S$  from the medium-resolution SDSS/SEGUE spectra for 39 stars with available high-resolution determinations from Aoki et al. (2013).

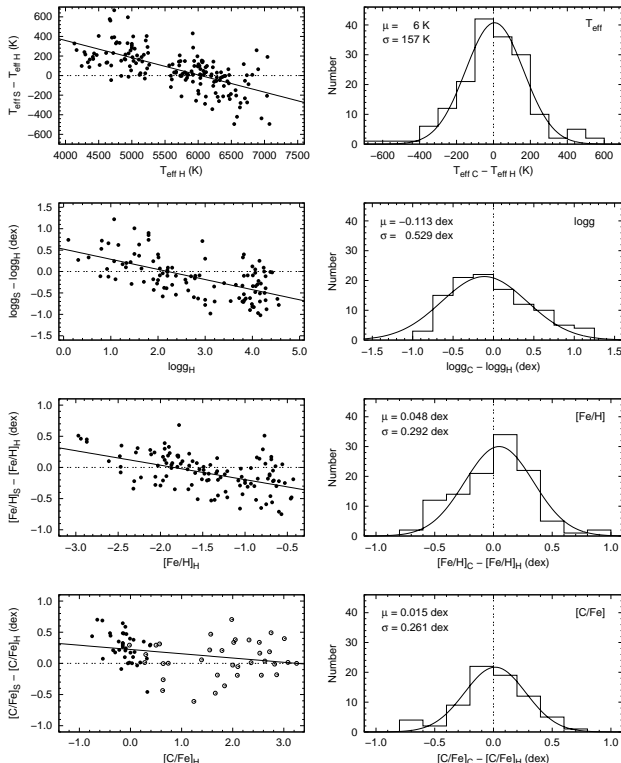


**Figure 3.** Left panels: Differences between the atmospheric parameters and carbon-abundance ratios determined by the n-SSPP,  $T_{\text{eff}}_S$ ,  $\log g_S$ ,  $[\text{Fe}/\text{H}]_S$ , and  $[\text{C}/\text{Fe}]_S$ , and the values from analyses of high-resolution spectroscopy,  $T_{\text{eff}}_H$ ,  $\log g_H$ ,  $[\text{Fe}/\text{H}]_H$ , and  $[\text{C}/\text{Fe}]_H$  reported in the literature, as a function of the high-resolution spectroscopic values. Filled symbols refer to our B&M program stars, while in the bottom panel the open symbols represent stars from Aoki et al. (2013), as described in the text. The dashed lines show the linear functions (Equations (1)-(4)) used to obtain corrections to the n-SSPP values, as described in the text. Right panels: Histograms of the residuals between the corrected n-SSPP and high-resolution parameters shown in the left panels. Each panel also lists the average offset and scatter determined from a Gaussian fit.

<sup>13</sup> <http://simbad.u-strasbg.fr/simbad/>

<sup>14</sup> <http://vizier.u-strasbg.fr/viz-bin/VizieR?-source=B/pastel>

Figure 3 illustrates, in the left-hand column of panels, comparisons of the n-SSPP estimates  $T_{\text{eff}}_S$ ,  $\log g_S$ ,  $[\text{Fe}/\text{H}]_S$ , and  $[\text{C}/\text{Fe}]_S$  with the averaged high-resolution spectroscopic results,  $T_{\text{eff}}_H$ ,  $\log g_H$ ,  $[\text{Fe}/\text{H}]_H$ , and  $[\text{C}/\text{Fe}]_H$ . The solid lines in these panels are linear fits to the residuals in the difference between the medium- and high-resolution results, as a function of the high-resolution determinations. We use these fits to correct our n-SSPP estimates from the medium-resolution spectra to come into better agreement with the external high-resolution estimates, in the form:

$$[\text{Fe}/\text{H}]_C = [\text{Fe}/\text{H}]_S - (-0.232 \cdot [\text{Fe}/\text{H}]_S - 0.428) \quad (1)$$

$$T_{\text{eff}}_C = T_{\text{eff}}_S - (-0.1758 \cdot T_{\text{eff}}_S + 1062) \quad (2)$$

$$\log g_C = \log g_S - (-0.237 \cdot \log g_S + 0.523) \quad (3)$$

$$[\text{C}/\text{Fe}]_C = [\text{C}/\text{Fe}]_S - (-0.068 \cdot [\text{C}/\text{Fe}]_S + 0.273) \quad (4)$$

The right-hand column of panels in Figure 3 shows the distribution of residuals between the corrected n-SSPP estimates ( $T_{\text{eff}}_C$ ,  $\log g_C$ , and  $[\text{Fe}/\text{H}]_C$ , listed in columns (16)-(18) of Table 1, and  $[\text{C}/\text{Fe}]_C$ , listed in column (6) of Table 1) and their corresponding high-resolution values. Note that, with the exception of a few individual stars, the agreement is quite satisfactory. Maximum-likelihood Gaussian fits to the distributions of residuals between these various estimates are shown in the right-hand column of panels. Taking into account the expected errors in the (non-uniformly analysed) high-resolution literature estimates of the effective temperature and surface gravity (100 K and 0.35 dex, respectively), we conclude that the external accuracies of  $T_{\text{eff}}_C$  and  $\log g_C$  are on the order of 125 K and 0.4 dex, respectively. The zero-point offsets of the n-SSPP estimates are acceptably small, on the order of 6 K and 0.1 dex for  $T_{\text{eff}}_C$  and  $\log g_C$ , respectively. The rather large external error in the surface gravity estimate is perhaps not surprising, since the spectra do not extend sufficiently redward to include the particularly gravity sensitive Mg I lines at  $\sim 5180 \text{ \AA}$ . Assuming that the expected errors in the literature estimates of metallicity and carbonicity are on the order of 0.20 dex (which may be generous), the external errors in  $[\text{Fe}/\text{H}]_C$  and  $[\text{C}/\text{Fe}]_C$  are both  $\sim 0.20$  dex.

### 3.2. Comparison to the NBP DDO-based Estimates

We now examine a comparison of our presently determined spectroscopic metallicity estimates with the DDO photometry-based estimates of metallicity given by NBP, and listed as  $[\text{Fe}/\text{H}]_N$  in column (19) of Table 1. The upper panels of Figure 4 show the complete sample, while the middle and lower panels for stars classified as dwarfs and giants by NBP, respectively.

The luminosity classes for our program stars are listed in column (20), in the form  $\text{TYPE}_{N/S}$ , where “N” indicates those assigned by NBP, while “S” indicates the classes assigned by the n-SSPP. The stars classified as dwarf, subgiant, and red giant map directly onto the classes considered by Beers et al. (2000) (note that we do not discriminate between subgiants and giants in the n-SSPP; they are all classified as giants). We consider the stars NBP classified as blue dwarfs to be main-sequence turnoff (TO) stars, while the blue giant and red horizontal-branch (RHB) classes are considered as field horizontal-branch (FHB) stars. The UV bright stars are

considered to be giants. Note that the classifications are commensurate, in most cases, although they differ for 43 stars (labeled with a ":" in column (20)). The great majority of these conflicting classifications (33 of 43) occur for stars with  $T_{\text{eff}}C \geq 6000$  K, the region where it becomes difficult to distinguish dwarfs from giants close to the main-sequence turnoff. We proceed with our analysis under the assumption the n-SSPP classification is superior, and make use of it for cases where the luminosity class is in doubt (except where noted).

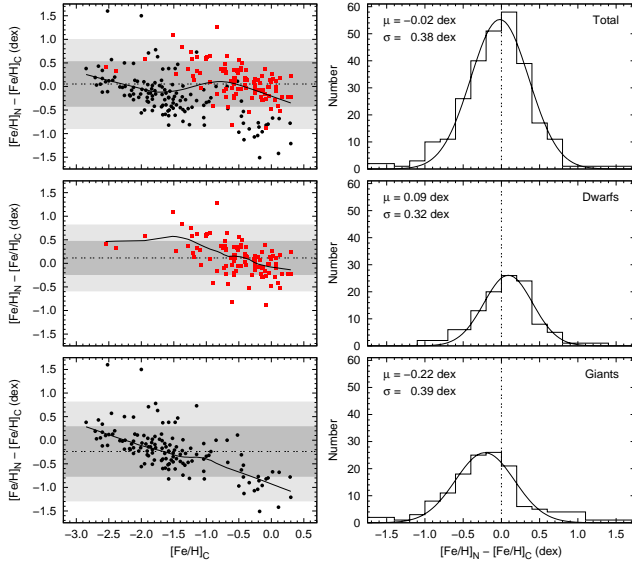


**Figure 4.** Comparison between the DDO photometry-based metallicities from NBP with our final metallicity estimates,  $[Fe/H]_C$ , for the entire sample (upper panels), dwarfs (middle panels), and giants (lower panels). Note that, for the purposes of this comparison, the taxonomy of NBP was used. The left-hand column of panels shows the residuals as a function of  $[Fe/H]_C$ , with the average (dashed horizontal line), while the darker and lighter shaded areas represent the 1- $\sigma$  and 2- $\sigma$  regions, respectively. The solid line is a *loess* (locally weighted regression) line. The right panels show Gaussian fits to the residuals. Note the clear offset to lower metallicities reported by NBP for the giants with metallicities  $[Fe/H]_C > -1.5$  (see text).

The average offset and scatter in the metallicity residuals, shown in Figure 4 for the complete sample, are  $(\mu, \sigma) = (-0.02 \text{ dex}, 0.38 \text{ dex})$ , while the values for the dwarfs and giants (as classified by NBP) are  $(+0.09 \text{ dex}, 0.32 \text{ dex})$  and  $(-0.22 \text{ dex}, 0.39 \text{ dex})$ , respectively. The solid lines in the left-hand panels indicate locally weighted regression (*loess*) lines that trace the data. As can be appreciated by inspection of the middle panels of Figure 4, the dwarfs exhibit general agreement with our spectroscopic metallicity estimates, with a tendency for  $[Fe/H]_N$  to be somewhat higher than  $[Fe/H]_C$  for metallicities  $[Fe/H]_C < -1.0$ . By way of contrast, the  $[Fe/H]_N$  for giants in the lower panels are clearly too low, compared to  $[Fe/H]_C$ , for  $[Fe/H]_C > -1.5$ , and somewhat higher than  $[Fe/H]_C$  for  $[Fe/H]_C < -1.5$ . It is the higher metallicity stars that disagree in the same sense described by Anthony-Twarog & Twarog (1994) and Ryan & Lambert (1995), and which were the source of concern for the validity of the original claim for a MWTD. What remains to be shown is whether the existence of a MWTD is supported, or refuted, by the analysis we carry out below,

using our improved estimates of metallicity and refined kinematics.

For the remainder of the paper, we drop the subscripts on  $[Fe/H]_C$  and  $[C/Fe]_C$ , and simply refer to our adopted metallicity and carbonicity estimates as  $[Fe/H]$  and  $[C/Fe]$ , respectively.

#### 4. DISTANCE ESTIMATES AND PROPER MOTIONS

##### 4.1. Distance Estimates

Distances to individual stars in this sample are estimated using the  $M_V$  vs.  $(B-V)_0$  relationships described by Beers et al. (2000). These relationships require that the likely evolutionary state (luminosity class) of a star be specified. For this, we make use of the taxonomy assigned by the n-SSPP (which assigns types according to the observed surface gravity estimate), the most recent discussion of which is provided by Beers et al. (2012). Note that this includes the reassignment, as necessary, of stars classified as main-sequence turnoff stars into dwarfs or giants when they otherwise appear in physically impossible positions in the color-magnitude diagram. See Beers et al. (2012) for additional details.

Once types are assigned, distance estimates can be obtained in a straightforward manner. The estimates have to be iterated, because both  $V_0$  (and therefore the distance estimate) and  $(B-V)_0$  depend on the adopted reddening. Although the  $M_V$  vs.  $(B-V)_0$  relationships depend on the metallicity as well, the change in metallicity with small alterations in reddening has little effect. With only a few iterations we obtain consistent estimates of the final reddening,  $E(B-V)_F$  (listed in column (11) of Table 1), and the photometric distance estimate,  $D_{\text{pho}}$ , listed in the fourth column of Table 1. Based on previous tests of this approach (e.g., Beers et al. 2000, 2012), we expect the photometric distances to be precise to on the order of 10–20%. For most instances, we apply a distance uncertainty of 15%, although in a few cases, larger uncertainties were adopted in order to reflect uncertainties in the determination of reddening corrections.

All but four stars among our program objects have parallaxes available from the Hipparcos astrometric catalog (ESA 1997; van Leeuwen 2007). These parallaxes, and their associated errors, are listed in columns (2) and (3) of Table 1.

To assess the reliability of our photometric distance estimates, Figure 5 shows the comparison between distances based on photometry,  $D_{\text{pho}}$ , with the distances based on Hipparcos parallaxes,  $D_{\text{HIP}} = 1/\pi_{\text{HIP}}$ , for the four different luminosity classes of the targets. Note that this plot only includes stars for which accurate trigonometric and photometric distance estimates are available (that is, we exclude stars with trigonometric parallaxes having  $\sigma_{\pi_{\text{HIP}}} / \pi_{\text{HIP}} > 0.20$ , listed in column (6) of Table 1, or located at the lowest latitudes,  $|b| \leq 10^\circ$ , where reddening, and hence extinction, to a given star is highly uncertain. As can be appreciated by inspection of Figure 5, the relationship between our derived photometric and Hipparcos distances is close to the one-to-one line. Only the few stars with distances greater than about 200 parsecs exhibit significant scatter.

For the purpose of our kinematic analysis below, we adopt distance estimates based on trigonometric parallaxes, where we judge them to be sufficiently accurate

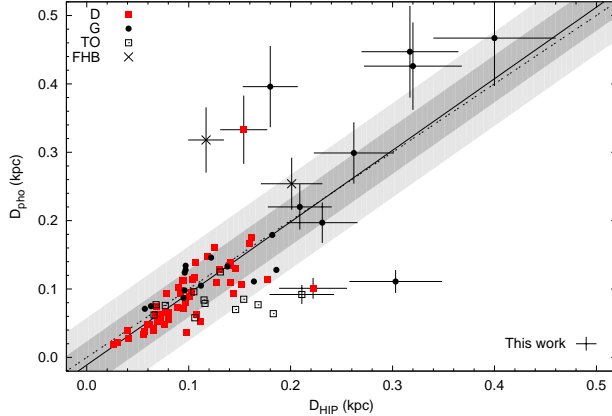


**Figure 5.** Comparison of the photometrically estimated distances,  $D_{\text{pho}}$ , with the trigonometric distance estimates,  $D_{\text{HIP}}$ , for stars with sufficiently accurate Hipparcos parallaxes ( $\sigma_{\pi_{\text{HIP}}} / \pi_{\text{HIP}} \leq 0.20$ ). The dashed line is the one-to-one line, while the solid line is a robust regression fit to the data. The darker and lighter shaded areas represent the 1- $\sigma$  and 2- $\sigma$  regions about the linear fit, respectively, based on a Gaussian fit to the residuals. The error bar in the lower right corner of the plot is the typical error for stars with distances less than 200 pc. For stars with distances (either photometric or astrometric) greater than 200 pc, individual error bars are shown.

(parallaxes satisfying  $\sigma_{\pi_{\text{HIP}}} / \pi_{\text{HIP}} \leq 0.20$ , and greater than zero). Otherwise, we adopt the derived photometric distance estimate. The final adopted distances,  $D_{\text{ado}}$ , are listed in column (7) of Table 1.

#### 4.2. Proper Motions

Proper motions for all of our program stars are available from the Hipparcos (ESA 1997; van Leeuwen 2007), Tycho-1 (ESA 1997; Hog et al. 1998), or Tycho-2 (ESA 1997; Høg et al. 2000) catalogs, with average precisions of 1.25 mas yr<sup>-1</sup> in  $\mu_\alpha$  (taking the  $\cos \delta$  term into account) and 1.03 mas yr<sup>-1</sup> in  $\mu_\delta$ . The precision of the presently available proper motions represent substantial improvements over those used by NBP. Furthermore, while all of our program stars have proper motion estimates, only about one-third of the stars in the NBP catalog had this information available. Columns (8) and (9) of Table 1 list the proper motions for our program stars, while columns (10) and (11) present their associated errors. The final column lists the identifier of the star in the Hipparcos or Tycho catalogs.

### 5. KINEMATIC ANALYSIS OF THE B&M SAMPLE

In this section we examine the kinematic properties of the B&M sample of stars studied by NBP.

Figure 6 shows the distribution of the absorption-corrected  $V_0$  magnitudes, de-reddened  $(B - V)_0$  colors, adopted distances,  $D_{\text{ado}}$ , and estimates of metallicities,  $[\text{Fe}/\text{H}]$ , for our sample of program stars. As is immediately clear from inspection of this figure, this is a very local sample of stars, with  $\sim 90\%$  of the stars located within 1 kpc from the Sun. Nevertheless, because of the metallicity bias in the original selection, some 70% have  $[\text{Fe}/\text{H}] \leq -0.5$ , suitable for exploration of the thick disk, MWTD, and inner-halo population. There are not large numbers of stars in this sample with  $[\text{Fe}/\text{H}] < -2.0$  ( $\sim 10\%$  of the sample), which limits its utility for examination of the outer-halo population.

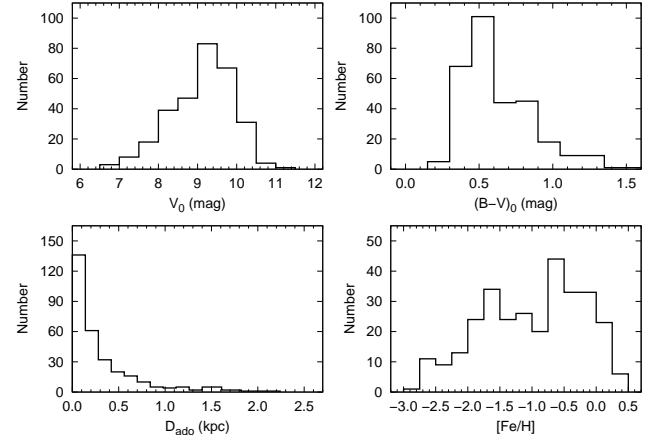


**Figure 6.** Distributions of (a) absorption-corrected  $V_0$  magnitudes, (b) de-reddened  $(B - V)_0$  colors, (c) adopted distance estimates,  $D_{\text{ado}}$ , and (d) metallicity estimates,  $[\text{Fe}/\text{H}]$ , for our program stars.

#### 5.1. Determination of Space Motions and Orbital Parameters

It is our intention to obtain the most precise kinematics for our program stars, taking advantage of the refinements that more modern data have provided in the 28 years since the publication of the first paper in this series.

Adopted distances are determined as described in subsection 4.1 above. Proper motions, almost all taken from the Hipparcos catalog, are described in subsection 4.2 above. From Table 1, we adopt the high-resolution spectroscopic determinations of radial velocities,  $RV_H$ , where available, which are expected to have precisions of 2 km s<sup>-1</sup> or better. When not available, we make use of the determinations based on medium-resolution spectroscopy, which were demonstrated in subsection 2.3 to exhibit precisions on the order of 5 km s<sup>-1</sup>.

We now derive the space motions and orbital parameters of our program stars, following the procedures described by Carollo et al. (2010).

Corrections for the motion of the Sun with respect to the Local Standard of Rest (LSR) are applied during the course of the calculation of the full space motions; here we adopt the values  $(U, V, W) = (9, 12, 7)$  km s<sup>-1</sup> (Mihalas & Binney 1981). Note that we follow the convention that  $U$  is positive in the direction away from the Galactic center,  $V$  is positive in the direction of Galactic rotation, and  $W$  is positive toward the north Galactic pole. For the purpose of this analysis it is also convenient to obtain the rotational component of a star's motion about the Galactic center in a cylindrical frame, denoted as  $V_\phi$ , and calculated assuming that the LSR is on a circular orbit with a value of 220 km s<sup>-1</sup> (Kerr & Lynden-Bell 1986). Our assumed values of  $R_\odot$  (8.5 kpc) and the circular velocity of the LSR are both consistent with two recent independent determinations of these quantities by Ghez et al. (2008) and Koposov et al. (2009). Bovy et al. (2012d) recently obtained an estimate of the Milky Way's circular velocity at the position of the Sun of  $V_c(R_\odot) = 218 \pm 6$  km s<sup>-1</sup>, based on an analysis of high-resolution spectroscopic determinations from the Apache Point Observatory Galactic Evolution Experiment (APOGEE; Majewski et al. 2010), part of

the Sloan Digital Sky Survey III (SDSS-III; Eisenstein et al. 2011), which is also consistent with our adopted value.

The orbital parameters of the stars, such as the perigalactic distance (the closest approach of an orbit to the Galactic center),  $r_{\text{peri}}$ , the apogalactic distance (the farthest extent of an orbit from the Galactic center),  $r_{\text{apo}}$ , of each stellar orbit, and the orbital eccentricity,  $e$ , defined as  $e = (r_{\text{apo}} - r_{\text{peri}})/(r_{\text{apo}} + r_{\text{peri}})$ , as well as  $Z_{\text{max}}$  (the maximum distance that a stellar orbit achieves above or below the Galactic plane), are derived by adopting an analytic Stäckel-type gravitational potential (which consists of a flattened, oblate disk, and a nearly spherical massive dark-matter halo; see the description given by Chiba & Beers 2000, Appendix A), and integrating their orbital paths based on the starting point obtained from the observations.

Table 1 provides a summary of the above calculations. Column (1) provides the star names. Columns (2) and (3) list the positions of the stars in the meridional ( $R, Z$ )-plane. The derived  $UVW$  velocity components are provided in columns (4)-(6); their associated errors are listed in columns (7)-(9). Column (10) lists the velocity projected onto the Galactic plane ( $V_R$ , positive in the direction away from the Galactic center), while column (11) lists the derived rotation velocity,  $V_\phi$ . The derived  $r_{\text{peri}}$  and  $r_{\text{apo}}$  are given in columns (12) and (13), respectively. Columns (14) and (15) list the derived  $Z_{\text{max}}$  and orbital eccentricity,  $e$ , respectively.

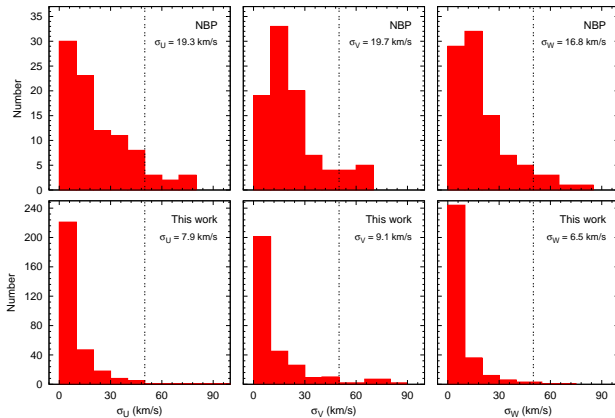


**Figure 7.** Errors in the estimation of the local velocity components of the space motions for stars in the B&M sample, for the stars reported by NBP (upper panels) and in the present work (lower panels). The vertical dashed lines at  $50 \text{ km s}^{-1}$  indicate the maximum individual errors allowed for a given star to be included in the subsequent kinematic analysis. The legends provide the mean errors for the accepted stars. Note the marked decrease in the errors for these quantities obtained by the present work.

Errors on our derived estimates of the individual components of the space motions take into account an estimated 15% error in the photometric distances (individual errors in Hipparcos distances, when adopted, are used), as well as the individual errors in the proper motions and the adopted radial velocities ( $2 \text{ km s}^{-1}$  for the high-resolution determinations,  $5 \text{ km s}^{-1}$  for the medium-resolution determinations). As expected, when compared to the previous results of NBP, the derived errors in these quantities are much improved. Figure 7

shows the distributions of these errors for both sets of analyses. After removing the stars with individual estimated errors in any one of the three components of space motion larger than  $50 \text{ km s}^{-1}$  from each of these samples (or which were dropped for other reasons), the average errors for the B&M sample are  $\sigma(U, V, W) = (7.9, 9.1, 6.5) \text{ km s}^{-1}$ . For NBP, the average errors were 2 to 2.5 times as high,  $\sigma(U, V, W) = (19.3, 19.7, 16.8) \text{ km s}^{-1}$ . The large errors in the individual space motions (and eccentricities) of some stars forced NBP to rather severely trim their sample from which inferences could be made about the nature of the underlying populations.

A total of 42 stars in our full sample of 302 stars are not used in the kinematic analysis, because they are either missing one or more of the input quantities used for the determination of their space motions, are located at Galactic latitudes  $|b| < 10^\circ$  and had only photometric distances available (and hence uncertain estimates of reddening), or had individual estimated errors in any one of the three components of space motion larger than  $50 \text{ km s}^{-1}$ . Such stars are noted in the final column of Table 1, where the first digit of the INOUT parameter set to “0” indicates that the star has been dropped from subsequent kinematical analysis.

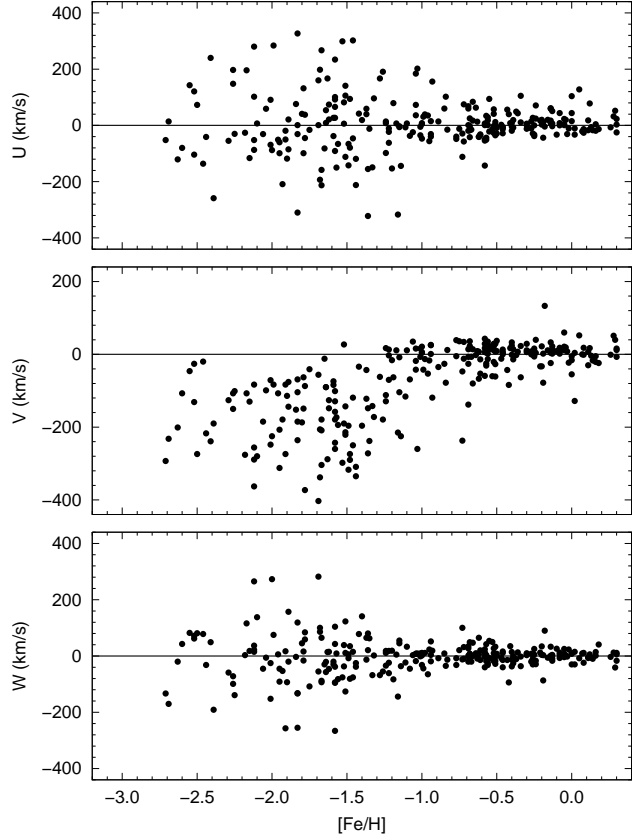
### 5.2. Distributions of $UVW$ , and $Z_{\text{max}}$ vs. $[\text{Fe}/\text{H}]$

Figure 8 presents the individual components of the space motions, as a function of  $[\text{Fe}/\text{H}]$ , for our program stars with accepted kinematic estimates. It is clear from inspection of this diagram that there exists a “core” of stars with relatively high net rotation and low velocity dispersion down to at least  $[\text{Fe}/\text{H}] = -1.3$ , and possibly a little lower. This immediately suggests the presence of low-metallicity stars in the disk system, well below the mean abundance typically associated with the canonical thick disk, on the order of  $[\text{Fe}/\text{H}] = -0.6$ .

Since the great majority of our program stars are located within 1 kpc, it is difficult to separate possible stellar populations on the basis of vertical distance from the Galactic plane. As an alternative, we have explored using the derived maximum distance from the plane,  $Z_{\text{max}}$ . Figure 9 shows the result of this exercise, where we have plotted the base-10 log of  $Z_{\text{max}}$  as a function of  $[\text{Fe}/\text{H}]$ . A reference line at  $Z_{\text{max}} = 3 \text{ kpc}$  is shown. From inspection of this figure, it is clear that significant numbers of stars with  $Z_{\text{max}} > 3 \text{ kpc}$  are not found for  $[\text{Fe}/\text{H}] \gtrsim -1.5$ . Although some overlap between the inner-halo population and the proposed MWTD population is unavoidable, we expect the majority of the stars with  $Z_{\text{max}} \leq 3 \text{ kpc}$  and in the metallicity interval  $-1.8 \leq [\text{Fe}/\text{H}] \leq -0.8$  (following Carollo et al. 2010) to be associated with the MWTD. As is shown below, stars in this metallicity interval also exhibit a lower net rotation than the stars of the canonical thick disk.

### 5.3. The $[\text{Fe}/\text{H}]$ vs. Eccentricity Diagram

One of the central arguments of NBP, that there exist numerous stars in the B&M sample (where none were found in the sample used by ELS to support their classic monolithic collapse model) in the regime  $[\text{Fe}/\text{H}] \leq -1.0$ ,  $e \leq 0.4$ , can now be re-examined using our improved kinematic results. The upper panel of Figure 10 is a plot of  $[\text{Fe}/\text{H}]$ , as a function of orbital eccentricity, for the



**Figure 8.** Local velocity components for stars in the B&M sample with available  $UVW$  estimates, as a function of metallicity,  $[Fe/H]$ . Note the existence of stars with low velocity dispersions in their estimated components down to at least  $[Fe/H] = -1.5$ , and possibly a little lower. Stars with errors in any of the individual derived components of motion exceeding  $50 \text{ km s}^{-1}$  are excluded.

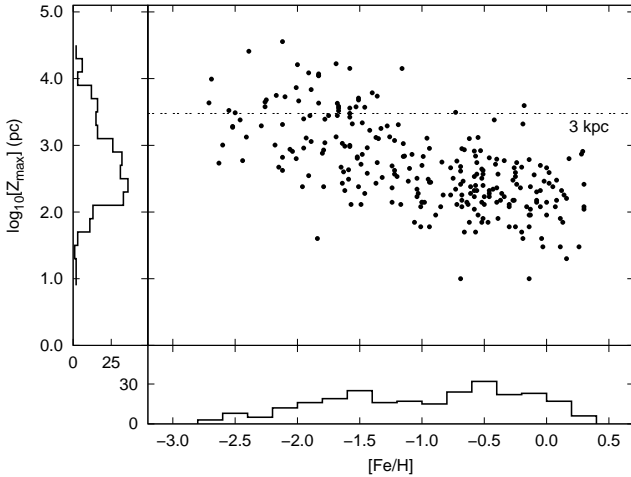


**Figure 9.** Distribution of  $Z_{\max}$ , the largest distance above or below the Galactic plane achieved by a star during the course of its orbit, as a function of metallicity, for the stars in the B&M sample. The marginal distributions of each variable are shown as histograms. The horizontal dashed line provides a reference at 3 kpc. Very few stars with metallicity  $[Fe/H] > -1.5$  achieve orbits that reach higher than this location. Note the logarithmic scale for  $Z_{\max}$ . Stars with errors in any of the individual derived components of motion exceeding  $50 \text{ km s}^{-1}$  are excluded.

sample of B&M stars from NBP (their Figure 14), where we have used their derived metallicities and eccentricities (restricted, as did they, to stars with estimated errors in the eccentricity  $\leq 0.1$ ). The lower panel of the figure shows the more comprehensive results for the B&M stars from the present analysis. All of our program stars with acceptable kinematic determinations have estimated errors in eccentricity less than 0.1. In both panels, for heuristic purposes, the red squares stand for red giants (NBP, upper panel) and giants (this work, lower panels), while black circles are used for all other objects. The two panels also show the original box ( $-2.0 \leq [Fe/H] \leq -1.0$ ,  $0.2 \leq e \leq 0.4$ ) used by NBP to contrast the locations of the stars in the ELS sample with their own. Note that there are roughly 10 stars in the NBP analysis that fall in the box (plus or minus a few that are right at the edges of the box) compared with none in the original ELS sample. As seen in the lower panel, the present analysis now includes almost twice as many stars in the same box.

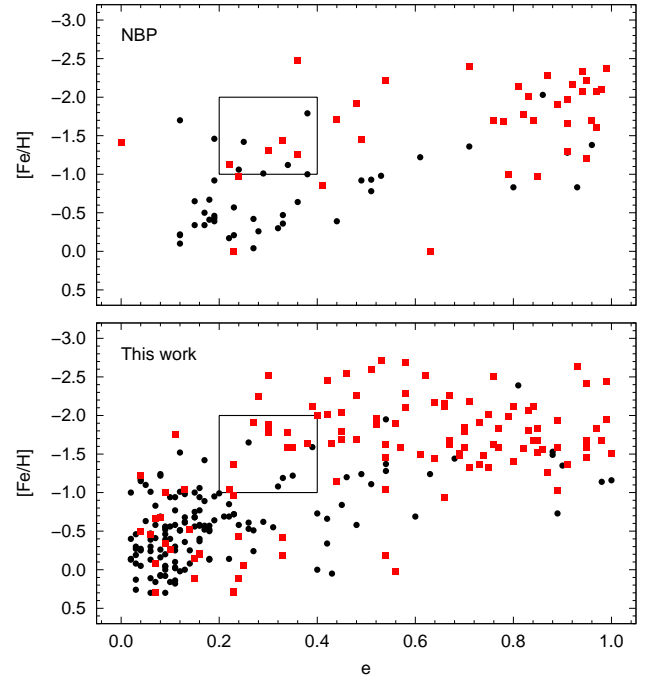


**Figure 10.** Distribution of metallicity,  $[Fe/H]$ , for stars in the B&M sample, as a function of derived orbital eccentricity,  $e$ . In both panels the red squares stand for red giants while black circles are used for all other objects. (Upper panel) The sample studied by NBP (and adopting their metallicities and eccentricities), which only included stars with eccentricities having errors less than 0.1. The box indicates the region of interest originally considered by NBP. (Lower panel) The present sample, all of which have errors in eccentricity less than 0.1. In addition to a much larger total sample, note that the box now contains about twice as many stars as for the NBP sample. Stars with errors in any of the individual derived components of motion exceeding  $50 \text{ km s}^{-1}$  are excluded.

Clearly, the addition of more stars with improved estimates of metallicities and eccentricities in the present sample *strengthens* the original thesis of NBP that the ELS model was incompatible with results obtained for the B&M sample of non-kinematically selected stars.

Of course, more modern analyses of even larger such samples (e.g., Chiba & Beers 2000; Carollo et al. 2007, 2010) have come to similar conclusions, and are consis-

tent with the expectations from contemporary hierarchical galaxy-assembly models. However, this idea had its observational origin for field stars in the work of NBP<sup>15</sup>.

#### 5.4. The Toomre and Lindblad Diagrams

The so-called Toomre diagram (a plot of  $(U^2 + W^2)^{1/2}$ , the quadratic addition of the  $U$  and  $W$  velocity components, as a function of the rotational component,  $V$ ) and the Lindblad diagram (a plot of the integrals of motion representing the total energy,  $E$ , and the vertical angular momentum component,  $L_Z$ ) are commonly used to investigate the nature of the kinematics of stellar populations in the Galaxy. Given the high quality of the estimated kinematics for the B&M sample, it is useful to examine these diagrams to glean any insight we can from them.

For the sake of comparison, we have also derived these diagrams based on the sample of RAVE stars reported by Ruchti et al. (2011)<sup>16</sup>. The Ruchti et al. sample is of similar size, and covers a similar metallicity range as the B&M sample, but carries along its own set of biases in the selection of the member stars (see Ruchti et al. 2010, for a discussion). In addition, the proper motions available to Ruchti et al. are not as precise, in general, as those in our sample, since few of their stars were included in the Hipparcos, Tycho, or Tycho-2 catalogs.

Figure 11 shows the Toomre diagrams for the two samples. The upper panel is the sample of Ruchti et al. (after removal of the 72 of 319 stars that are either missing the input quantities used for determination of their space motions, or that have individual estimated errors in any one of the three components of space motion larger than  $50 \text{ km s}^{-1}$ ). Following the removal of these stars, the average errors in the derived space motions are  $\sigma(U, V, W) = (14.4, 15.6, 12.2) \text{ km s}^{-1}$ , about twice as high as from our analysis of the B&M sample, but still better than obtained from the NBP analysis.

The lower panel shows the Toomre diagram for the B&M sample. The legend indicates the metallicity intervals that are distinguished in the two panels. These were chosen to roughly separate stars expected to belong to the thick (or thin) disk ( $[\text{Fe}/\text{H}] > -0.8$ ), the suggested MWTD ( $-1.8 < [\text{Fe}/\text{H}] \leq -0.8$ ), and the halo system ( $[\text{Fe}/\text{H}] \leq -1.8$ ), taking our guidance in selecting these intervals from Carollo et al. (2010). As expected, the more metal-rich stars in both samples are primarily found in the region with low  $(U^2 + W^2)^{1/2}$  and high orbital rotation velocities ( $(U^2 + W^2)^{1/2} \lesssim 100 \text{ km s}^{-1}$ ,  $-100 < V < 100 \text{ km s}^{-1}$ ), while stars with intermediate metallicities are divided between those inside and outside this region.

The Lindblad diagrams for these two samples of stars, calculated following the prescription described by Carollo

<sup>15</sup> J.E.N. acknowledges here the validity of the criticism of the NBP abundances for red giants by Anthony-Twarog & Twarog (1994) and Ryan & Lambert (1995); for historians of science, he notes that the discrepancy results from errors in the limited DDO abundance calibration adopted for (absolutely) fainter, more metal-rich giants. That said, inspection of the present Figure 10 shows that, with the present abundance calibration, giants exist in the region where ELS (due to their selection criteria) found no stars.

<sup>16</sup> We have updated the estimates of  $[\text{Fe}/\text{H}]$  and the derived  $UVW$  used for the Ruchti et al. sample based on revised information kindly supplied by G. Ruchti (private communication), based on a newer version of the RAVE pipeline outputs.

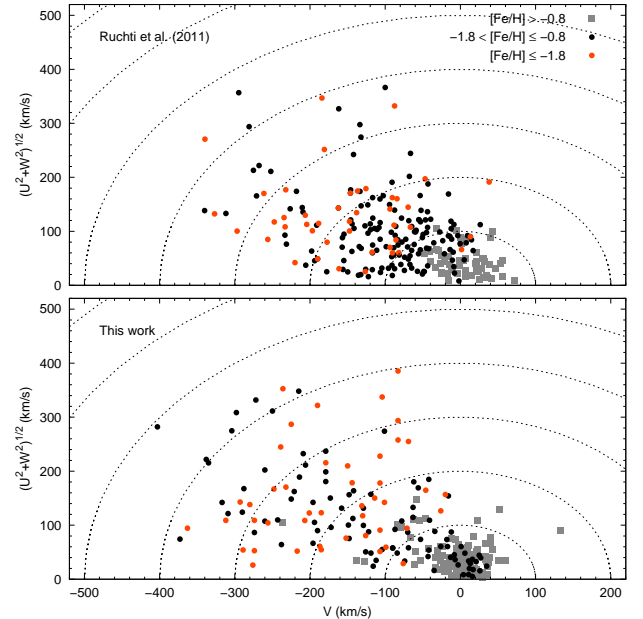


**Figure 11.** Toomre diagram of  $(U^2 + W^2)^{1/2}$  vs.  $V$  for the stars with available  $UVW$  velocity components, in three regimes of metallicity, for stars in the sample of RAVE stars from Ruchti et al. (2011) (upper panel) and in the B&M sample (lower panel). Note the presence of the intermediate-metallicity ( $-1.8 < [\text{Fe}/\text{H}] \leq -0.8$ ) stars both inside and outside the region with low  $(U^2 + W^2)^{1/2}$  and high orbital rotation velocities ( $(U^2 + W^2)^{1/2} \lesssim 100 \text{ km s}^{-1}$ ,  $-100 < V < 100 \text{ km s}^{-1}$ ). Stars with errors in any of the individual derived components of motion exceeding  $50 \text{ km s}^{-1}$  are excluded.

et. al (2014), are shown in Figure 12. As can be appreciated from inspection of the left-hand panel, which applies to the B&M sample, there is rather clear separation of a region corresponding to a rotationally supported disk system, indicated by the dashed line shown to guide the eye. The same line is drawn in the right-hand panel, which applies to the Ruchti et al. sample. The stars to the right of the line are expected to be dominated by members of the disk system (thin, thick, and MWTD) while those to the left of the line are likely to be dominated by inner-halo members. Note that the separation of stars across this line is somewhat less clear for the Ruchti et al. sample, presumably because of the larger errors in the derived kinematics. Also note that this kinematic division does not isolate only the more metal-rich stars, but in both samples appears to include relatively large fractions of stars in the intermediate metallicity interval,  $-1.8 < [\text{Fe}/\text{H}] \leq -0.8$ , and a few stars with even lower metallicity.

#### 5.5. Distributions of $V_\phi$ for the B&M and Ruchti et al. Samples

We now examine, in greater detail, the motions of the stars isolated above by their location in the Lindblad diagrams. The top row of the upper grouping of panels in Figure 13 shows stripe density plots of the distribution of  $V_\phi$  for the full sets of stars with metallicities  $-0.8 < [\text{Fe}/\text{H}] \leq -0.5$  from the B&M (left) and Ruchti et al. (right) samples. The lower row in this grouping shows the stars in this same metallicity interval selected to the right of the segregation line in Figure 12, labeled as the “Disk sample.” This metallicity interval is expected

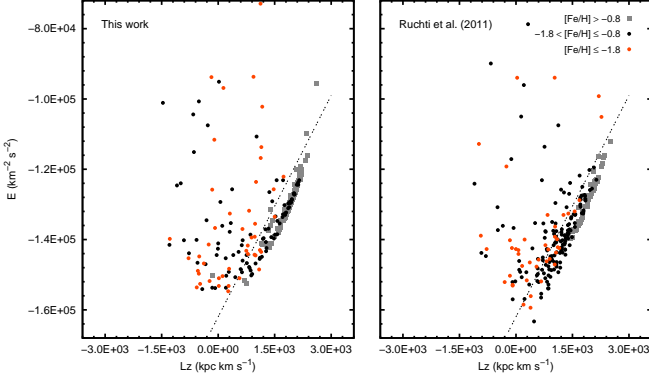


**Figure 12.** Lindblad diagram of two integrals of motion, the total energy,  $E$ , and the vertical angular momentum component,  $L_z$ , in three regimes of metallicity, for the B&M sample (left panel) and for the sample of RAVE stars from Ruchti et al. (2011) (right panel). The dashed line is drawn in order to separate likely members of rotation-supported populations (see text). Note that the same line is drawn in both figures. Stars with errors in any of the individual derived components of motion exceeding  $50 \text{ km s}^{-1}$  are excluded.

to primarily comprise thick-disk stars, but some overlap with the thin disk and MWTD is inevitable. Stars that are likely members of the disk system are identified by a “1” in the second digit of the INOUT parameter in column (18) of Table 1. Stars with metallicities in the high range noted in this upper grouping of panels are identified by a “1” in the third digit of the INOUT parameter.

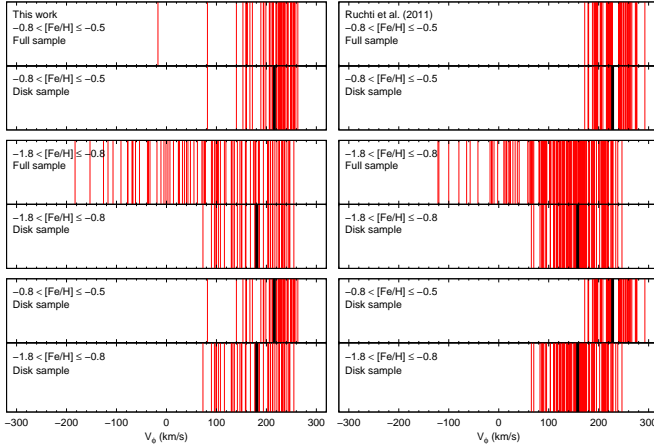


**Figure 13.** Stripe density plots of the orbital rotation velocity,  $V_\phi$ , for stars in the B&M sample (left panels) and the sample of RAVE stars from Ruchti et al. (2011) (right panels). The panels labeled “Disk sample” only include stars that lie below the line drawn in Figure 12, and are expected to be dominated by stars in the disk system. The black vertical lines indicate the mean rotational velocity for each subsample,  $\langle V_\phi \rangle$ . The upper grouping of panels shows the subsets of stars in a metallicity regime ( $-0.8 < [\text{Fe/H}] \leq -0.5$ ) that is expected to be mainly occupied by thick-disk population stars. The middle grouping of panels is the subset of intermediate-metallicity ( $-1.8 < [\text{Fe/H}] \leq -0.8$ ) stars, which are expected to include stars from both the inner-halo population and the MWTD. The lower grouping of panels gathers the stars in the Disk samples together, in order to contrast the difference in the  $V_\phi$  distributions between the canonical thick disk and the MWTD. Stars with errors in any of the individual derived components of motion exceeding  $50 \text{ km s}^{-1}$  are excluded.

The middle grouping of panels are similar plots, but now for stars from each sample with intermediate metal-

licities,  $-1.8 < [\text{Fe/H}] \leq -0.8$ , which corresponds to an interval expected to have a significant contribution of MWTD stars (again with possible overlap from other stellar populations). Once more the top row of plots is the full sample of stars, and the bottom row is the subset in this interval that falls in the disk sample. Stars in the upper panel of this grouping would presumably include members of the “local halo” component proposed by Morrison et al. (2009). Unfortunately, neither the B&M sample nor the Ruchti et al. sample contains a sufficient number of stars to explore this issue in further detail. So here we simply note the possibility of its presence. Stars with metallicities in the intermediate range noted in this grouping of panels are identified by a “2” in the third digit of the INOUT parameter in column (18) of Table 1.

The lower grouping of panels compares the distribution of  $V_\phi$  for the two metallicity intervals considered previously, but only for the stars in the disk samples. We employ a two-sample K-S test to check if the subset of disk stars chosen from the B&M sample and Ruchti et al. samples in the high- and intermediate-metallicity intervals are consistent with selection from the same parent population. Indeed, this test cannot reject the common-parent null hypothesis for either metallicity interval, in spite of the fact that the samples were clearly chosen in different ways. In contrast, it is unsurprising that the same K-S test applied *between* the disk stars in the different metallicity intervals for each of the B&M and Ruchti et al. samples clearly discriminates between their distributions of  $V_\phi$ .

The black vertical lines mark the location of the  $\langle V_\phi \rangle$  for each disk subsample. The means and dispersions of the stars we would associate with the canonical thick-disk population for the B&M sample (the metallicity interval  $-0.8 < [\text{Fe/H}] \leq -0.5$ ) are  $\langle V_\phi \rangle = 216 \text{ km s}^{-1}$ ,  $\sigma_{V_\phi} = 37 \text{ km s}^{-1}$ , while those for the Ruchti et al. sample are  $\langle V_\phi \rangle = 229 \text{ km s}^{-1}$ ,  $\sigma_{V_\phi} = 30 \text{ km s}^{-1}$ . Note that the values we obtain for the mean rotational velocity of the thick-disk population from this crude analysis are somewhat higher, and the velocity dispersions somewhat lower, than those reported by Carollo et al. (2010) ( $\langle V_\phi \rangle = 182 \text{ km s}^{-1}$ ,  $\sigma_{V_\phi} = 51 \text{ km s}^{-1}$ ). It stands to reason that contamination from stars of the thin-disk population in this interval may be at least in part responsible for this result. However, it is also worth noting that Chiba & Beers (2000), and other authors since, have reported that the asymmetric drift of the thick disk exhibits a strong gradient with distance above the Galactic plane, on the order of  $\Delta \langle V_\phi \rangle / \Delta |Z| = 36 \text{ km s}^{-1} \text{ kpc}^{-1}$ , according to Carollo et al. The B&M sample and the Ruchti et al. disk sample are both located very close to the plane, and hence would be expected to be in more rapid rotation. In the case of stars we would associate with a MWTD population (the metallicity interval  $-1.8 < [\text{Fe/H}] \leq -0.8$ ), we obtain  $\langle V_\phi \rangle = 181 \text{ km s}^{-1}$ ,  $\sigma_{V_\phi} = 53 \text{ km s}^{-1}$ , while those for the Ruchti et al. sample are  $\langle V_\phi \rangle = 166 \text{ km s}^{-1}$ ,  $\sigma_{V_\phi} = 47 \text{ km s}^{-1}$ . The rotational velocity of the MWTD in the present analysis is again somewhat higher than reported by Carollo et al., who obtained a mean rotational velocity of this component of  $\langle V_\phi \rangle \sim 100 - 150 \text{ km s}^{-1}$ , with a dispersion in the range 35 to  $45 \text{ km s}^{-1}$ , which is a

little lower than our derived value. Contamination of the B&M and Ruchti et al. samples from metal-poor stars of the inner-halo population is possibly responsible for this result. The difference in the mean rotational velocity might also be accounted for if, as speculated by Carollo et al., the MWTD also exhibits a gradient in its rotational velocity with distance from the plane; future tests with larger samples should prove illuminating.

#### 5.6. Distribution of [C/Fe] for the B&M sample

Figure 14 shows the distribution of carbonicity, [C/Fe], as a function of [Fe/H], for the stars in the B&M sample. The general increase in the level of [C/Fe] with decreasing [Fe/H], as has been seen in numerous previous samples, is evident. There are 12 stars in this sample which are classified as CEMP stars (and tagged as such in Table 1). Their frequency appears to increase with declining [Fe/H], again as noted in previous samples. Based on their metallicities, we expect that the majority of these stars will be classified as CEMP-s, rather than CEMP-no, once high-resolution spectroscopy has been carried out.

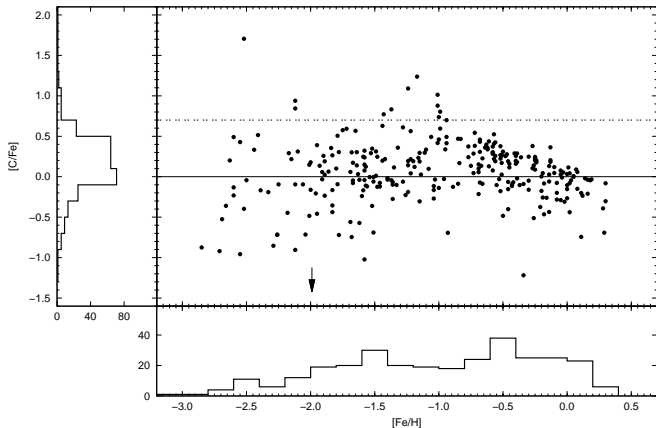


**Figure 14.** Carbonicity, [C/Fe], as a function of the metallicity, [Fe/H], for stars in the B&M sample with available measurements; downward arrows indicate derived upper limits for [C/Fe]. The marginal distributions of each variable are shown as histograms. The horizontal dashed line marks the definition of CEMP stars used in this work,  $[C/Fe] \geq +0.7$ .

#### 6. DISCUSSION AND CONCLUSIONS

As noted in the introduction, a large number of recent papers on the nature, origin, and evolution of the disk (and halo) system of the Milky Way have raised new and important questions concerning issues that were once considered “solved.” In this paper, we have sought to explore what can be learned from a modern analysis of a pioneering dataset, the “weak-metal” sample of Bidelman & MacConnell (1973) studied by Norris, Bessell, & Pickles (1985), Paper I of this series. Many of the ideas and insights from Paper I have spawned research directions that have not yet, even today, been completely explored to their conclusion. Here, we have focused on resolving one of the most important claims from that paper, the suggested existence for what has come to be known as the metal-weak thick disk. As we have shown, the worries raised by a number of authors, subsequent to

the publication of Paper I, were indeed valid. The faulty calibration of a photometric DDO-based metallicity determination led to the production of a false signature in the analysis of Paper I, which may (or may not) have unduly influenced claims for the existence of a MWTD.

The combination of high-quality, high-S/N medium-resolution spectroscopic data with a set of tools capable of producing accurate, and well-tested, estimates of the atmospheric parameters (and carbonicity, [C/Fe]) for the same sample of stars as analysed in Paper I, has allowed us to carry out a new (and expanded) consideration of the presence of stars that might be associated with a MWTD. We also have the advantage that we could make use of much-improved radial velocities and proper motions than were available to the previous study, adding substantially to the size of the dataset suitable for kinematic study, while simultaneously improving the quality of the derived kinematics.

We conclude that the dataset from Paper I does indeed comprise stars that can be associated with a MWTD. A comparison of these data with a similar-size sample from the RAVE survey (and with atmospheric parameters determined from a completely different set of techniques) yields essentially the same conclusion. We note, however, as pointed out by an anonymous referee, that both samples of stars we have considered are impacted by metallicity-selection biases (and in the case of the Ruchti et al. sample, by kinematic-selection bias as well). Thus, the relative numbers of stars present in any given metallicity interval should clearly not be taken as representative of the underlying parent population. We have also not addressed in this paper whether or not a MWTD is indeed best considered a separate component from the rest of the disk system, or whether it is somehow causally linked to the same formation processes (themselves still actively debated) involved with the origin of the thick (and even thin) disks. We leave these issues to future work.

We thank an anonymous referee for remarks which served to improve our manuscript. T.C.B. acknowledges partial support from grant PHY 08-22648; Physics Frontier Center/JINA, awarded by the US National Science Foundation. J.E.N. acknowledges support from Australian Research Council grants DP0663562 and DP0984924. V.M.P. acknowledges support from the Gemini Observatory. S.R. acknowledge partial support from FAPESP, CNPq, and Capes. Y.S.L. is a Tombaugh Fellow.

#### REFERENCES

- Adibekyan, V. Z., Figueira, P., Santos, N. C., et al. 2013, A&A, 554, A44
- Allende Prieto, C., Sivarani, T., Beers, T. C., et al. 2008, AJ, 136, 2070
- Allende Prieto, C., Fernandez-Alvar, E., Schlesinger, K., et al. 2014, A&A, submitted
- An, D., Beers, T.C., Johnson, J.A., et al. 2013, ApJ, 763, 65
- Anthony-Twarog, B. J., & Twarog, B. A. 1994, AJ, 107, 1577
- Aoki, W., Beers, T. C., Lee, Y. S., et al. 2013, AJ, 145, 13
- Arifayto, M. I., Fuchs, B., Jahreiß, H., & Wielen, R. 2005, A&A, 433, 911
- Beers, T. C., Chiba, M., Yoshii, Y., et al. 2000, AJ, 119, 2866
- Beers, T. C., Drilling, J. S., Rossi, S., et al. 2002, AJ, 124, 931

- Beers, T. C., Preston, G. W., & Shectman, S. A. 1985, AJ, 90, 2089  
 —. 1992, AJ, 103, 1987  
 Beers, T. C., Rossi, S., Norris, J. E., Ryan, S. G., & Shefler, T. 1999, AJ, 117, 981  
 Beers, T. C., & Sommer-Larsen, J. 1995, ApJS, 96, 175  
 Beers, T. C., Carollo, D., Ivezić, Ž., et al. 2012, ApJ, 746, 34  
 Bensby, T., Feltzing, S., & Oey, S. 2014, A&A, 562, 71  
 Bidelman, W. P., & MacConnell, D. J. 1973, AJ, 78, 687  
 Boeche, C., Chiappini, C., Minchev, I., et al. 2013a, A&A, 553, 19  
 Boeche, C., Siebert, A., Piffl, T., et al. 2013b, A&A, 559, 59  
 Bovy, J., Rix, H.-W., & Hogg, D. W. 2012a, ApJ, 751, 131  
 Bovy, J., Rix, H.-W., Hogg, D. W., et al. 2012b, ApJ, 755, 115  
 Bovy, J., Rix, H.-W., Liu, C., et al. 2012c, ApJ, 753, 148  
 —. 2012d, ApJ, 753, 148  
 Carney, B. W., Latham, D. W., Laird, J. B., & Aguilar, L. A. 1994, AJ, 107, 2240  
 Carollo, D., Beers, T. C., Lee, Y. S., et al. 2007, Nature, 450, 1020  
 Carollo, D., Beers, T. C., Chiba, M., et al. 2010, ApJ, 712, 692  
 Carollo, D., Beers, T.C., Bovy, J., et. al 2012, ApJ, 744, 195  
 Carollo, D., Freeman, K., Beers, T.C., et. al 2014, ApJ, 788, 180  
 Carré, K., Chen, Y., & Zhao, G. 2012, AJ, 144, 185  
 Cayrel de Strobel, G., Soubiran, C., & Ralite, N. 2001, A&A, 373, 159  
 Cheng, J. Y., Rockosi, C. M., Morrison, H. L., et al. 2012a, ApJ, 752, 51  
 —. 2012b, ApJ, 746, 149  
 Chiba, M., & Beers, T. C. 2000, AJ, 119, 2843  
 Chiba, M., & Yoshii, Y. 1998, AJ, 115, 168  
 Drilling, J. S., & Bergeron, L. E. 1995, PASP, 107, 846  
 Eggen, O. J., Lynden-Bell, D., & Sandage, A. R. 1962, ApJ, 136, 748  
 Eisenstein, D. J., Weinberg, D. H., Agol, E., et al. 2011, AJ, 142, 72  
 ESA. 1997, VizieR Online Data Catalog, 1239, 0  
 Frebel, A. 2010, Astronomische Nachrichten, 331, 474  
 Ghez, A. M., Salim, S., Weinberg, N. N., et al. 2008, ApJ, 689, 1044  
 Gilmore, G. 1984, MNRAS, 207, 223  
 Gilmore, G., Wyse, R. F. G., & Norris, J. E. 2002, ApJ, 574, L39  
 Haywood, M., Di Matteo, P., Lehnert, M. D., Katz, D., & Gómez, A. 2013, A&A, 560, A109  
 Hog, E., Kuzmin, A., Bastian, U., et al. 1998, A&A, 335, L65  
 Högl, E., Fabricius, C., Makarov, V. V., et al. 2000, A&A, 355, L27  
 Jayaraman, A., Gilmore, G., Wyse, R. F. G., Norris, J. E., & Belokurov, V. 2013, MNRAS, 431, 930  
 Kerr, F. J., & Lynden-Bell, D. 1986, MNRAS, 221, 1023  
 Koposov, S. E., Yoo, J., Rix, H.-W., et al. 2009, ApJ, 696, 2179  
 Kordopatis, G., Recio-Blanco, A., de Laverny, P., et al. 2011, A&A, 535, A107  
 Kordopatis, G., Hill, V., Irwin, M., et al. et al. 2013a, A&A, 555, 12  
 Kordopatis, G., Gilmore, G., Wyse, R. F. G., et al. 2013b, MNRAS, 436, 3231  
 Layden, A. C. 1995, AJ, 110, 2288  
 Lee, Y. S., Beers, T. C., Sivarani, T., et al. 2008a, AJ, 136, 2022  
 —. 2008b, AJ, 136, 2050  
 Lee, Y. S., Beers, T. C., Allende Prieto, C., et al. 2011, AJ, 141, 90  
 Lee, Y. S., Beers, T. C., Masseron, T., et al. 2013, AJ, 146, 132  
 Majewski, S. R., Wilson, J. C., Hearty, F., Schiavon, R. R., & Skrutskie, M. F. 2010, in IAU Symposium, Vol. 265, IAU Symposium, ed. K. Cunha, M. Spite, & B. Barbuy, 480  
 Martin, J. C., & Morrison, H. L. 1998, AJ, 116, 1724  
 Mihalas, D., & Binney, J. 1981, Galactic astronomy: Structure and kinematics /2nd edition/, (San Francisco, CA: Freeman)  
 Minchev, I., Chiappini, C., Martig, M., et al. 2014, ApJ, 781, L20  
 Morrison, H. L., Flynn, C., & Freeman, K. C. 1990, AJ, 100, 1191  
 Morrison, H. L., Helmi, A., Sun, J., et al. 2009, ApJ, 694, 130  
 Norris, J. E., Bessell, M. S., & Pickles, A. J. 1985, ApJS, 58, 463 (Paper I)  
 Norris, J. E., Ryan, S. G., & Beers, T. C., 1999, ApJS, 123, 639  
 Pasetto, S., Grebel, E.K., Zwitter, T., et al. 2012, A&A, 547, 70  
 Ruchti, G. R., Fulbright, J. P., Wyse, R. F. G., et al. 2010, ApJ, 721, L92  
 —. 2011, ApJ, 737, 9  
 Ryan, S. G., & Lambert, D. L. 1995, AJ, 109, 2068  
 Schlegel, D. J., Finkbeiner, D. P., & Davis, M. 1998, ApJ, 500, 525  
 Schönrich, R., Asplund, M., & Casagrande, L. 2011, MNRAS, 415, 3807  
 Shortridge, K. 1993, in Astronomical Society of the Pacific Conference Series, Vol. 52, Astronomical Data Analysis Software and Systems II, ed. R. J. Hanisch, R. J. V. Brissenden, & J. Barnes, 219  
 Skrutskie, M. F., Cutri, R. M., Stiening, R., et al. 2006, AJ, 131, 1163  
 Smolinski, J. P., Lee, Y. S., Beers, T. C., et al. 2011, AJ, 141, 89  
 Soubiran, C., Le Campion, J.-F., Cayrel de Strobel, G., & Caillol, A. 2010, A&A, 515, A111  
 Steinmetz, M., Zwitter, T., Siebert, A., et al. 2006, AJ, 132, 1645  
 Suda, T., Katsuta, Y., Yamada, S., et al. 2008, PASJ, 60, 1159  
 van Leeuwen, F. 2007, A&A, 474, 653  
 Villalobos, Á., & Helmi, A. 2009, MNRAS, 399, 166  
 Yanny, B., Rockosi, C., Newberg, H. J., et al. 2009, AJ, 137, 4377  
 York, D. G., Adelman, J., Anderson, Jr., J. E., et al. 2000, AJ, 120, 1579

**Table 1**  
Photometric Information and Adopted Reddening

BM Name (1)	Star Name (2)	LON ( $^{\circ}$ ) (3)	LAT ( $^{\circ}$ ) (4)	V (mag) (5)	B – V (mag) (6)	J (mag) (7)	J – K (mag) (8)	E(B – V) <sub>S</sub> (mag) (9)	E(B – V) <sub>A</sub> (mag) (10)	E(B – V) <sub>F</sub> (mag) (11)
BM-001	HD 702	94.3	-69.0	9.81	0.51	8.767	0.308	0.034	0.03	0.02
BM-002	HD 2796	97.6	-78.7	8.49	0.74	6.853	0.597	0.020	0.02	0.01
BM-003	HD 3567	113.1	-70.9	9.26	0.46	8.218	0.329	0.036	0.04	0.02
BM-004	HD 3715	110.5	-76.9	9.46	0.45	8.523	0.254	0.020	0.02	0.01
BM-005	HD 4306	118.1	-72.4	9.01	0.74	7.424	0.601	0.036	0.04	0.04
BM-006	HD 6461	136.6	-75.4	7.64	0.79	6.149	0.562	0.025	0.03	0.01
BM-007	HD 7041	297.8	-60.6	9.02	0.80	7.459	0.558	0.021	0.02	0.01
BM-008	BD-11:220	138.6	-72.7	9.19	0.58	8.083	0.365	0.030	0.03	0.01
BM-009	HD 7983	143.9	-70.7	8.90	0.60	7.718	0.364	0.035	0.04	0.01
BM-010	HD 7985	151.9	-76.1	9.46	0.43	8.563	0.300	0.017	0.02	0.01
BM-011	HD 11038	195.1	-76.2	9.45	0.54	8.417	0.339	0.010	0.01	0.01
BM-012	BD-10:388	163.8	-67.4	10.34	0.44	9.317	0.320	0.023	0.02	0.01
BM-013	HD 11569	296.6	-44.5	9.02	0.37	8.203	0.229	0.035	0.04	0.02
BM-014	HD 11582	245.2	-75.0	9.57	0.66	8.124	0.472	0.015	0.01	0.01
BM-015	BD-14:363	175.8	-70.0	9.66	0.65	8.395	0.423	0.015	0.01	0.00
BM-016	HD 13359	197.7	-71.0	9.70	0.71	8.274	0.462	0.015	0.01	0.01
BM-017	HD 13889	259.0	-67.7	9.57	0.55	8.398	0.365	0.015	0.01	0.00
BM-018	HD 14229	280.4	-57.8	9.52	0.46	8.518	0.290	0.034	0.03	0.02
BM-019	HD 15395	277.1	-57.5	9.44	0.56	8.269	0.346	0.026	0.03	0.01
BM-021	BD-17:484	194.4	-64.8	10.47	0.44	9.464	0.328	0.026	0.03	0.02
BM-022	HD 16031	186.5	-61.8	9.77	0.44	8.790	0.333	0.022	0.02	0.01
BM-023	BD-10:514	182.0	-59.8	10.13	0.62	8.953	0.435	0.026	0.03	0.02
BM-024	CD-50:776	267.4	-59.6	10.11	0.77	8.595	0.496	0.027	0.03	0.03
BM-025	HD 17020	298.5	-34.7	9.17	0.54	8.150	0.382	0.091	0.09	0.03
BM-026	HD 17233	274.2	-55.6	9.04	0.79	7.547	0.499	0.036	0.04	0.02
BM-028	CD-36:1052	240.2	-63.8	9.94	0.46	8.849	0.337	0.023	0.02	0.00
BM-029	HD 18710	262.9	-57.3	9.66	0.90	8.033	0.595	0.021	0.02	0.02
BM-030	HD 20038	275.5	-50.2	8.90	0.85	7.332	0.552	0.020	0.02	0.01
BM-032	BD-04:571	187.0	-47.7	9.57	0.45	8.638	0.236	0.036	0.04	0.02
BM-033	HD 21022	232.5	-57.0	9.19	0.95	7.330	0.699	0.014	0.01	0.01
BM-034	HD 21581	184.3	-43.7	8.71	0.82	6.975	0.561	0.103	0.10	0.05
BM-035	CD-24:1782	217.8	-52.3	9.91	0.63	8.497	0.538	0.019	0.02	0.02
BM-036	HD 22879	189.8	-43.1	6.70	0.54	5.588	0.409	0.066	0.07	0.01
BM-037	HD 23332	268.0	-48.3	8.91	0.90	7.241	0.607	0.025	0.03	0.02
BM-038	HD 23592	262.7	-49.4	9.47	0.86	7.831	0.556	0.014	0.01	0.01
BM-039	HD 23798	229.2	-51.7	8.31	1.09	6.276	0.759	0.008	0.01	0.01
BM-040	HD 26169	289.8	-36.3	8.85	0.74	7.172	0.538	0.077	0.08	0.05
BM-041	HD 26297	209.7	-43.0	7.47	1.11	5.379	0.748	0.032	0.03	0.01
BM-042	HD 26298	210.3	-43.2	8.16	0.36	7.382	0.171	0.028	0.03	0.02
BM-043	BD+06:648	185.9	-30.7	9.10	1.29	6.562	0.764	0.265	0.21	0.00
BM-044	HD 27928	239.7	-44.7	9.56	0.71	7.986	0.538	0.031	0.03	0.02
BM-045	HD 29574	210.3	-35.4	8.34	1.41	5.726	0.886	0.201	0.17	0.00
BM-046	CP-57:680	267.0	-40.5	9.26	0.91	7.588	0.631	0.009	0.01	0.01
BM-047	BD-13:959N	210.7	-34.5	...	...	9.772	0.410	0.254	0.20	0.00
BM-048	HD 30229	276.4	-37.9	9.40	0.66	7.940	0.516	0.047	0.05	0.04
BM-049	BD-09:978	207.0	-32.1	9.31	0.92	7.664	0.551	0.057	0.06	0.03
BM-050	BD-22:926	221.7	-36.1	10.37	0.43	9.418	0.284	0.045	0.04	0.00
BM-051	HD 31128	227.7	-37.0	9.14	0.49	8.032	0.294	0.037	0.04	0.01
BM-052	CP-62:394	272.2	-37.6	10.13	0.84	8.344	0.594	0.028	0.03	0.03
BM-053	HD 33073	230.4	-34.3	9.52	0.69	8.010	0.484	0.013	0.01	0.01
BM-054	HD 268957	281.3	-34.6	9.79	0.48	8.603	0.312	0.175	0.15	0.00
BM-055	CD-53:1089	260.3	-37.1	10.55	0.48	9.634	0.274	0.012	0.01	0.01
BM-056	HD 33771	241.7	-35.3	9.50	0.86	7.663	0.642	0.030	0.03	0.02
BM-057	CP-57:752	266.1	-36.1	9.82	0.87	8.202	0.585	0.016	0.02	0.01
BM-058	HD 34048	272.3	-35.4	9.98	0.55	8.722	0.403	0.024	0.02	0.02
BM-059	HD 34328	268.6	-35.5	9.43	0.48	8.316	0.318	0.026	0.03	0.01
BM-060	CD-48:1741	255.3	-35.1	10.69	0.50	9.514	0.419	0.027	0.03	0.01
BM-061	HD 35179	216.4	-26.1	9.48	0.98	7.715	0.616	0.095	0.10	0.05
BM-062	HD 35416	235.2	-31.6	7.53	0.39	6.689	0.280	0.012	0.01	0.00
BM-063	HD 36702	243.4	-31.4	8.37	1.21	6.126	0.797	0.028	0.03	0.01
BM-064	HD 274939	254.4	-32.5	9.43	0.72	7.856	0.557	0.031	0.03	0.02
BM-065	HD 274681	251.2	-31.8	10.07	0.56	9.412	0.331	0.037	0.04	0.01
BM-067	HD 37828	215.2	-20.7	6.88	1.13	4.889	0.825	0.219	0.18	0.00
BM-068	HD 38043	274.6	-32.1	9.43	0.26	8.853	0.216	0.062	0.06	0.05
BM-069	HD 38510	231.6	-25.7	8.22	0.53	7.114	0.372	0.030	0.03	0.00
BM-070	HD 38893	274.7	-31.5	9.48	0.72	8.024	0.534	0.068	0.07	0.03
BM-071	HD 40259	204.9	-10.9	7.86	0.38	7.062	0.193	1.115	0.76	0.00

**Table 1** — *Continued*

BM Name (1)	Star Name (2)	LON ( $^{\circ}$ ) (3)	LAT ( $^{\circ}$ ) (4)	$V$ (mag) (5)	$B - V$ (mag) (6)	$J$ (mag) (7)	$J - K$ (mag) (8)	$E(B - V)_S$ (mag) (9)	$E(B - V)_A$ (mag) (10)	$E(B - V)_F$ (mag) (11)
BM-072	HD 40361	252.8	-28.4	9.04	0.98	7.268	0.587	0.047	0.05	0.02
BM-073	BD+04:1107	203.7	-8.9	10.05	0.60	8.947	0.367	0.570	0.41	0.00
BM-074	HD 41406	226.8	-19.4	8.69	0.48	7.775	0.243	0.058	0.06	0.01
BM-075	HD 43592	222.7	-14.4	10.04	0.47	9.066	0.282	0.227	0.18	0.00
BM-076	HD 43641	290.6	-28.8	9.92	0.55	8.795	0.309	0.127	0.12	0.00
BM-077	HD 44007	222.7	-13.8	8.06	0.84	6.340	0.637	0.223	0.18	0.00
BM-078	HD 44165	286.1	-28.7	7.34	0.96	5.610	0.626	0.122	0.11	0.00
BM-079	BD-19:1422	227.1	-15.1	9.67	0.81	7.950	0.572	0.114	0.11	0.00
BM-080	HD 44517	214.5	-9.0	7.95	0.54	6.917	0.329	0.388	0.29	0.00
BM-081	HD 45282	207.1	-3.9	8.02	0.67	6.591	0.502	0.806	0.56	0.00
BM-082	HD 45610	240.2	-18.8	7.19	0.81	5.548	0.634	0.048	0.05	0.01
BM-083	HD 47147	253.9	-21.7	9.20	0.41	8.105	0.326	0.049	0.05	0.04
BM-084	CD-33:3169	242.8	-16.3	9.84	0.45	8.947	0.241	0.088	0.09	0.03
BM-085	BD+07:1444	205.8	+2.2	9.68	0.78	8.270	0.558	0.639	0.45	0.00
BM-086	CD-33:3337	243.9	-14.0	9.08	0.47	8.007	0.341	0.198	0.16	0.00
BM-087	BD+00:1804	214.3	+3.6	9.59	0.42	8.690	0.233	0.356	0.27	0.00
BM-088	HD 54759	210.3	+6.6	9.37	0.48	8.350	0.301	0.201	0.17	0.00
BM-089	HD 59392	250.8	-9.7	9.70	0.47	8.633	0.295	0.386	0.29	0.00
BM-090	HD 60370	246.8	-6.6	9.19	0.48	8.285	0.306	0.418	0.31	0.00
BM-091	HD 60552	230.2	+3.0	6.70	0.47	5.791	0.286	0.384	0.28	0.00
BM-092	HD 61383	223.3	+8.0	7.57	0.61	6.371	0.403	0.131	0.12	0.00
BM-093	HD 61632	229.6	+4.8	8.29	0.64	7.024	0.392	0.292	0.22	0.00
BM-095	HD 63066	223.8	+10.0	9.09	0.66	7.840	0.406	0.165	0.14	0.00
BM-096	BD-18:2065	236.4	+4.4	9.62	0.96	7.878	0.612	0.332	0.25	0.00
BM-097	HD 66015	238.2	+5.7	8.39	0.44	7.471	0.302	0.177	0.15	0.00
BM-099	CD-44:4311	262.0	-4.9	9.76	0.99	7.878	0.685	0.921	0.63	0.00
BM-100	BD-20:2583	243.3	+11.1	10.00	0.65	8.580	0.433	0.083	0.08	0.06
BM-101	HD 74000	240.8	+15.3	9.69	0.43	8.716	0.326	0.051	0.05	0.01
BM-102	HD 74205	248.7	+10.0	9.20	0.42	8.393	0.191	0.122	0.11	0.00
BM-103	BD-12:2669	239.1	+18.2	10.24	0.30	9.489	0.190	0.065	0.07	0.03
BM-104	HD 78737	253.7	+13.9	8.93	0.41	8.016	0.280	0.130	0.12	0.00
BM-105	HD 78747	271.1	-1.9	7.71	0.57	6.542	0.363	3.421	2.26	0.00
BM-106	HD 81223	285.2	-12.8	8.41	0.98	6.516	0.684	0.140	0.13	0.00
BM-107	HD 81290	271.8	+0.8	8.89	0.33	8.037	0.216	2.600	1.73	0.00
BM-108	HD 81517	271.7	+1.2	8.98	0.50	8.010	0.311	2.844	1.88	0.00
BM-109	HD 81713	251.5	+21.2	8.91	0.95	7.142	0.619	0.055	0.06	0.02
BM-110	CD-36:5714	264.5	+9.8	9.91	0.66	8.406	0.512	0.186	0.16	0.00
BM-111	HD 82590	249.9	+24.3	9.43	0.47	8.300	0.358	0.061	0.06	0.05
BM-112	CD-72:544	289.5	-15.7	9.21	0.48	8.266	0.230	0.213	0.17	0.00
BM-113	HD 83201	275.1	+0.0	8.87	0.54	7.787	0.281	2.082	1.39	0.00
BM-114	HD 83212	253.3	+22.7	8.35	1.09	6.307	0.698	0.057	0.06	0.02
BM-115	HD 83220	273.3	+2.1	8.55	0.40	7.638	0.279	1.321	0.89	0.00
BM-117	HD 83277	258.8	+17.7	8.31	0.31	7.531	0.230	0.096	0.10	0.05
BM-118	HD 84326	276.1	+0.7	9.28	0.55	8.189	0.310	1.868	1.25	0.00
BM-119	HD 84612	274.7	+2.9	8.04	0.52	7.143	0.292	0.705	0.49	0.00
BM-120	HD 84903	269.8	+9.3	8.01	1.17	5.656	0.774	0.522	0.37	0.00
BM-121	CD-22:7696	257.9	+24.1	9.39	1.16	7.230	0.725	0.046	0.05	0.03
BM-122	CD-24:8642	260.5	+23.5	9.66	0.83	8.050	0.559	0.058	0.06	0.03
BM-123	HD 86847	276.7	+4.3	9.00	0.45	8.041	0.277	0.467	0.34	0.00
BM-125	HD 88554	277.8	+6.0	9.32	0.33	8.536	0.221	0.226	0.18	0.00
BM-126	CD-44:6435	277.5	+9.9	9.32	0.44	8.385	0.267	0.182	0.15	0.00
BM-127	HD 90175	280.2	+5.9	7.90	0.50	6.933	0.309	0.331	0.25	0.00
BM-128	HD 90676	282.4	+3.4	9.19	0.49	8.308	0.214	0.500	0.36	0.00
BM-129	HD 90948	289.7	-8.3	8.34	0.56	7.279	0.334	0.245	0.19	0.00
BM-130	HD 91345	292.2	-11.7	9.03	0.56	7.877	0.359	0.130	0.12	0.00
BM-131	HD 91540	292.3	-11.6	9.34	0.58	8.314	0.315	0.130	0.12	0.00
BM-132	HD 92368	285.0	+2.4	9.25	0.48	8.309	0.254	1.303	0.88	0.00
BM-133	CD-30:8626	272.4	+24.3	9.69	0.77	8.087	0.536	0.064	0.06	0.03
BM-134	HD 93529	270.6	+29.6	9.30	0.89	7.503	0.630	0.079	0.08	0.04
BM-135	CD-35:6811	278.0	+20.4	10.14	0.50	9.094	0.289	0.060	0.06	0.02
BM-136	CD-35:6934	279.6	+21.7	10.28	0.60	9.011	0.417	0.091	0.09	0.04
BM-138	HD 97320	292.7	-4.6	8.16	0.48	7.137	0.347	0.874	0.60	0.00
BM-139	HD 99383	285.2	+21.0	9.08	0.47	8.025	0.381	0.083	0.08	0.01
BM-140	HD 99682	291.3	+5.1	8.67	0.51	7.667	0.310	0.680	0.48	0.00
BM-141	HD 99978	291.6	+5.2	8.65	0.97	6.837	0.651	0.456	0.33	0.00
BM-142	HD 100906	279.5	+40.5	9.68	0.84	8.031	0.538	0.044	0.04	0.02
BM-143	HD 100980	287.6	+21.2	8.73	0.44	7.746	0.312	0.117	0.11	0.00
BM-144	HD 101063	284.0	+31.3	9.46	0.75	7.882	0.510	0.063	0.06	0.03

**Table 1** — *Continued*

BM Name (1)	Star Name (2)	LON (°) (3)	LAT (°) (4)	V (mag) (5)	B – V (mag) (6)	J (mag) (7)	J – K (mag) (8)	E(B – V) <sub>S</sub> (mag) (9)	E(B – V) <sub>A</sub> (mag) (10)	E(B – V) <sub>F</sub> (mag) (11)
BM-146	HD 102200	291.2	+15.3	8.76	0.46	7.688	0.305	0.101	0.10	0.02
BM-147	CP-70:1436	298.0	-8.5	9.34	0.91	7.275	0.698	0.323	0.24	0.00
BM-148	HD 103295	287.9	+32.5	9.60	0.81	7.945	0.571	0.080	0.08	0.04
BM-149	CD-35:7576	291.1	+25.4	10.11	0.53	8.908	0.383	0.085	0.09	0.08
BM-150	HD 104059	293.0	+18.2	9.10	0.36	8.333	0.209	0.108	0.11	0.00
BM-151	HD 104222	287.1	+40.6	10.37	0.58	9.205	0.393	0.049	0.05	0.02
BM-152	CD-26:8918	289.4	+34.3	11.02	0.48	9.933	0.312	0.074	0.07	0.06
BM-153	HD 104893	290.8	+32.6	9.21	1.23	7.001	0.744	0.064	0.06	0.04
BM-155	CD-37:7677	293.7	+23.4	9.94	0.86	8.138	0.652	0.065	0.07	0.04
BM-157	HD 106411	296.0	+18.3	9.26	0.57	8.100	0.359	0.111	0.11	0.00
BM-158	CD-28:9374	293.4	+32.6	10.25	0.81	8.652	0.536	0.054	0.05	0.03
BM-159	HD 106670	297.1	+12.6	8.86	0.84	7.221	0.557	0.169	0.14	0.00
BM-160	HD 107885	299.3	+4.8	7.73	0.56	6.699	0.376	0.788	0.55	0.00
BM-161	HD 108405	298.8	+14.6	9.27	0.58	8.051	0.413	0.117	0.11	0.00
BM-164	HD 109801	301.6	-3.0	8.44	0.38	...	...	0.928	0.64	0.00
BM-165	CD-27:8817	300.6	+34.7	10.44	0.44	9.524	0.278	0.090	0.09	0.09
BM-166	HD 110621	301.5	+18.2	9.91	0.46	8.852	0.286	0.098	0.10	0.02
BM-167	HD 111289	302.6	+6.0	8.62	0.45	7.665	0.248	0.670	0.47	0.00
BM-168	CD-45:8032	302.5	+16.7	9.70	0.48	8.729	0.284	0.093	0.09	0.02
BM-169	HD 111503	302.7	+16.7	9.52	0.50	8.519	0.312	0.093	0.09	0.06
BM-170	HD 111721	302.9	+49.4	7.97	0.79	6.347	0.561	0.053	0.05	0.02
BM-171	HD 111971	303.2	+5.2	8.00	0.53	6.949	0.323	0.616	0.44	0.00
BM-172	HD 111980	303.5	+44.4	8.36	0.54	7.176	0.408	0.053	0.05	0.01
BM-173	BD-20:3741	304.1	+41.5	10.64	0.50	9.662	0.308	0.075	0.07	0.07
BM-174	HD 113083	305.7	+35.4	8.05	0.54	6.964	0.388	0.080	0.08	0.02
BM-175	HD 113153	304.0	-6.0	8.55	0.54	7.527	0.293	0.313	0.24	0.00
BM-176	CD-23:10879	306.4	+38.4	9.95	0.50	8.958	0.289	0.143	0.13	0.00
BM-177	HD 114649	306.1	+8.8	8.50	0.51	7.527	0.327	0.608	0.43	0.00
BM-178	CD-28:9945	308.5	+33.0	9.87	0.88	8.296	0.565	0.059	0.06	0.03
BM-179	HD 115772	308.9	+22.6	9.64	0.84	8.090	0.501	0.102	0.10	0.04
BM-180	HD 116064	309.3	+23.2	8.79	0.47	7.698	0.392	0.072	0.07	0.01
BM-181	HD 117220	311.2	+24.7	9.00	0.84	7.386	0.584	0.064	0.06	0.02
BM-182	HD 118055	317.8	+45.3	8.86	1.29	6.573	0.849	0.092	0.09	0.05
BM-183	CD-33:9314	315.7	+27.6	9.95	0.80	8.319	0.529	0.052	0.05	0.03
BM-185	HD 120797	311.4	+5.2	9.05	0.53	8.012	0.306	0.542	0.39	0.00
BM-186	HD 121261	317.1	+25.0	9.22	1.25	6.983	0.797	0.073	0.07	0.03
BM-187	HD 121387	308.0	-10.1	8.60	0.43	7.695	0.264	0.329	0.25	0.00
BM-188	HD 122196	317.7	+22.8	8.73	0.46	7.629	0.354	0.089	0.09	0.02
BM-189	HD 122232	312.7	+5.4	9.20	0.46	8.277	0.293	0.472	0.34	0.00
BM-190	HD 122956	328.3	+44.4	7.22	1.01	5.230	0.667	0.083	0.08	0.03
BM-191	HD 124358	332.4	+46.0	9.45	0.93	7.643	0.639	0.065	0.07	0.05
BM-192	HD 124879	312.6	-1.8	8.38	0.48	7.398	0.245	2.588	1.72	0.00
BM-193	HD 125764	317.0	+8.6	9.62	0.49	8.590	0.341	0.372	0.28	0.00
BM-194	BD+01:2916	346.1	+55.9	9.61	1.35	7.273	0.801	0.030	0.03	0.02
BM-195	HD 126238	320.4	+16.0	7.66	0.81	5.975	0.637	0.124	0.12	0.00
BM-196	HD 126587	330.4	+35.5	9.12	0.83	7.258	0.590	0.099	0.10	0.08
BM-197	HD 126842	314.7	-0.2	9.00	0.42	8.156	0.226	13.879	9.06	0.00
BM-198	HD 127537	312.2	-7.7	8.54	0.43	7.670	0.282	0.352	0.26	0.00
BM-199	HD 128188	339.7	+43.9	9.98	1.01	8.089	0.705	0.113	0.11	0.00
BM-200	HD 128204	331.1	+32.0	9.99	0.48	8.984	0.301	0.088	0.09	0.08
BM-201	HD 128279	329.1	+28.4	8.02	0.64	6.568	0.503	0.099	0.10	0.03
BM-202	HD 128636	319.0	+6.5	8.31	0.48	7.250	0.326	0.595	0.42	0.00
BM-203	HD 128959	331.2	+30.1	9.20	0.60	7.981	0.409	0.101	0.10	0.04
BM-204	HD 129055	323.1	+14.6	8.78	0.46	7.823	0.286	0.127	0.12	0.00
BM-205	HD 129546	328.1	+23.1	10.09	0.44	9.158	0.288	0.076	0.08	0.03
BM-206	HD 130551	317.0	-1.4	7.15	0.45	6.202	0.286	2.354	1.57	0.00
BM-207	HD 131299	321.7	+6.9	8.82	0.61	7.663	0.368	0.681	0.48	0.00
BM-208	HD 132475	338.4	+31.9	8.55	0.55	7.327	0.415	0.108	0.11	0.00
BM-209	BD-11:3853	345.5	+39.5	10.14	0.52	9.089	0.356	0.074	0.07	0.03
BM-210	HD 132686	332.3	+22.7	9.24	0.41	8.423	0.200	0.163	0.14	0.00
BM-211	HD 133119	322.1	+4.5	9.22	0.67	7.986	0.373	0.813	0.56	0.00
BM-212	BD-08:3901	349.6	+41.7	9.47	0.91	7.627	0.634	0.084	0.08	0.05
BM-213	HD 135449	335.0	+20.8	9.37	0.44	8.383	0.232	0.321	0.24	0.00
BM-214	HD 137502	325.1	+2.5	8.77	0.48	7.809	0.302	1.720	1.15	0.00
BM-215	CD-33:10593	337.6	+17.8	9.56	0.50	8.515	0.339	0.464	0.34	0.00
BM-216	HD 139497	347.2	+26.9	9.64	0.56	8.381	0.355	0.171	0.15	0.00
BM-217	HD 140283	356.3	+33.6	7.21	0.49	6.014	0.426	0.161	0.14	0.00
BM-218	HD 140681	324.7	-2.6	8.93	0.65	7.678	0.396	0.705	0.49	0.00

**Table 1** — *Continued*

BM Name (1)	Star Name (2)	LON ( $^{\circ}$ ) (3)	LAT ( $^{\circ}$ ) (4)	$V$ (mag) (5)	$B - V$ (mag) (6)	$J$ (mag) (7)	$J - K$ (mag) (8)	$E(B - V)_S$ (mag) (9)	$E(B - V)_A$ (mag) (10)	$E(B - V)_F$ (mag) (11)
BM-219	HD 141107	343.5	+19.8	7.68	0.41	6.759	0.265	0.186	0.16	0.00
BM-220	HD 141702	334.8	+8.8	8.10	0.53	7.076	0.339	0.388	0.29	0.00
BM-221	CD-31:12353	341.9	+16.8	10.11	0.87	8.369	0.537	0.144	0.13	0.00
BM-222	HD 141864	313.1	-17.6	9.00	0.67	7.514	0.467	0.061	0.06	0.02
BM-223	HD 142081	328.4	+0.4	8.57	0.47	7.608	0.270	22.681	14.78	0.00
BM-224	HD 142948	328.6	-0.6	8.00	0.98	6.139	0.626	8.565	5.60	0.00
BM-225	HD 145293	359.3	+26.9	10.00	0.67	8.502	0.427	0.236	0.19	0.00
BM-226	HD 149130	325.8	-10.3	8.47	0.34	7.729	0.189	0.195	0.16	0.00
BM-227	HD 149153	342.2	+4.9	9.23	0.60	8.147	0.336	1.329	0.90	0.00
BM-228	HD 150419	348.9	+8.8	9.04	0.63	7.869	0.355	0.492	0.35	0.00
BM-229	HD 150875	14.6	+26.6	8.29	0.58	7.017	0.359	0.245	0.19	0.00
BM-230	HD 152924	326.0	-13.5	7.96	0.46	7.035	0.295	0.140	0.13	0.00
BM-231	HD 156954	10.4	+13.3	7.68	0.29	7.010	0.151	0.439	0.32	0.00
BM-232	HD 159370	22.8	+16.5	9.56	0.53	...	...	0.221	0.18	0.00
BM-233	HD 160617	350.0	-5.5	8.73	0.45	7.628	0.317	0.522	0.37	0.00
BM-234	CP-71:2179	322.2	-20.9	8.50	0.42	7.705	0.224	0.067	0.07	0.01
BM-235	CD-68:1881	324.6	-20.2	9.48	1.05	7.537	0.657	0.077	0.08	0.03
BM-236	HD 161770	16.9	+9.5	9.60	0.67	8.099	0.432	0.939	0.65	0.00
BM-237	HD 161986	355.0	-4.2	8.67	0.47	7.795	0.295	0.692	0.48	0.00
BM-238	HD 162541	359.4	-2.2	9.64	0.46	8.635	0.262	1.603	1.08	0.00
BM-239	HD 162892	351.8	-7.1	9.02	0.49	8.163	0.251	0.294	0.23	0.00
BM-240	HD 166161	20.3	+5.2	8.09	0.98	5.998	0.654	1.412	0.95	0.00
BM-241	HD 166913	335.1	-18.9	8.20	0.45	7.200	0.280	0.118	0.11	0.00
BM-242	HD 167300	332.6	-20.1	9.15	0.60	8.013	0.385	0.068	0.07	0.01
BM-243	HD 168220	340.4	-17.6	8.85	1.09	6.987	0.651	0.104	0.10	0.03
BM-244	HD 171496	9.4	-7.7	8.44	1.10	6.294	0.700	0.376	0.28	0.00
BM-245	HD 174578	10.2	-11.4	9.47	1.24	7.031	0.755	0.378	0.28	0.00
BM-246	HD 175606	345.1	-22.0	9.78	0.44	8.709	0.323	0.063	0.06	0.02
BM-247	HD 176203	13.0	-12.1	8.77	0.74	7.203	0.491	0.200	0.17	0.00
BM-248	HD 176609	18.5	-10.1	8.04	0.45	7.100	0.243	0.257	0.20	0.00
BM-249	HD 177088	32.0	-3.8	9.85	0.81	7.963	0.413	0.772	0.54	0.00
BM-251	HD 178443	354.2	-21.5	9.98	0.72	8.414	0.503	0.090	0.09	0.05
BM-252	HD 181007	17.4	-15.1	9.58	0.82	7.855	0.550	0.115	0.11	0.00
BM-253	HD 181743	353.0	-24.3	9.66	0.46	8.624	0.350	0.091	0.09	0.03
BM-254	HD 182163	325.2	-28.6	8.76	0.41	7.908	0.217	0.074	0.07	0.03
BM-255	HD 184266	22.8	-16.7	7.60	0.58	6.252	0.422	0.141	0.13	0.00
BM-257	HD 184711	359.4	-25.3	7.98	1.33	5.513	0.805	0.156	0.14	0.00
BM-258	HD 186478	22.8	-19.5	9.15	0.97	7.117	0.674	0.125	0.12	0.00
BM-259	HD 186784	336.0	-30.5	8.01	0.50	7.035	0.247	0.075	0.07	0.02
BM-260	HD 187111	28.3	-18.1	7.72	1.23	5.366	0.816	0.186	0.16	0.00
BM-261	HD 188031	357.1	-29.2	10.17	0.44	9.163	0.306	0.074	0.07	0.03
BM-262	HD 188178	18.6	-23.5	9.83	0.56	8.632	0.347	0.137	0.12	0.00
BM-264	BD-18:5550	23.4	-22.8	9.25	0.92	7.202	0.647	0.190	0.16	0.00
BM-265	HD 190178	13.5	-27.6	9.50	0.52	8.416	0.342	0.103	0.10	0.03
BM-266	HD 190287	6.3	-29.6	8.53	0.75	6.970	0.529	0.115	0.11	0.00
BM-267	HD 190984	331.6	-32.9	8.75	0.54	7.671	0.352	0.055	0.06	0.01
BM-268	HD 192718	36.0	-22.3	8.38	0.57	7.237	0.351	0.068	0.07	0.01
BM-269	HD 193242	23.7	-28.1	9.16	0.78	7.468	0.579	0.077	0.08	0.04
BM-270	BD-22:5393	21.3	-28.9	10.08	0.64	8.785	0.418	0.080	0.08	0.02
BM-271	HD 193565	22.2	-28.9	7.77	0.41	6.869	0.274	0.061	0.06	0.02
BM-272	HD 194702	342.9	-35.8	9.45	0.39	8.656	0.214	0.050	0.05	0.03
BM-273	CD-45:13852	354.7	-35.9	10.28	0.51	8.620	0.482	0.034	0.03	0.01
BM-274	CD-23:16310	20.8	-31.9	10.37	0.85	8.620	0.586	0.059	0.06	0.06
BM-276	HD 196892	26.9	-32.3	8.25	0.49	7.182	0.358	0.044	0.04	0.01
BM-277	HD 197031	0.3	-37.8	10.21	0.58	9.062	0.306	0.037	0.04	0.02
BM-279	BD-20:6008	25.8	-33.1	9.84	0.87	8.023	0.627	0.042	0.04	0.04
BM-280	CD-30:18140	14.2	-36.3	9.91	0.43	8.955	0.300	0.073	0.07	0.03
BM-281	CD-48:13714	351.4	-40.0	10.68	0.51	9.635	0.344	0.031	0.03	0.02
BM-282	HD 199370	6.8	-40.3	9.83	0.45	8.893	0.296	0.075	0.07	0.04
BM-284	HD 199854	33.1	-35.2	8.91	0.42	7.855	0.318	0.046	0.05	0.04
BM-285	CD-62:1346	333.8	-39.5	9.81	0.73	8.500	0.491	0.036	0.04	0.03
BM-286	HD 200654	348.8	-41.9	9.08	0.64	7.648	0.494	0.028	0.03	0.02
BM-287	HD 201019	341.7	-41.4	8.35	0.34	7.621	0.259	0.035	0.04	0.03
BM-288	HD 201187	357.1	-42.8	9.72	0.42	8.875	0.278	0.032	0.03	0.02
BM-289	HD 205156	348.0	-46.4	8.11	0.63	6.955	0.438	0.022	0.02	0.00
BM-290	HD 205547	1.2	-48.0	8.60	1.26	6.450	0.793	0.025	0.03	0.02
BM-291	HD 206178	27.8	-46.8	9.78	0.46	8.873	0.299	0.051	0.05	0.03
BM-292	CD-34:15270	11.6	-50.5	10.16	0.41	9.388	0.263	0.028	0.03	0.03

**Table 1** — *Continued*

BM Name (1)	Star Name (2)	LON ( $^{\circ}$ ) (3)	LAT ( $^{\circ}$ ) (4)	$V$ (mag) (5)	$B - V$ (mag) (6)	$J$ (mag) (7)	$J - K$ (mag) (8)	$E(B - V)_S$ (mag) (9)	$E(B - V)_A$ (mag) (10)	$E(B - V)_F$ (mag) (11)
BM-293	HD 207692	28.1	-49.3	7.04	0.47	5.884	0.301	0.038	0.04	0.01
BM-294	HD 208061	349.8	-50.1	9.68	0.48	8.675	0.341	0.021	0.02	0.01
BM-295	HD 208069	17.5	-51.3	9.21	0.71	7.756	0.515	0.025	0.03	0.02
BM-297	HD 208360	346.7	-49.9	7.70	0.71	6.222	0.492	0.025	0.03	0.01
BM-298	HD 208603	354.2	-51.4	8.28	0.40	7.547	0.243	0.013	0.01	0.00
BM-299	HD 209068	26.9	-51.8	10.01	0.39	9.121	0.241	0.035	0.04	0.03
BM-300	HD 209083	8.2	-53.0	8.87	0.38	8.084	0.217	0.017	0.02	0.01
BM-301	HD 210295	44.4	-50.0	9.56	0.91	7.839	0.656	0.039	0.04	0.03
BM-302	HD 211236	30.9	-54.7	7.44	0.24	6.941	0.102	0.025	0.03	0.02
BM-303	HD 211744	353.2	-55.2	9.12	0.76	7.642	0.525	0.018	0.02	0.01
BM-304	HD 212038	342.6	-53.3	8.74	0.84	7.080	0.570	0.016	0.02	0.00
BM-305	HD 213467	16.9	-59.4	8.50	0.73	7.041	0.562	0.014	0.01	0.01
BM-306	HD 213487	35.1	-57.9	9.85	0.84	8.265	0.570	0.035	0.04	0.03
BM-307	HD 213657	355.9	-58.3	9.65	0.42	8.672	0.326	0.013	0.01	0.01
BM-308	HD 214161	358.4	-59.3	9.11	0.79	7.462	0.608	0.017	0.02	0.02
BM-309	HD 214164	328.2	-50.0	8.69	0.43	7.806	0.284	0.022	0.02	0.01
BM-310	HD 214362	33.9	-59.5	9.09	0.50	7.924	0.389	0.026	0.03	0.03
BM-311	HD 214925	38.0	-59.8	9.28	1.52	6.757	0.849	0.028	0.03	0.02
BM-313	HD 215801	346.8	-59.2	10.03	0.44	9.016	0.374	0.011	0.01	0.01
BM-314	CD-41:15048	356.0	-61.5	10.14	0.55	8.930	0.400	0.014	0.01	0.01
BM-315	HD 217305	8.5	-65.1	9.72	0.39	8.901	0.198	0.018	0.02	0.01
BM-316	HD 217515	46.3	-63.2	9.41	0.37	8.578	0.203	0.034	0.03	0.02
BM-317	CD-63:1588	321.9	-50.1	9.40	0.86	7.723	0.617	0.020	0.02	0.01
BM-318	HD 217808	346.8	-62.3	9.30	0.75	7.688	0.538	0.010	0.01	0.01
BM-319	HD 218810	19.6	-67.8	8.43	0.39	7.525	0.256	0.024	0.02	0.01
BM-320	CD-17:6692	52.9	-64.4	8.95	0.73	7.397	0.524	0.036	0.04	0.03
BM-321	HD 219145	331.6	-58.7	9.44	0.47	8.534	0.273	0.011	0.01	0.01
BM-322	HD 219221	336.9	-61.3	8.54	0.40	7.624	0.246	0.011	0.01	0.00
BM-323	HD 220127	334.5	-61.8	10.15	0.69	8.691	0.500	0.011	0.01	0.01
BM-325	HD 222925	316.0	-53.5	9.02	0.59	7.747	0.409	0.021	0.02	0.02
BM-326	HD 223224	320.9	-59.6	9.57	0.78	8.106	0.548	0.008	0.01	0.01

**Table 2**  
 Radial Velocities, Line Indices, Atmospheric Parameters, and Type  
 Assignments

BM Name	N	$RV_M$ km s $^{-1}$	$RV_H$ km s $^{-1}$	KP (Å)	HP2 (Å)	GP (Å)	HG2 (Å)	LACF (9)	Teff $_S$ (K) (10)	logg $_S$ (cgs) (11)	[Fe/H] $_S$ (12)	Teff $_H$ (K) (13)	logg $_H$ (cgs) (14)	[Fe/H] $_H$ (15)	Teff $_C$ (K) (16)	logg $_C$ (cgs) (17)	[Fe/H] $_C$ (18)	[Fe/H] $_N$ (19)	TYPE $_{N/S}$ (20)
(1)	(2)	(3)	(4)	(5)	(6)	(7)	(8)	(9)	(10)	(11)	(12)	(13)	(14)	(15)	(16)	(17)	(18)	(19)	(20)
BM-001	1	45	...	7.90	2.85	3.39	2.53	0.204	6007	3.75	-0.80	...	...	...	6001	4.11	-0.56	-0.44	D / D
BM-002	2	-48	-61	6.37	1.06	1.66	1.25	-0.347	5065	1.15	-2.46	4901	1.44	-2.30	4894	0.90	-2.60	-2.43	RG / G
BM-003	1	-32	-48	6.39	3.51	1.64	3.45	-0.233	6105	3.58	-1.27	6004	4.06	-1.21	6117	3.90	-1.14	-0.82	D / TO
BM-004	1	29	...	6.70	4.19	2.24	4.06	0.027	6355	3.75	-0.66	...	...	...	6411	4.11	-0.39	-0.42	D / D
BM-005	1	-68	-66	4.86	1.62	2.60	1.14	-0.662	5266	1.70	-2.42	4935	1.98	-2.73	5130	1.58	-2.55	-2.45	RG / G
BM-006	3	9	8	10.01	0.84	5.65	1.15	0.472	5123	2.39	-1.19	5116	2.30	-0.93	4962	2.43	-1.04	-1.44	RG / G
BM-007	1	122	119	9.84	0.71	5.47	0.87	0.605	5285	2.69	-0.69	5079	2.79	-0.83	5152	2.80	-0.42	-1.55	RG / G
BM-008	1	47	...	8.52	2.00	4.56	1.88	0.439	5821	4.29	-0.35	6006	...	...	5783	4.78	0.00	-0.47	D / D
BM-009	1	7	-5	8.74	1.91	4.65	1.77	0.402	5693	4.37	-0.82	5664	4.38	-0.71	5632	4.88	-0.58	-0.78	D / D
BM-010	1	28	23	6.38	4.28	1.98	4.12	-0.037	6354	3.62	-0.80	...	...	...	6409	3.95	-0.56	-0.38	D / TO
BM-011	1	15	8	8.56	2.70	3.99	2.42	0.393	5950	4.39	-0.41	6035	...	...	5934	4.91	-0.08	-0.34	D / D
BM-012	1	46	36	2.54	3.95	0.40	3.50	-1.004	6203	3.16	-1.96	6060	3.83	-2.27	6232	3.38	-1.99	-2.05	D / G :
BM-013	1	1	...	4.59	5.35	1.09	5.15	-0.405	6687	4.11	-0.88	...	...	...	6801	4.56	-0.66	-1.10	BD / D
BM-014	1	25	22	8.41	1.19	4.06	1.26	0.070	5420	2.78	-1.57	...	...	...	5311	2.91	-1.51	-1.97	RG / G
BM-015	1	-5	-9	9.08	1.34	5.13	1.29	0.488	5536	4.48	-0.79	5748	...	...	5448	5.02	-0.55	-0.72	D / D
BM-016	1	25	31	9.33	1.20	4.53	1.51	0.287	5322	2.19	-1.34	...	...	...	5196	2.19	-1.22	-1.66	RG / G
BM-017	1	72	76	8.22	1.97	4.02	2.04	0.186	5766	4.32	-1.22	...	...	...	5718	4.82	-1.08	-1.12	D / D
BM-018	1	-2	-13	6.95	3.94	2.53	4.02	0.115	6261	3.55	-0.67	...	...	...	6300	3.87	-0.40	-0.37	D / TO
BM-019	1	54	...	8.49	1.99	4.26	2.05	0.291	5791	4.33	-0.84	...	...	...	5747	4.83	-0.61	-1.42	D / D
BM-021	2	232	235	4.23	3.60	1.12	3.75	-0.536	6176	3.15	-1.59	6240	...	...	6200	3.37	-1.53	-1.28	D / G :
BM-022	1	18	24	4.29	3.64	1.14	3.70	-0.654	6154	3.15	-1.64	6119	4.12	-1.74	6174	3.37	-1.59	-1.79	D / G :
BM-023	1	26	...	9.09	1.61	5.08	1.60	0.498	5607	4.26	-0.48	...	...	...	5531	4.74	-0.16	-0.39	D / D
BM-024	1	28	...	5.54	1.13	7.32	1.85	0.255	5305	2.22	-2.39	5000	3.00	-2.23	5176	2.22	-2.52	-0.92	SG / G
BM-025	2	-1	...	7.95	4.01	2.84	4.11	0.235	6220	3.32	-0.57	...	...	...	6252	3.58	-0.27	+0.05	D / TO
BM-026	2	2	-6	9.64	0.87	6.06	0.84	0.699	5310	3.52	-0.25	...	...	...	5182	3.83	+0.12	-0.56	SG / D :
BM-028	1	318	305	1.12	3.41	0.93	3.61	-0.273	6151	2.80	-1.63	...	...	...	6171	2.94	-1.58	-2.40	RHB / G :
BM-029	1	-22	...	10.69	...	6.27	0.41	0.778	5097	2.40	-0.12	...	...	...	4931	2.44	+0.28	-2.40	RG / FHB :
BM-030	2	38	...	10.45	0.62	5.95	0.94	0.599	5197	2.28	-0.56	5009	2.38	-0.69	5049	2.30	-0.26	-1.33	RG / G
BM-032	1	-33	...	7.21	4.27	2.30	4.51	0.049	6401	3.64	-0.55	...	...	...	6465	3.98	-0.25	-0.30	D / TO
BM-033	2	125	122	8.57	0.48	3.52	0.94	0.025	4777	1.35	-2.12	...	...	...	4555	1.15	-2.18	-2.36	RG / G
BM-034	1	146	152	9.03	0.77	4.66	1.07	0.142	5118	2.30	-1.63	4903	2.21	-1.66	4956	2.32	-1.58	-2.20	RG / G
BM-035	1	95	101	4.19	1.30	1.89	1.40	-0.750	5569	2.60	-2.33	5210	...	...	5486	2.69	-2.44	-2.31	RG / G
BM-036	3	122	120	8.08	2.16	3.55	2.15	0.171	5809	4.17	-1.03	5832	4.28	-0.85	5769	4.63	-0.84	-1.00	D / D
BM-037	2	-2	-2	10.51	0.31	6.11	0.57	0.728	5124	2.26	-0.41	...	...	...	4963	2.27	-0.08	-0.90	RG / G
BM-038	3	-31	...	10.42	0.52	6.06	0.78	0.640	5245	2.35	-0.46	...	...	...	5105	2.38	-0.14	-1.10	RG / G
BM-039	1	98	89	9.29	0.46	3.34	0.64	0.181	4680	1.31	-2.00	4470	1.07	-2.03	4441	1.10	-2.04	-2.27	RG / G
BM-040	2	-20	-31	5.91	1.20	3.60	1.23	-0.361	5318	2.10	-2.11	5043	2.20	-2.46	5191	2.07	-2.17	-2.37	RG / G
BM-041	1	23	14	10.61	0.64	4.70	0.72	0.445	4587	1.61	-1.79	4417	0.95	-1.80	4332	1.47	-1.78	-1.94	RG / G
BM-042	1	73	82	5.58	5.39	1.45	5.26	-0.039	6824	4.36	-0.31	6816	...	...	6962	4.87	+0.05	-0.24	BD / D
BM-043	1	-152	-143	9.49	0.61	5.31	1.08	0.208	4447	2.29	-2.34	4360	1.07	-2.06	4167	2.31	-2.46	-1.89	RG / G
BM-044	1	41	...	5.97	1.13	3.20	1.23	-0.449	5279	2.03	-2.09	...	...	...	5145	1.99	-2.15	-2.23	RG / G
BM-045	1	23	22	9.98	0.80	3.86	0.78	0.563	4462	0.58	-2.29	4134	0.31	-1.93	4185	0.19	-2.39	-2.06	RG / G
BM-046	3	32	...	10.89	0.35	6.21	0.55	0.728	4992	2.19	-0.52	4840	2.20	-0.69	4808	2.19	-0.21	-1.25	RG / G
BM-047	2	27	...	8.92	2.03	4.80	1.80	0.611	5906	3.76	-0.35	...	...	...	5883	4.13	0.00	...	D / D
BM-048	1	320	307	1.88	1.18	1.89	1.19	-0.446	5534	2.48	-1.98	...	...	...	5445	2.54	-2.01	-2.17	RG / G
BM-049	1	-8	...	10.74	0.22	5.95	0.47	0.798	4985	2.28	-0.90	...	...	...	4800	2.30	-0.68	-0.68	RG / G
BM-050	1	15	...	7.84	3.72	2.99	3.65	0.274	6210	4.42	-0.41	...	...	...	6240	4.94	-0.08	-0.97	RG / D :
BM-051	1	121	112	6.00	2.68	1.73	2.48	-0.311	5934	3.89	-1.68	5920	4.28	-1.59	5916	4.29	-1.64	-1.71	D / D

Table 2 — *Continued*

BM Name	N	$\text{RV}_M$ km s $^{-1}$	$\text{RV}_H$ km s $^{-1}$	KP (Å)	HP2 (Å)	GP (Å)	HG2 (Å)	LACF	Teff $_S$ (K)	logg $_S$ (cgs)	[Fe/H] $_S$	Teff $_H$ (K)	logg $_H$ (cgs)	[Fe/H] $_H$	Teff $_C$ (K)	logg $_C$ (cgs)	[Fe/H] $_C$	[Fe/H] $_N$	TYPE $_{N/S}$
(1)	(2)	(3)	(4)	(5)	(6)	(7)	(8)	(9)	(10)	(11)	(12)	(13)	(14)	(15)	(16)	(17)	(18)	(19)	(20)
BM-052	1	179	...	6.61	0.75	2.72	0.96	-0.314	4990	1.52	-2.38	...	...	...	4806	1.36	-2.50	-2.38	RG / G
BM-053	1	89	...	9.11	1.04	2.68	1.29	0.101	5244	1.82	-1.64	...	...	...	5104	1.73	-1.59	-2.11	RG / G
BM-054	1	181	173	3.86	4.11	0.88	3.78	-0.204	6263	2.95	-1.74	...	...	...	6302	3.12	-1.72	-1.70	RHB / FHB
BM-055	1	32	...	8.11	3.98	2.95	3.94	0.195	6263	3.81	-0.23	...	...	...	6302	4.19	+0.14	+0.32	D / D
BM-056	1	-18	-14	8.69	0.72	4.58	1.04	-0.030	4920	1.78	-1.97	...	...	...	4723	1.68	-2.00	-2.56	RG / G
BM-057	1	37	...	10.09	0.54	6.20	0.58	0.735	5167	2.42	-0.72	...	...	...	5014	2.47	-0.46	-0.77	RG / G
BM-058	1	273	...	6.67	1.92	1.68	1.89	-0.032	5759	2.65	-1.56	...	...	...	5710	2.75	-1.49	-1.70	RHB / FHB
BM-059	1	239	235	5.76	2.52	1.66	1.98	-0.340	5929	3.89	-1.71	5921	4.53	-1.68	5910	4.29	-1.68	-1.69	D / D
BM-060	1	302	302	4.58	1.96	1.75	1.87	-0.234	5833	4.12	-1.93	5800	4.00	-1.40	5797	4.57	-1.95	-1.36	D / D
BM-061	2	18	...	10.25	0.29	6.55	0.74	0.741	4950	2.23	-0.89	4720	1.60	-0.67	4759	2.23	-0.67	-1.14	RG / G
BM-062	2	-9	-11	4.92	5.42	1.57	5.39	-0.079	6581	4.30	-1.11	...	...	...	6676	4.79	-0.94	-0.30	D / D
BM-063	1	125	123	9.24	0.49	3.33	0.82	0.285	4530	0.83	-2.21	4366	0.95	-2.06	4265	0.50	-2.29	-2.31	RG / G
BM-064	1	173	...	8.56	0.89	4.09	1.10	0.065	5166	2.34	-1.70	5196	3.00	-1.76	5013	2.37	-1.67	-2.07	RG / G
BM-065	1	-3	...	8.10	3.67	3.11	3.90	0.210	6127	3.92	-0.72	...	...	...	6143	4.32	-0.46	-0.07	D / D
BM-067	1	200	194	11.19	...	4.92	0.51	0.687	4473	1.42	-1.58	4337	1.32	-1.48	4198	1.23	-1.52	-1.48	RG / G
BM-068	1	-9	-3	2.74	7.60	1.00	7.58	-0.492	7379	4.86	-0.72	...	...	...	7615	5.49	-0.46	...	BG / D :
BM-069	1	195	184	7.75	2.32	3.33	2.53	0.119	5842	3.73	-1.39	5826	4.07	-0.87	5807	4.09	-1.28	-0.92	D / D
BM-070	1	119	...	8.83	1.07	4.56	1.46	0.229	5191	2.11	-1.68	...	...	...	5042	2.09	-1.64	-1.92	RG / G
BM-071	1	35	24	5.72	5.49	1.48	5.43	-0.021	6738	4.24	-0.38	6734	...	...	6861	4.72	-0.04	-0.25	BD / D
BM-072	1	20	...	10.71	...	6.66	0.41	0.871	5163	2.18	-0.10	...	...	...	5009	2.17	+0.30	-0.91	RG / G
BM-073	1	21	...	8.87	2.76	4.20	2.44	0.404	5810	3.57	-0.71	...	...	...	5770	3.89	-0.45	+0.04	D / TO
BM-074	1	2	...	6.44	3.97	3.30	4.16	0.213	6204	3.63	-1.17	...	...	...	6233	3.97	-1.01	-0.42	D / TO
BM-075	1	-31	...	6.94	4.64	2.06	4.67	0.101	6390	4.06	-0.75	...	...	...	6452	4.50	-0.50	+0.07	D / D
BM-076	1	-16	-6	7.39	3.53	3.11	3.69	0.050	6053	3.77	-0.88	...	...	...	6056	4.14	-0.66	-0.25	D / D
BM-077	1	161	162	9.18	0.73	4.64	0.95	0.206	5060	1.79	-1.66	4890	2.18	-1.59	4888	1.69	-1.62	-2.01	RG / G
BM-078	2	-57	...	10.81	...	6.43	0.56	0.796	5115	2.15	-0.39	...	...	...	4953	2.14	-0.05	-0.85	RG / G
BM-079	1	58	57	8.64	0.99	2.78	1.18	0.031	5063	1.37	-1.94	...	...	...	4891	1.17	-1.96	-1.86	RG / G
BM-080	2	18	15	7.38	2.93	3.41	3.08	0.170	5937	2.94	-1.15	...	...	...	5919	3.11	-0.99	...	BG / FHB
BM-081	2	311	306	8.24	0.99	3.21	1.10	0.106	5371	2.84	-1.63	5261	3.19	-1.43	5254	2.99	-1.58	...	RG / G
BM-082	3	92	87	9.93	0.75	5.17	1.06	0.300	5000	2.23	-1.53	...	...	...	4817	2.23	-1.46	-1.85	RG / G
BM-083	1	304	...	0.64	4.08	0.34	3.79	-0.648	6329	3.04	-2.07	...	...	...	6380	3.24	-2.12	-2.40	RHB / FHB
BM-084	1	4	...	7.31	4.48	2.44	4.44	0.205	6446	3.95	-0.29	...	...	...	6518	4.36	+0.07	+0.18	D / D
BM-085	2	-2	...	9.63	0.93	5.91	0.93	0.610	5367	2.74	-1.28	...	...	...	5249	2.87	-1.15	-0.42	D / G :
BM-086	1	78	72	5.57	3.21	1.91	2.96	-0.325	6042	3.33	-1.77	6029	3.95	-1.32	6043	3.59	-1.75	-1.12	D / G :
BM-087	1	32	...	6.31	4.73	2.05	4.59	-0.003	6305	3.95	-0.75	6630	...	...	6352	4.36	-0.50	-0.32	D / D
BM-088	1	15	13	6.50	3.80	2.34	3.71	-0.114	6197	3.60	-1.11	6112	...	...	6225	3.93	-0.94	-0.46	D / TO
BM-089	1	266	269	4.45	3.14	1.17	3.14	-0.510	6045	3.18	-1.52	6040	4.00	-1.62	6046	3.41	-1.44	-0.97	D / G :
BM-090	1	43	27	7.53	3.86	2.80	3.77	0.184	6204	3.71	-0.73	...	...	...	6233	4.06	-0.47	-0.13	D / D
BM-091	5	10	12	6.15	3.80	3.30	4.08	0.157	6178	3.48	-1.35	...	...	...	6203	3.78	-1.24	-0.50	D / TO
BM-092	4	51	51	9.38	1.88	4.63	1.80	0.418	5670	3.92	-0.78	5638	4.01	-0.53	5605	4.32	-0.53	-0.21	D / D
BM-093	4	60	58	9.26	1.63	5.14	1.61	0.450	5585	4.01	-0.76	5587	...	...	5505	4.44	-0.51	-0.57	D / D
BM-095	1	3	6	9.16	1.62	4.86	1.54	0.491	5471	3.03	-1.58	5588	...	...	5371	3.22	-1.52	-0.42	D / G :
BM-096	1	120	...	10.58	0.29	5.88	0.64	0.723	5088	2.14	-0.70	4700	1.90	-0.76	4921	2.12	-0.43	-0.96	RG / G
BM-097	1	-17	-12	7.37	4.15	2.46	4.11	0.098	6242	3.61	-0.76	...	...	...	6278	3.94	-0.51	-0.22	D / TO
BM-099	2	-24	...	10.69	0.26	6.22	0.28	0.826	4662	2.23	-1.04	...	...	...	4420	2.23	-0.85	-0.85	RG / G
BM-100	1	273	...	7.43	1.46	2.02	1.55	0.022	5554	1.77	-1.63	...	...	...	5469	1.67	-1.58	-1.20	RHB / FHB
BM-101	2	208	205	3.20	3.92	0.58	3.59	-0.810	6306	3.76	-1.65	6221	4.26	-1.95	6353	4.13	-1.60	-2.03	D / D
BM-102	1	13	7.03	5.03	2.03	4.92	0.048	6581	4.33	-0.32	7075	...	...	6676	4.83	+0.03	+0.18	BD / D	
BM-103	1	53	41	1.71	6.74	0.30	6.44	-0.893	7140	4.37	-1.53	6881	...	-1.49	7334	4.88	-1.46	-1.19	BD / D

Table 2 — Continued

BM Name	N	$RV_M$ km s $^{-1}$	$RV_H$ km s $^{-1}$	KP (Å)	HP2 (Å)	GP (Å)	HG2 (Å)	LACF	Teff $_S$ (K)	logg $_S$ (cgs)	[Fe/H] $_S$	Teff $_H$ (K)	logg $_H$ (cgs)	[Fe/H] $_H$	Teff $_C$ (K)	logg $_C$ (cgs)	[Fe/H] $_C$	[Fe/H] $_N$	TYPE $_{N/S}$
(1)	(2)	(3)	(4)	(5)	(6)	(7)	(8)	(9)	(10)	(11)	(12)	(13)	(14)	(15)	(16)	(17)	(18)	(19)	(20)
BM-104	1	-26	-28	6.39	4.67	1.95	4.64	-0.024	6387	3.72	-0.93	6392	3.82	-0.63	6448	4.08	-0.72	-0.36	D / D
BM-105	3	-3	-1	8.81	2.06	4.45	2.06	0.335	5739	4.25	-0.91	5740	4.25	-0.73	5686	4.73	-0.69	-0.92	D / D
BM-106	3	7	...	10.79	0.59	6.18	0.45	0.741	4765	1.99	-1.19	4630	2.30	-0.89	4541	1.94	-1.04	-1.11	RG / G
BM-107	1	19	23	2.92	6.15	1.22	5.91	-0.472	6795	4.32	-1.17	...	...	...	6928	4.82	-1.01	...	BD / D
BM-108	2	42	35	7.57	3.57	3.13	3.81	0.352	6172	3.79	-0.43	...	...	...	6195	4.16	-0.10	+0.28	D / D
BM-109	3	58	...	10.40	...	6.26	0.54	0.765	5089	2.54	-0.51	4760	1.80	-0.56	4922	2.62	-0.20	-0.97	RG / G
BM-110	2	337	...	6.78	1.31	1.58	1.30	-0.234	5387	1.64	-1.88	...	...	...	5272	1.50	-1.89	-2.03	RG / G
BM-111	1	214	215	4.38	3.70	1.09	3.56	-0.149	6199	2.50	-1.52	6063	3.20	-1.29	6227	2.57	-1.44	-1.60	RHB / FHB
BM-112	1	18	11	6.44	4.67	1.98	4.65	0.094	6464	3.88	-0.67	6738	...	...	6539	4.27	-0.40	...	BG / D :
BM-113	1	17	10	8.48	3.66	3.12	3.77	0.366	6200	3.26	-0.31	...	...	...	6228	3.51	+0.05	...	BG / D :
BM-114	1	106	109	10.60	0.49	4.82	0.70	0.553	4622	1.53	-1.66	4514	1.33	-1.45	4373	1.37	-1.62	-1.76	RG / G
BM-115	2	-11	-23	6.13	4.88	1.62	4.89	-0.054	6474	3.91	-0.96	6468	4.13	-0.46	6551	4.31	-0.75	-0.43	D / D
BM-117	1	33	...	2.39	6.95	0.80	6.64	-0.547	7163	4.41	-1.14	...	...	...	7361	4.93	-0.98	...	BG / D :
BM-118	1	3	-4	8.48	2.49	4.35	2.75	0.383	5982	4.28	-0.46	...	...	...	5972	4.77	-0.14	-0.42	D / D
BM-119	2	-1	-3	8.49	2.85	4.03	2.91	0.360	6024	4.31	-0.55	...	...	...	6021	4.81	-0.25	-0.39	D / D
BM-120	5	84	...	5.91	0.84	1.93	0.91	-0.274	4905	1.33	-2.66	4500	0.80	-2.32	4706	1.12	-2.85	-2.47	RG / G
BM-121	1	150	...	7.93	0.52	2.87	0.81	0.009	4656	0.98	-2.53	4430	0.92	-2.31	4413	0.69	-2.69	-2.66	RG / G
BM-122	1	125	...	9.91	0.64	5.57	0.95	0.507	5066	2.06	-1.28	4970	2.10	-0.97	4895	2.02	-1.15	-1.45	RG / G
BM-123	1	-28	-25	6.30	4.43	2.03	4.72	-0.002	6369	3.84	-0.90	6573	...	...	6427	4.23	-0.68	-0.04	D / D
BM-125	1	17	...	3.29	6.21	1.46	6.23	-0.350	6831	4.15	-1.01	7038	...	...	6970	4.61	-0.82	...	BG / D :
BM-126	1	14	16	7.19	4.27	2.50	4.52	0.095	6357	4.20	-0.55	...	...	...	6413	4.67	-0.25	-0.21	D / D
BM-127	2	-31	-27	8.07	3.39	3.36	3.71	0.238	6116	4.23	-0.77	...	...	...	6130	4.71	-0.52	-0.18	D / D
BM-128	1	-20	-15	7.77	4.28	3.05	4.43	0.267	6377	4.30	-0.34	...	...	...	6436	4.79	+0.01	+0.27	D / D
BM-129	1	9	13	7.96	2.42	4.22	2.63	0.367	5902	4.27	-0.91	6116	...	...	5878	4.76	-0.69	-0.40	D / D
BM-130	2	37	37	8.24	1.88	3.72	1.86	0.198	5729	4.40	-1.07	5614	4.15	-1.05	5675	4.92	-0.89	-1.30	D / D
BM-131	3	20	20	8.25	3.94	3.18	3.93	0.367	6165	4.10	-0.22	6586	...	...	6187	4.55	+0.16	...	BG / D :
BM-132	1	1	2	8.10	3.81	3.09	3.87	0.323	6257	4.02	-0.35	...	...	...	6295	4.45	0.00	+0.10	D / D
BM-133	1	268	266	8.45	0.85	2.46	0.84	0.069	5143	1.40	-1.90	...	...	...	4986	1.21	-1.91	-2.14	RG / G
BM-134	1	148	146	9.74	0.48	4.94	0.79	0.308	5115	1.46	-2.02	4774	1.70	-1.67	4953	1.28	-2.06	-1.95	RG / G
BM-135	1	-16	-15	7.65	3.47	3.08	3.53	0.190	6126	3.51	-0.82	...	...	...	6141	3.82	-0.58	-0.24	D / TO
BM-136	1	29	22	7.97	2.80	3.64	2.69	0.248	5862	3.42	-1.17	...	...	...	5831	3.71	-1.01	-0.70	SG / TO
BM-138	3	49	53	6.13	3.19	2.31	3.21	-0.215	6008	3.81	-1.69	6033	4.11	-1.21	6003	4.19	-1.65	-1.01	D / D
BM-139	1	235	229	4.84	3.12	1.28	2.85	-0.398	6091	3.23	-1.48	5996	3.86	-1.49	6100	3.47	-1.40	-1.70	D / G :
BM-140	1	-12	-10	8.02	3.53	3.19	3.45	0.213	6101	4.11	-0.93	6034	4.06	-0.45	6112	4.56	-0.72	-0.24	D / D
BM-141	2	67	...	10.42	0.60	6.12	0.73	0.663	4792	1.75	-1.35	4689	2.13	-1.06	4573	1.64	-1.24	-1.41	RG / G
BM-142	2	-16	...	11.14	0.91	2.84	0.67	0.722	5237	2.40	-0.62	4980	2.00	-0.43	5096	2.44	-0.34	-1.24	RG / G
BM-143	1	13	12	6.68	4.03	2.27	3.73	-0.049	6262	3.70	-0.97	6281	...	...	6301	4.05	-0.77	-0.41	D / D
BM-144	1	183	183	9.37	0.89	4.45	1.01	0.320	5324	3.12	-1.18	5000	...	-1.13	5198	3.34	-1.03	-1.85	RG / G
BM-146	1	159	161	6.05	3.34	1.61	3.13	-0.245	6127	3.65	-1.35	6098	4.16	-1.24	6143	3.99	-1.24	-1.22	D / TO
BM-147	1	328	...	4.86	0.82	2.70	0.70	-0.368	5197	1.73	-2.24	...	...	...	5049	1.62	-2.33	-2.34	RG / G
BM-148	1	14	3	9.94	0.92	5.45	0.91	0.460	5177	2.34	-1.19	4950	2.60	-1.04	5025	2.37	-1.04	-1.70	RG / G
BM-149	1	119	...	5.61	3.19	1.37	2.97	-0.009	6099	2.61	-1.42	...	...	...	6110	2.70	-1.32	-1.60	RHB / FHB
BM-150	1	17	17	4.07	5.58	1.08	5.90	-0.144	6771	3.88	-1.15	...	...	...	6900	4.27	-0.99	-0.36	BD / D
BM-151	1	-13	-7	8.72	2.40	4.48	2.28	0.392	5814	3.83	-0.66	6103	...	...	5775	4.21	-0.39	-0.24	D / D
BM-152	1	-14	-17	7.51	3.98	2.71	4.02	0.153	6282	3.74	-0.54	6388	...	...	6325	4.10	-0.24	...	D / D
BM-153	1	27	24	8.90	0.62	3.44	0.88	0.205	4603	0.92	-2.18	4412	1.10	-1.97	4351	0.61	-2.26	-2.45	RG / G
BM-155	1	197	...	8.84	0.62	2.78	0.91	0.064	4944	1.36	-1.93	...	...	...	4752	1.16	-1.95	-2.45	RG / G
BM-157	1	63	70	7.93	2.08	3.93	2.10	0.236	5767	3.34	-1.34	5811	3.65	-0.75	5719	3.61	-1.22	-0.64	D / G :
BM-158	2	32	31	9.79	0.83	6.13	0.68	0.737	5283	3.13	-0.50	5000	3.40	-0.79	5150	3.35	-0.19	-1.05	RG / G

**Table 2** — *Continued*

BM Name	N	$RV_M$ km s $^{-1}$	$RV_H$ km s $^{-1}$	KP (Å)	HP2 (Å)	GP (Å)	HG2 (Å)	LACF	Teff $_S$ (K)	logg $_S$ (cgs)	[Fe/H] $_S$	Teff $_H$ (K)	logg $_H$ (cgs)	[Fe/H] $_H$	Teff $_C$ (K)	logg $_C$ (cgs)	[Fe/H] $_C$	[Fe/H] $_N$	TYPE $_{N/S}$
(1)	(2)	(3)	(4)	(5)	(6)	(7)	(8)	(9)	(10)	(11)	(12)	(13)	(14)	(15)	(16)	(17)	(18)	(19)	(20)
BM-159	1	-33	-30	9.83	1.01	5.26	1.25	0.384	4938	1.72	-1.72	4950	1.90	-1.06	4744	1.60	-1.69	-1.56	RG / G
BM-160	1	45	49	8.68	2.75	4.27	2.52	0.346	5869	3.99	-0.81	...	...	...	5839	4.41	-0.57	-0.49	D / D
BM-161	2	-4	0	8.40	2.26	4.00	1.96	0.248	5729	4.22	-1.31	5730	3.82	-0.60	5675	4.70	-1.19	-1.06	D / D
BM-164	1	10	...	5.63	6.64	1.34	6.68	-0.013	6989	4.07	-0.14	...	...	...	7156	4.51	+0.26	+0.03	BD / D
BM-165	1	20	...	6.61	4.84	1.88	4.90	0.099	6597	4.21	-0.33	...	...	...	6695	4.68	+0.02	...	BG / D :
BM-166	1	220	222	4.59	3.56	1.12	3.33	-0.538	6186	3.23	-1.44	5989	3.99	-1.66	6212	3.47	-1.35	-1.38	D / G :
BM-167	2	-12	-10	7.38	4.15	2.54	4.26	0.069	6305	3.76	-0.68	6493	...	...	6352	4.13	-0.41	-0.22	D / D
BM-168	1	-58	-74	7.01	4.54	2.28	4.67	0.064	6427	4.22	-0.54	...	...	...	6495	4.70	-0.24	-0.10	D / D
BM-169	1	-4	1	7.46	4.06	2.58	4.13	0.218	6359	3.76	-0.45	6639	...	...	6415	4.13	-0.13	...	BG / D :
BM-170	1	22	21	9.89	0.95	5.32	1.05	0.331	5175	2.16	-1.39	5025	2.76	-1.33	5023	2.15	-1.28	-1.75	RG / G
BM-171	4	-6	-6	7.55	2.88	3.37	2.93	0.144	5948	4.13	-1.24	5800	3.80	-0.68	5932	4.58	-1.10	-0.81	D / D
BM-172	1	148	152	7.62	2.40	2.89	2.26	0.017	5819	3.29	-1.29	5715	3.82	-1.08	5780	3.55	-1.16	-0.83	D / G :
BM-173	1	-19	46	8.00	4.08	2.86	4.22	0.331	6322	3.84	-0.20	...	...	...	6372	4.23	+0.18	...	BG / D :
BM-174	1	234	228	7.84	1.90	3.17	1.87	0.195	5856	4.40	-0.94	5849	4.42	-0.93	5824	4.92	-0.73	-0.83	D / D
BM-175	1	31	24	8.85	3.57	4.21	3.19	0.406	6077	3.70	0.00	6294	...	...	6084	4.05	+0.30	+0.53	D / D
BM-176	1	-16	-10	6.30	4.70	1.87	4.77	0.024	6383	4.19	-1.02	6462	...	...	6444	4.66	-0.83	+0.44	D / D
BM-177	1	25	20	8.39	3.59	2.99	3.46	0.281	6053	3.29	-0.71	6314	...	...	6056	3.55	-0.45	...	BG / FHB
BM-178	1	-76	...	10.67	0.55	5.24	0.60	0.765	5190	3.21	-0.11	...	...	...	5041	3.45	+0.29	-0.49	RG / G
BM-179	2	-30	...	9.75	0.64	6.15	1.04	0.563	5420	2.70	-1.16	5020	1.80	-0.70	5311	2.82	-1.00	-1.34	RG / G
BM-180	1	142	145	3.67	3.52	0.82	3.37	-0.636	6210	3.46	-1.57	5924	4.16	-1.90	6240	3.76	-1.51	-1.78	D / TO
BM-181	2	-12	-10	10.09	0.83	5.96	0.80	0.613	5536	2.59	-0.70	4940	2.70	-0.86	5448	2.68	-0.43	-1.21	RG / G
BM-182	1	-103	-101	10.35	0.46	4.54	0.79	0.494	4342	0.67	-2.18	4244	0.78	-1.83	4044	0.31	-2.26	-1.76	RG / G
BM-183	1	406	408	8.48	...	3.45	0.27	0.296	5201	2.10	-1.45	...	...	...	5054	2.07	-1.36	-2.10	RG / G
BM-185	2	28	28	8.07	3.27	3.37	3.24	0.264	6048	3.43	-0.66	6543	...	...	6050	3.72	-0.39	-0.04	D / TO
BM-186	1	93	100	10.49	0.41	3.92	0.75	0.544	4642	1.44	-1.63	...	...	...	4396	1.26	-1.58	-1.82	RG / G
BM-187	1	-29	-34	6.26	4.32	2.06	4.43	-0.083	6349	3.65	-0.87	5918	2.94	-0.66	6404	3.99	-0.64	-0.55	D / TO
BM-188	3	-24	-26	4.13	3.37	1.06	3.20	-0.602	6089	3.09	-1.10	5939	3.79	-1.78	6098	3.30	-0.93	-1.17	D / G :
BM-189	1	-15	-16	7.74	3.79	2.71	3.83	0.208	6222	3.85	-0.51	...	...	...	6254	4.24	-0.20	-0.07	D / D
BM-190	1	169	166	9.83	0.53	4.58	0.77	0.310	4748	1.64	-1.83	4617	1.42	-1.73	4521	1.50	-1.83	-2.03	RG / G
BM-191	1	326	325	8.86	0.41	2.33	0.80	0.177	4975	1.58	-1.72	4722	...	...	4788	1.43	-1.69	-2.12	RG / G
BM-192	1	8	9	7.62	3.95	2.78	3.98	0.175	6285	4.16	-0.55	...	...	...	6328	4.62	-0.25	-0.10	D / D
BM-193	1	-17	-14	7.77	3.75	2.96	3.68	0.306	6164	4.40	-0.49	6376	...	...	6186	4.92	-0.18	-0.10	D / D
BM-194	1	-6	-12	10.38	0.79	4.24	0.75	0.532	4428	0.84	-2.07	4167	0.10	-1.93	4145	0.52	-2.12	-2.14	RG / G
BM-195	1	260	249	8.37	0.74	4.18	0.87	0.095	5041	1.84	-1.91	4988	2.38	-1.63	4866	1.75	-1.93	-2.01	RG / G
BM-196	1	148	149	4.58	1.01	2.16	1.05	-0.636	5149	1.80	-2.48	4815	2.00	-2.94	4993	1.70	-2.63	-2.58	RG / G
BM-197	1	16	18	7.05	4.75	2.03	4.79	0.124	6518	4.18	-0.37	6955	...	...	6602	4.65	-0.03	-0.05	D / D
BM-198	1	-4	-3	7.04	4.89	1.99	4.94	0.135	6469	3.70	-0.46	...	...	...	6545	4.05	-0.14	+0.09	D / D
BM-199	1	-17	...	10.08	0.67	5.92	0.82	0.487	4642	1.48	-1.88	4688	1.91	-1.36	4396	1.31	-1.89	-1.18	RG / G
BM-200	1	-34	-33	6.84	4.44	2.13	4.58	0.031	6382	3.56	-0.64	6440	...	...	6442	3.88	-0.36	...	BG / D :
BM-201	1	-73	-75	5.93	1.49	2.59	1.41	-0.400	5477	2.62	-1.90	5245	2.78	-2.18	5378	2.72	-1.91	-2.22	RG / G
BM-202	1	29	32	7.07	3.51	2.84	3.53	0.171	6140	4.33	-1.16	...	...	...	6158	4.83	-1.00	-0.40	D / D
BM-203	1	21	25	7.91	2.30	4.02	2.28	0.266	5748	3.34	-1.28	5751	...	...	5697	3.61	-1.15	-0.52	SG / G
BM-204	1	-22	-22	6.63	4.10	2.17	4.08	-0.029	6253	3.49	-0.90	6460	...	...	6291	3.79	-0.68	-0.55	D / TO
BM-205	1	-15	-16	6.38	4.66	1.86	4.69	-0.049	6415	3.57	-0.76	6564	...	...	6481	3.89	-0.51	-0.22	D / TO
BM-206	1	32	33	6.92	3.80	2.53	3.77	0.029	6218	3.61	-0.82	6273	4.28	-0.60	6250	3.94	-0.58	-0.46	D / TO
BM-207	1	16	18	9.13	1.94	4.85	1.93	0.473	5736	3.82	-0.28	...	...	...	5683	4.20	+0.08	+0.06	D / D
BM-208	1	179	176	6.51	1.92	2.39	1.99	-0.210	5707	3.46	-1.79	5667	3.79	-1.51	5649	3.76	-1.78	-1.00	D / D
BM-209	1	15	12	7.08	2.33	4.62	2.61	0.154	5845	3.42	-1.46	6000	4.30	-0.81	5811	3.71	-1.37	-0.54	D / G :
BM-210	1	4	...	4.70	6.51	1.24	6.56	-0.259	6899	4.05	-0.59	...	...	...	7050	4.49	-0.30	...	BG / D :

Table 2 — Continued

BM Name	N	$RV_M$ km s $^{-1}$	$RV_H$ km s $^{-1}$	KP (Å)	HP2 (Å)	GP (Å)	HG2 (Å)	LACF	Teff <sub>S</sub> (K)	logg <sub>S</sub> (cgs)	[Fe/H] <sub>S</sub>	Teff <sub>H</sub> (K)	logg <sub>H</sub> (cgs)	[Fe/H] <sub>H</sub>	Teff <sub>C</sub> (K)	logg <sub>C</sub> (cgs)	[Fe/H] <sub>C</sub>	[Fe/H] <sub>N</sub>	TYPE <sub>N/S</sub>
(1)	(2)	(3)	(4)	(5)	(6)	(7)	(8)	(9)	(10)	(11)	(12)	(13)	(14)	(15)	(16)	(17)	(18)	(19)	(20)
BM-211	1	-27	-21	9.24	3.14	4.35	2.89	0.484	5945	3.40	-0.33	...	...	...	5929	3.68	+0.02	+0.04	SG / TO
BM-212	1	-103	-109	10.11	0.75	5.36	1.02	0.330	4854	1.57	-1.80	...	...	...	4646	1.42	-1.79	-1.88	RG / G
BM-213	1	-41	-43	3.38	6.21	0.93	6.09	-0.425	6934	3.51	-1.04	...	...	...	7091	3.82	-0.85	-0.80	RHB / TO :
BM-214	1	-8	-6	7.80	3.58	3.07	3.58	0.168	6123	3.62	-0.67	6228	...	...	6138	3.95	-0.40	-0.26	D / TO
BM-215	1	35	37	7.53	3.07	3.12	3.08	0.140	6004	3.50	-1.11	...	...	...	5998	3.80	-0.94	-0.85	D / TO
BM-216	1	71	54	6.95	3.55	2.72	3.30	0.002	6085	3.67	-1.12	6263	...	...	6093	4.02	-0.95	...	SG / D :
BM-217	1	-169	-170	2.75	2.76	0.94	2.61	-0.921	5851	2.85	-2.30	5709	3.54	-2.48	5818	3.00	-2.41	-2.21	D / G :
BM-218	1	-8	-7	8.76	3.15	3.69	2.96	0.384	5720	2.76	-1.51	...	...	...	5664	2.89	-1.43	...	BG / FHB
BM-219	1	-14	-16	7.62	4.39	1.99	4.46	0.036	6351	3.52	-0.50	6365	...	...	6406	3.83	-0.19	-0.26	D / TO
BM-220	1	7	1	8.23	3.07	3.56	2.97	0.235	5947	3.29	-0.76	...	...	...	5931	3.55	-0.51	-0.22	D / TO
BM-221	1	33	...	10.17	0.72	5.70	0.63	0.683	5201	2.48	-0.33	...	...	...	5054	2.54	+0.02	-0.65	RG / G
BM-222	1	317	...	7.63	1.10	1.99	1.36	0.041	5391	1.79	-1.70	...	...	...	5277	1.69	-1.67	-2.27	RG / G
BM-223	2	24	22	7.86	3.68	3.13	3.74	0.207	6215	3.71	-0.43	6202	...	...	6246	4.06	-0.10	-0.26	D / D
BM-224	1	29	...	10.57	0.54	6.16	0.70	0.662	5401	2.11	-0.26	4734	2.04	-0.80	5289	2.09	+0.11	-1.31	RG / G
BM-225	1	77	79	5.90	2.75	1.67	2.76	-0.036	6000	2.57	-1.55	...	...	...	5993	2.65	-1.48	-1.10	RHB / FHB
BM-226	1	12	...	4.19	6.65	1.21	6.61	-0.110	6970	4.20	-0.79	6905	...	...	7134	4.67	-0.55	...	BG / D :
BM-227	1	-25	-25	9.04	2.44	4.66	2.34	0.525	5870	4.19	-0.26	6213	...	...	5840	4.66	+0.11	-0.30	D / D
BM-228	1	-41	-38	9.22	2.69	4.45	2.62	0.421	5889	3.80	-0.35	...	...	...	5863	4.18	0.00	+0.24	D / D
BM-229	1	-22	-16	6.47	4.57	1.98	4.49	0.094	6318	3.11	-0.59	6340	...	...	6367	3.32	-0.30	...	RHB / FHB
BM-230	1	27	31	7.13	3.94	2.59	3.93	0.005	6230	3.81	-0.84	6132	3.90	-0.71	6264	4.19	-0.61	-0.64	D / D
BM-231	1	-9	...	3.90	7.36	1.07	7.45	-0.231	7236	4.81	-0.24	7045	...	...	7447	5.42	+0.13	-0.39	BD / D
BM-232	1	-7	...	4.73	5.96	1.38	5.85	-0.199	6833	3.34	-0.57	...	...	...	6973	3.61	-0.27	-0.50	RHB / FHB
BM-233	1	97	100	4.39	3.16	0.91	2.97	-0.575	6040	3.10	-1.61	5942	3.72	-1.80	6040	3.31	-1.56	-1.66	D / G :
BM-234	1	44	...	5.83	4.50	2.07	4.74	0.014	6472	3.64	-0.81	6704	...	...	6548	3.98	-0.57	-0.39	D / TO
BM-235	1	127	...	10.28	0.36	4.53	0.87	0.359	4719	1.47	-1.83	...	...	...	4487	1.29	-1.83	-1.81	RG / G
BM-236	1	-135	-130	6.80	2.44	2.28	2.41	-0.249	5627	2.59	-1.84	5223	...	-2.12	5555	2.68	-1.84	-1.89	RG / G
BM-237	1	37	62	6.69	4.41	2.07	4.47	0.097	6378	4.03	-0.74	...	...	...	6438	4.46	-0.48	...	BG / D :
BM-238	1	-11	-4	7.38	5.07	2.11	5.22	0.194	6497	3.68	-0.19	...	...	...	6578	4.03	+0.19	...	BG / D :
BM-239	1	-12	-9	8.68	3.85	3.19	3.92	0.314	6237	3.68	-0.22	6477	...	...	6272	4.03	+0.16	-0.07	D / D
BM-240	1	63	68	8.79	1.31	4.20	1.42	0.186	5336	1.52	-1.62	5147	2.10	-1.28	5212	1.36	-1.57	-2.07	RG / G
BM-241	1	-53	-49	4.89	3.55	1.43	3.63	-0.495	6127	3.15	-1.50	6079	4.17	-1.57	6143	3.37	-1.42	-1.46	D / G :
BM-242	1	3	7	8.94	1.99	4.56	2.15	0.358	5711	4.04	-0.72	5968	...	...	5653	4.47	-0.46	-0.51	D / D
BM-243	1	26	...	11.01	...	6.41	...	0.979	4664	2.47	-0.77	...	...	...	4422	2.53	-0.52	-0.41	RG / G
BM-244	1	-43	-39	11.96	0.56	6.10	0.69	0.640	5243	2.65	-0.72	4666	1.80	-0.80	5103	2.75	-0.46	-1.09	RG / G
BM-245	1	0	...	10.77	0.28	6.30	0.37	0.757	5326	2.65	-0.49	...	...	...	5201	2.75	-0.18	-1.69	RG / G
BM-246	1	161	165	2.98	3.37	0.59	3.29	-0.917	6149	3.49	-1.89	...	...	...	6168	3.79	-1.90	-1.86	D / TO
BM-247	1	61	69	7.93	1.56	3.06	1.79	0.097	5409	1.91	-1.63	...	...	...	5298	1.84	-1.58	-1.81	RG / G
BM-248	1	25	29	6.91	3.97	2.41	3.93	0.025	6280	4.00	-0.85	6326	...	...	6322	4.42	-0.62	-0.26	D / D
BM-249	2	56	...	1.30	4.63	0.44	3.61	-0.538	...	...	...	...	...	...	...	...	...	UVB / HOT	
BM-251	1	341	...	7.05	1.17	1.63	1.22	-0.158	5393	1.72	-1.83	5180	1.65	-2.07	5279	1.60	-1.83	-2.34	RG / G
BM-252	1	-6	-2	8.67	1.21	4.71	1.09	0.102	5127	1.91	-1.86	4735	1.50	-1.93	4967	1.84	-1.86	-2.00	RG / G
BM-253	1	24	18	4.61	3.01	1.36	2.87	-0.547	6119	3.78	-1.60	6019	4.56	-1.79	6133	4.15	-1.54	-1.96	D / D
BM-254	1	-47	...	6.59	4.74	1.95	4.87	-0.013	6566	3.96	-0.45	...	...	...	6659	4.37	-0.13	-0.41	D / D
BM-256	1	-355	-349	1.20	1.89	0.84	1.96	-0.110	5881	2.34	-1.53	5733	2.01	-1.68	5853	2.37	-1.46	-1.60	RHB / FHB
BM-257	2	93	102	7.61	0.66	2.60	0.85	-0.017	4525	0.86	-2.55	4285	0.53	-2.47	4259	0.54	-2.71	-2.52	RG / G
BM-258	1	19	31	7.30	0.84	3.24	0.92	-0.260	4843	1.42	-2.51	4612	1.25	-2.61	4633	1.23	-2.66	-2.23	RG / G
BM-259	1	-4	-1	8.51	3.68	3.44	3.71	0.344	6218	3.65	-0.28	...	...	...	6250	3.99	+0.08	-0.01	D / TO
BM-260	1	-194	-186	10.76	0.76	4.43	0.77	0.495	4515	1.53	-1.57	4299	0.81	-1.74	4247	1.37	-1.51	-1.86	RG / G
BM-261	1	-146	-139	3.84	3.85	0.99	3.78	-0.695	6207	3.20	-1.62	6054	4.03	-1.79	6237	3.43	-1.57	-1.56	D / G :

Table 2 — Continued

BM Name	N	$RV_M$ km s $^{-1}$	$RV_H$ km s $^{-1}$	KP (Å)	HP2 (Å)	GP (Å)	HG2 (Å)	LACF	Teff $_S$ (K)	logg $_S$ (cgs)	[Fe/H] $_S$	Teff $_H$ (K)	logg $_H$ (cgs)	[Fe/H] $_H$	Teff $_C$ (K)	logg $_C$ (cgs)	[Fe/H] $_C$	[Fe/H] $_N$	TYPE $_{N/S}$
(1)	(2)	(3)	(4)	(5)	(6)	(7)	(8)	(9)	(10)	(11)	(12)	(13)	(14)	(15)	(16)	(17)	(18)	(19)	(20)
BM-262	1	-47	...	8.09	3.54	3.13	3.48	0.178	6032	3.93	-0.65	...	...	...	6031	4.34	-0.37	-0.23	D / D
BM-264	1	-133	-126	4.34	1.13	2.38	1.11	-0.658	5239	1.78	-2.46	4677	1.16	-2.97	5098	1.68	-2.60	-2.72	RG / G
BM-265	1	10	20	6.70	3.55	2.52	3.58	-0.040	6095	3.30	-1.21	6000	3.00	-1.00	6105	3.56	-1.06	-0.53	D / TO
BM-266	1	142	143	9.15	0.96	4.59	1.18	0.202	5225	2.13	-1.43	5202	3.11	-1.34	5082	2.11	-1.33	-1.86	RG / G
BM-267	1	11	20	8.24	2.63	3.77	2.75	0.205	5859	3.25	-0.97	5921	...	...	5827	3.50	-0.77	-0.53	D / TO
BM-268	1	-123	-110	8.92	1.99	4.30	2.37	0.323	5783	4.33	-0.62	5765	4.24	-0.64	5738	4.83	-0.34	-0.87	D / D
BM-269	1	-134	-128	8.44	1.17	4.23	1.35	-0.028	5205	2.26	-1.81	...	...	...	5058	2.27	-1.80	-2.22	RG / G
BM-270	1	-84	-78	8.92	1.83	4.59	1.88	0.263	5617	3.49	-0.91	...	...	...	5543	3.79	-0.69	-0.74	D / D
BM-271	1	-44	-30	6.34	4.43	2.00	4.49	-0.138	6378	3.66	-0.85	6344	...	...	6438	4.00	-0.62	-0.51	D / D
BM-272	1	33	...	5.35	5.08	1.43	5.12	-0.196	6625	4.07	-0.82	...	...	...	6728	4.51	-0.58	-0.53	D / D
BM-273	1	-5	...	7.20	4.43	2.30	4.59	0.142	6454	4.20	-0.36	...	...	...	6527	4.67	-0.02	+0.11	D / D
BM-274	1	-87	...	8.27	1.05	1.94	1.44	0.061	5115	1.28	-1.98	...	...	...	4953	1.06	-2.01	...	UVB / FHB
BM-276	1	-38	-34	7.47	2.99	2.77	3.10	-0.059	5944	3.67	-1.25	5900	4.01	-1.07	5927	4.02	-1.11	-0.93	D / D
BM-277	1	-7	...	8.64	2.00	4.41	2.16	0.390	5880	4.38	-0.59	...	...	...	5852	4.89	-0.30	-0.54	D / D
BM-279	1	16	22	6.06	0.96	2.13	1.03	-0.449	5021	1.57	-2.39	...	...	...	4842	1.42	-2.52	-2.63	RG / G
BM-280	1	12	12	3.46	4.06	0.71	4.01	-0.810	6373	4.03	-1.56	6230	4.06	-1.95	6432	4.46	-1.49	-1.73	D / D
BM-281	1	23	28	6.98	2.90	2.37	2.98	-0.144	5962	3.59	-1.35	...	...	...	5949	3.92	-1.24	-0.81	D / TO
BM-282	1	-63	...	7.15	3.87	2.50	4.07	0.030	6258	3.63	-0.77	...	...	...	6297	3.97	-0.52	-0.34	D / TO
BM-284	1	18	4	3.99	4.33	1.07	4.29	-0.199	6496	3.44	-1.34	...	...	...	6576	3.73	-1.22	-1.70	RHB / FHB
BM-285	1	127	127	6.38	1.12	5.09	1.79	0.177	5303	1.97	-2.07	5230	1.60	-1.56	5174	1.91	-2.12	-1.63	RG / G
BM-286	1	-45	...	3.54	1.54	2.04	1.51	-0.833	5529	2.22	-2.46	5237	2.85	-2.87	5439	2.22	-2.60	-2.26	RG / G
BM-287	1	-8	-10	3.54	5.89	1.46	5.89	-0.336	6804	4.17	-1.30	6687	...	...	6939	4.63	-1.17	...	BG / D :
BM-288	1	-19	-14	7.03	4.42	2.16	4.60	0.054	6405	3.85	-0.56	6408	...	...	6469	4.24	-0.26	-0.17	D / D
BM-289	4	98	93	8.77	1.60	4.84	1.67	0.466	5564	3.90	-1.32	5603	4.18	-0.57	5481	4.30	-1.20	-0.98	D / D
BM-290	1	61	...	10.63	0.57	4.55	0.84	0.528	4541	1.45	-1.71	...	...	...	4278	1.27	-1.68	-1.85	RG / G
BM-291	1	-3	...	6.69	4.01	2.46	4.12	-0.015	6312	3.64	-0.80	6282	...	...	6360	3.98	-0.56	-0.45	D / TO
BM-292	1	2	...	5.69	5.06	1.81	5.30	0.017	6647	4.23	-0.39	...	...	...	6754	4.71	-0.05	...	BG / D :
BM-293	4	-36	-43	8.04	3.62	3.11	3.85	0.259	6193	3.84	-0.46	6197	...	...	6220	4.23	-0.14	-0.24	SG / D :
BM-294	1	87	...	6.98	3.42	2.44	3.46	-0.057	6097	3.23	-0.94	6086	...	...	6107	3.47	-0.73	-0.43	D / G :
BM-295	1	-167	-166	8.21	1.27	4.23	1.52	-0.011	5345	2.56	-1.67	...	...	...	5223	2.64	-1.63	-2.22	RG / G
BM-297	2	81	76	9.03	1.32	3.32	1.65	0.187	5369	1.95	-1.45	...	...	...	5251	1.89	-1.36	-1.85	RG / G
BM-298	1	-7	...	6.45	5.50	1.80	5.72	-0.073	6671	4.31	-0.39	6759	...	...	6782	4.81	-0.05	-0.06	BD / D
BM-299	1	-63	...	5.93	4.87	1.70	4.98	-0.258	6552	3.74	-0.81	...	...	...	6642	4.10	-0.57	-0.50	D / D
BM-300	1	23	10	6.14	5.27	1.80	5.53	0.029	6653	3.85	-0.45	6706	...	...	6761	4.24	-0.13	-0.21	BD / D
BM-301	2	-18	-16	10.74	0.74	5.68	0.86	0.451	4838	1.95	-1.45	4841	2.04	-1.29	4627	1.89	-1.36	-1.35	RG / G
BM-302	1	-17	-4	4.30	8.87	1.33	8.99	-0.010	7619	4.66	+0.38	...	...	...	7897	5.24	+0.30	+0.08	BD / D
BM-303	1	-7	...	9.84	0.99	5.31	1.20	0.405	5155	2.23	-1.46	5130	2.20	-1.03	5000	2.23	-1.37	-1.59	RG / G
BM-304	1	-8	0	10.48	0.95	5.49	...	1.037	5190	4.64	-0.91	5063	...	...	5041	5.21	-0.69	-0.39	D / D
BM-305	1	-69	-72	9.35	1.07	4.69	1.22	0.218	5301	2.79	-1.37	5157	2.88	-1.41	5171	2.93	-1.26	-2.07	RG / G
BM-306	1	0	4	9.95	0.70	5.97	1.01	0.523	5316	2.48	-0.75	...	...	...	5189	2.54	-0.50	-1.47	RG / G
BM-307	1	49	45	3.53	3.87	0.84	3.72	-0.788	6216	3.05	-1.80	6069	3.95	-1.97	6247	3.25	-1.79	-1.71	D / G :
BM-308	1	-368	...	6.91	0.90	2.75	0.92	-0.115	5061	1.74	-2.07	...	...	...	4889	1.63	-2.12	-2.28	RG / G
BM-309	1	-3	...	5.83	4.35	1.99	4.51	-0.040	6374	3.46	-1.16	...	...	...	6433	3.76	-1.00	-0.32	D / TO
BM-310	1	-82	-92	4.23	2.96	1.06	3.18	-0.338	5929	2.51	-1.83	5722	1.50	-1.90	5910	2.58	-1.83	-2.10	RHB / FHB
BM-311	1	-325	-328	8.32	1.12	2.50	0.65	0.596	4371	0.26	-2.42	...	...	...	4078	-0.20	-2.55	-2.14	RG / G
BM-313	1	-86	...	2.77	3.51	0.71	3.43	-0.900	6121	3.10	-2.05	6005	3.81	-2.29	6135	3.31	-2.10	-1.97	D / G :
BM-314	1	234	...	3.87	2.38	0.95	2.63	-0.375	5776	2.27	-1.97	...	...	...	5730	2.28	-2.00	-0.50	RHB / FHB
BM-315	1	21	...	5.39	5.04	1.53	5.21	-0.033	6669	4.21	-0.77	...	...	...	6780	4.68	-0.52	-0.23	D / D
BM-316	1	-5	-6	4.48	5.45	1.23	5.52	-0.268	6753	4.20	-0.82	...	...	...	6879	4.67	-0.58	-0.82	BD / D

**Table 2** — *Continued*

BM Name	N	$RV_M$ km s $^{-1}$	$RV_H$ km s $^{-1}$	KP (Å)	HP2 (Å)	GP (Å)	HG2 (Å)	LACF	Teff $_S$ (K)	logg $_S$ (cgs)	[Fe/H] $_S$	Teff $_H$ (K)	logg $_H$ (cgs)	[Fe/H] $_H$	Teff $_C$ (K)	logg $_C$ (cgs)	[Fe/H] $_C$	[Fe/H] $_N$	TYPE $_{N/S}$
(1)	(2)	(3)	(4)	(5)	(6)	(7)	(8)	(9)	(10)	(11)	(12)	(13)	(14)	(15)	(16)	(17)	(18)	(19)	(20)
BM-317	1	135	...	9.70	0.53	5.17	1.12	0.391	4975	1.99	-1.55	...	...	...	4788	1.94	-1.48	-2.09	RG / G
BM-318	1	151	...	7.57	0.96	2.18	1.21	-0.189	5109	1.06	-2.17	...	...	...	4946	0.79	-2.25	-2.25	RG / G
BM-319	1	6	...	5.30	4.96	1.58	5.05	-0.144	6582	3.72	-0.86	...	...	...	6678	4.08	-0.63	-0.65	D / D
BM-320	1	-162	-170	7.21	1.21	4.02	1.46	-0.155	5269	2.39	-1.88	5106	2.58	-1.87	5134	2.43	-1.89	-2.22	RG / G
BM-321	1	38	...	7.31	3.95	2.80	4.09	0.145	6288	3.75	-0.55	...	...	...	6332	4.11	-0.25	-0.29	D / D
BM-322	2	34	24	5.28	4.81	1.59	4.95	-0.130	6520	3.56	-0.90	6455	...	...	6605	3.88	-0.68	-0.67	D / TO
BM-323	1	84	...	8.61	1.13	4.34	1.39	0.143	5346	2.89	-1.48	...	...	...	5224	3.05	-1.40	-1.85	RG / G
BM-325	1	-34	...	6.73	1.99	1.90	2.38	0.030	5668	2.20	-1.70	5564	2.64	-1.51	5603	2.20	-1.67	-1.30	RHB / FHB
BM-326	1	65	...	9.98	0.87	5.28	1.08	0.515	5261	2.42	-1.13	...	...	...	5124	2.47	-0.96	-1.28	SG / G

**Note.** — A ":" appended to column (20) indicates a disagreement between the type assignment (based on photometry) in Paper I and that assigned based on the atmospheric parameters determined by the n-SSPP.

**Table 3**  
Carbon Abundance Ratio Estimates

BM Name (1)	[C/Fe] <sub>S</sub> (2)	DETECT (3)	CC (4)	[C/Fe] <sub>H</sub> (5)	[C/Fe] <sub>C</sub> (6)
BM-001	+0.39	D	0.999	...	+0.19
BM-002	+0.09	D	0.998	-0.40	-0.13
BM-003	+0.23	D	0.989	...	+0.03
BM-004	+0.48	D	0.995	...	+0.29
BM-005	+0.61	D	0.994	+0.26	+0.43
BM-006	+0.05	D	1.000	...	-0.17
BM-007	+0.14	D	0.998	-0.15	-0.07
BM-008	+0.07	D	0.997	...	-0.15
BM-009	+0.28	D	0.999	...	+0.08
BM-010	+0.45	D	0.996	...	+0.26
BM-011	+0.14	D	0.997	...	-0.08
BM-012	-0.84	U	0.811	...	-0.84
BM-013	+0.13	D	0.983	...	-0.09
BM-014	+0.20	D	1.000	...	-0.01
BM-015	+0.11	D	0.999	...	-0.10
BM-016	+0.25	D	0.998	...	+0.04
BM-017	+0.30	D	0.999	...	+0.10
BM-018	+0.45	D	0.996	...	+0.26
BM-019	+0.33	D	0.999	...	+0.13
BM-021	+0.48	D	0.953	...	+0.29
BM-022	+0.44	D	0.953	+0.06	+0.25
BM-023	-0.04	D	0.994	...	-0.26
BM-024	+1.81	D	0.998	...	+1.71 <sup>a</sup>
BM-025	+0.31	D	0.994	...	+0.10
BM-026	-0.01	D	0.995	...	-0.24
BM-028	+0.43	D:	0.619	...	+0.24
BM-029	-0.16	D	0.993	...	-0.39
BM-030	-0.27	D	0.979	-0.18	-0.51
BM-032	+0.44	D	0.990	...	+0.25
BM-033	-0.21	D	0.996	...	-0.45
BM-034	+0.17	D	0.999	-0.15	-0.04
BM-035	+0.52	D	0.993	...	+0.33
BM-036	+0.37	D	0.999	...	+0.17
BM-037	-0.06	D	0.997	...	-0.28
BM-038	-0.20	D	0.993	...	-0.44
BM-039	-0.46	D	0.999	-0.81	-0.71
BM-040	+0.48	D	0.996	+0.20	+0.29
BM-041	-0.47	D	0.997	-0.54	-0.72
BM-042	+0.21	D	0.954	...	0.00
BM-043	+2.48	D	0.985	...	+2.43 <sup>a</sup>
BM-044	+0.41	D	0.997	...	+0.22
BM-045	+0.05	D	0.942	-0.65	-0.17
BM-046	-0.14	D	0.993	...	-0.38
BM-047	-0.04	D	0.998	...	-0.27
BM-048	+0.35	D	0.997	...	+0.15
BM-049	+0.14	D	0.998	...	-0.07
BM-050	+0.02	D	0.996	...	-0.20
BM-051	+0.49	D	0.998	...	+0.30
BM-052	+0.17	D	1.000	...	-0.04
BM-053	+0.05	D	0.997	...	-0.17
BM-054	+0.76	D:	0.660	...	+0.59
BM-055	+0.19	D	0.994	...	-0.02
BM-056	+0.06	D	0.997	...	-0.16
BM-057	+0.07	D	0.998	...	-0.15
BM-058	+0.50	D	0.904	...	+0.31
BM-059	+0.49	D	0.998	...	+0.30
BM-060	+0.57	D	0.993	...	+0.39
BM-061	+0.33	D	0.998	...	+0.13
BM-062	+0.86	D	0.991	...	+0.70 <sup>a</sup>
BM-063	-0.59	D	0.996	...	-0.85
BM-064	+0.14	D	0.999	...	-0.08
BM-065	+0.39	D	0.998	...	+0.19
BM-067	-0.13	D	0.995	-0.34	-0.36
BM-068	...	N	...	...	...
BM-069	+0.78	D	0.995	...	+0.61
BM-070	+0.34	D	0.995	...	+0.14
BM-071	+0.20	D	0.975	...	-0.01
BM-072	-0.08	D	0.999	...	-0.30
BM-073	+0.32	D	0.999	...	+0.11

**Table 3** — *Continued*

BM Name (1)	[C/Fe] <sub>S</sub> (2)	DETECT (3)	CC (4)	[C/Fe] <sub>H</sub> (5)	[C/Fe] <sub>C</sub> (6)
BM-074	+1.16	D	0.993	...	+1.01 <sup>a</sup>
BM-075	+0.50	D	0.992	...	+0.31
BM-076	+0.42	D	0.998	...	+0.23
BM-077	+0.17	D	1.000	0.00	-0.04
BM-078	-0.06	D	0.999	...	-0.29
BM-079	+0.02	D	0.998	...	-0.21
BM-080	+0.77	D	0.992	...	+0.59
BM-081	+0.35	D	0.994	-0.13	+0.15
BM-082	+0.10	D	1.000	...	-0.12
BM-083	+1.09	D:	0.582	...	+0.94
BM-084	+0.29	D	0.994	...	+0.09
BM-085	+0.38	D	0.994	...	+0.19
BM-086	+0.75	D	0.996	...	+0.58
BM-087	...	N	...	...	...
BM-088	+0.67	D	0.997	...	+0.49
BM-089	+0.39	D	0.988	...	+0.20
BM-090	+0.47	D	0.997	...	+0.28
BM-091	+1.23	D	0.993	...	+1.09 <sup>a</sup>
BM-092	+0.18	D	0.999	...	-0.03
BM-093	+0.23	D	1.000	...	+0.03
BM-095	+0.53	D	0.994	...	+0.35
BM-096	+0.10	D	0.994	...	-0.12
BM-097	+0.46	D	0.995	...	+0.27
BM-099	+0.13	D	0.998	...	-0.09
BM-100	+0.51	D	0.959	...	+0.32
BM-101	-0.02	D	0.843	-0.03	-0.24
BM-102	+0.17	D	0.994	...	-0.05
BM-103	...	N	...	...	...
BM-104	+0.72	D	0.992	...	+0.54
BM-105	+0.30	D	0.999	...	+0.10
BM-106	-0.04	D	0.999	...	-0.27
BM-107	+1.03	D	0.984	...	+0.88 <sup>a</sup>
BM-108	+0.25	D	0.991	...	+0.05
BM-109	+0.04	D	1.000	...	-0.18
BM-110	+0.23	D	0.979	...	+0.02
BM-111	+0.80	D:	0.669	-1.05	+0.63
BM-112	+0.36	D	0.979	...	+0.16
BM-113	+0.22	D	0.991	...	+0.01
BM-114	-0.33	D	0.997	-0.41	-0.57
BM-115	+0.33	D	0.824	...	+0.13
BM-117	...	N	...	...	...
BM-118	+0.15	D	0.998	...	-0.06
BM-119	+0.29	D	0.999	...	+0.09
BM-120	-0.61	D	0.998	...	-0.87
BM-121	-0.28	D	0.989	-0.72	-0.53
BM-122	-0.08	D	0.997	...	-0.31
BM-123	+0.61	D	0.983	...	+0.43
BM-125	+0.71	L	0.935	...	+0.71
BM-126	+0.43	D	0.994	...	+0.24
BM-127	+0.42	D	0.998	...	+0.22
BM-128	+0.32	D	0.995	...	+0.11
BM-129	+0.35	D	0.999	...	+0.15
BM-130	+0.09	D	0.996	...	-0.13
BM-131	+0.01	D	0.996	...	-0.21
BM-132	+0.24	D	0.997	...	+0.03
BM-133	+0.18	D	0.994	...	-0.03
BM-134	+0.12	D	0.999	-0.23	-0.10
BM-135	+0.49	D	0.997	...	+0.30
BM-136	+0.60	D	0.998	...	+0.42
BM-138	+0.74	D	0.993	...	+0.57
BM-139	+0.18	D	0.992	...	-0.04
BM-140	+0.57	D	0.998	...	+0.38
BM-141	+0.03	D	0.994	+0.03	-0.19
BM-142	-0.93	D	0.994	...	-1.22
BM-143	+0.56	D	0.999	...	+0.37
BM-144	+0.18	D	1.000	-0.15	-0.04
BM-146	+0.39	D	0.987	-0.08	+0.19
BM-147	+0.03	D	0.999	...	-0.19
BM-148	+0.10	D	0.998	...	-0.12

**Table 3** — *Continued*

BM Name (1)	[C/Fe] <sub>S</sub> (2)	DETECT (3)	CC (4)	[C/Fe] <sub>H</sub> (5)	[C/Fe] <sub>C</sub> (6)
BM-149	+0.54	D	0.817	...	+0.36
BM-150	+0.96	D	0.791	...	+0.80 <sup>a</sup>
BM-151	+0.19	D	0.999	...	-0.02
BM-152	+0.37	D	0.997	...	+0.18
BM-153	-0.46	D	0.993	...	-0.72
BM-155	-0.22	D	0.997	...	-0.46
BM-157	+0.41	D	0.998	...	+0.22
BM-158	-0.03	D	0.993	...	-0.26
BM-159	+0.26	D	0.997	...	+0.06
BM-160	+0.41	D	0.999	...	+0.22
BM-161	+0.32	D	0.999	...	+0.12
BM-164	...	N	...	...	...
BM-165	+0.25	D	0.984	...	+0.04
BM-166	+0.32	D	0.992	...	+0.11
BM-167	+0.48	D	0.997	...	+0.29
BM-168	+0.40	D	0.993	...	+0.20
BM-169	+0.38	D	0.990	...	+0.18
BM-170	+0.15	D	0.998	-0.09	-0.06
BM-171	+0.52	D	0.998	...	+0.33
BM-172	+0.43	D	0.999	...	+0.23
BM-173	+0.17	D	0.984	...	-0.05
BM-174	+0.25	D	0.998	...	+0.05
BM-175	+0.13	D	0.998	...	-0.08
BM-176	+0.65	D	0.984	...	+0.47
BM-177	+0.36	D	0.994	...	+0.16
BM-178	-0.44	D	0.998	...	-0.69
BM-179	+0.08	D	0.997	...	-0.14
BM-180	+0.15	D	0.951	+0.05	-0.06
BM-181	+0.12	D	0.999	...	-0.10
BM-182	-0.46	D	0.997	-0.66	-0.72
BM-183	+0.12	D	1.000	...	-0.10
BM-185	+0.38	D	0.997	...	+0.18
BM-186	-0.75	D	0.991	...	-1.02
BM-187	+0.55	D	0.994	...	+0.36
BM-188	-0.44	D	0.862	...	-0.69
BM-189	+0.21	D	0.996	...	0.00
BM-190	-0.12	D	0.999	-0.30	-0.36
BM-191	-0.32	D	0.993	-0.75	-0.56
BM-192	+0.40	D	0.998	...	+0.20
BM-193	+0.13	D	0.997	...	-0.08
BM-194	-0.64	D	0.997	...	-0.90
BM-195	+0.34	D	0.999	-0.15	+0.14
BM-196	+0.40	D	0.999	+0.32	+0.20
BM-197	+0.26	D	0.990	...	+0.05
BM-198	+0.33	D	0.990	...	+0.13
BM-199	-0.01	D	0.999	-0.11	-0.24
BM-200	+0.43	D	0.985	...	+0.24
BM-201	+0.26	D	0.995	+0.08	+0.06
BM-202	+0.64	D	0.998	...	+0.46
BM-203	+0.49	D	0.998	...	+0.30
BM-204	+0.50	D	0.995	...	+0.31
BM-205	+0.45	D	0.989	...	+0.26
BM-206	+0.49	D	0.996	...	+0.30
BM-207	+0.07	D	0.999	...	-0.15
BM-208	+0.49	D	0.999	-0.15	+0.31
BM-209	+0.99	D	0.998	...	+0.83 <sup>a</sup>
BM-210	+0.44	D	0.830	...	+0.25
BM-211	+0.13	D	0.999	...	-0.08
BM-212	+0.12	D	0.999	...	-0.09
BM-213	+0.65	D	0.932	...	+0.47
BM-214	+0.39	D	0.998	...	+0.20
BM-215	+0.60	D	0.998	...	+0.41
BM-216	+0.53	D	0.996	...	+0.34
BM-217	+0.69	D	0.965	+0.39	+0.51
BM-218	+0.93	D	0.975	...	+0.77 <sup>a</sup>
BM-219	+0.25	D	0.985	...	+0.04
BM-220	+0.37	D	0.997	...	+0.17
BM-221	-0.20	D	0.991	...	-0.44
BM-222	+0.16	D	0.991	...	-0.05

**Table 3** — *Continued*

BM Name (1)	[C/Fe] <sub>S</sub> (2)	DETECT (3)	CC (4)	[C/Fe] <sub>H</sub> (5)	[C/Fe] <sub>C</sub> (6)
BM-223	+0.32	D	0.997	...	+0.12
BM-224	-0.49	D	0.955	-0.35	-0.74
BM-225	+0.44	D	0.909	...	+0.25
BM-226	...	N	...	...	...
BM-227	+0.02	D	0.997	...	-0.20
BM-228	+0.11	D	0.998	...	-0.11
BM-229	+0.16	D	0.975	...	-0.05
BM-230	+0.62	D	0.998	...	+0.44
BM-231	...	N	...	...	...
BM-232	+0.56	D	0.923	...	+0.38
BM-233	+0.10	D	0.974	+0.13	-0.12
BM-234	+0.70	D	0.992	...	+0.52
BM-235	-0.20	D	0.997	...	-0.44
BM-236	+0.54	D	0.995	...	+0.36
BM-237	+0.45	D	0.989	...	+0.25
BM-238	+0.18	D	0.982	...	-0.03
BM-239	+0.17	D	0.998	...	-0.04
BM-240	+0.11	D	0.998	-0.10	-0.11
BM-241	+0.41	D	0.986	...	+0.22
BM-242	+0.15	D	1.000	...	-0.07
BM-243	+0.04	D	0.996	...	-0.18
BM-244	-0.17	D	0.943	-0.15	-0.40
BM-245	-0.23	D	0.987	...	-0.46
BM-246	+0.45	D	0.984	...	+0.26
BM-247	+0.28	D	0.990	...	+0.08
BM-248	+0.54	D	0.995	...	+0.36
BM-249	...	N	...	...	...
BM-251	+0.05	D	0.992	-0.39	-0.17
BM-252	+0.27	D	0.999	...	+0.06
BM-253	+0.20	D	0.993	+0.19	-0.01
BM-254	+0.40	D	0.992	...	+0.20
BM-256	+0.14	D	0.864	-0.55	-0.08
BM-257	-0.65	D	0.987	-0.59	-0.92
BM-258	-0.13	D	0.999	+0.33	-0.36
BM-259	+0.26	D	0.998	...	+0.06
BM-260	-0.44	D	0.998	-0.60	-0.69
BM-261	+0.33	D	0.974	...	+0.12
BM-262	+0.11	D	0.999	...	-0.10
BM-264	-0.01	D	0.994	-0.02	-0.23
BM-265	+0.67	D	0.997	...	+0.49
BM-266	+0.11	D	0.999	-0.15	-0.10
BM-267	+0.44	D	0.999	...	+0.24
BM-268	+0.12	D	0.999	...	-0.09
BM-269	+0.30	D	1.000	...	+0.10
BM-270	+0.26	D	1.000	...	+0.06
BM-271	+0.53	D	0.990	...	+0.34
BM-272	+0.56	D	0.979	...	+0.37
BM-273	-0.08	D	0.856	...	-0.31
BM-274	-0.25	D	0.929	...	-0.49
BM-276	+0.49	D	0.998	-0.10	+0.30
BM-277	+0.06	D	0.995	...	-0.16
BM-279	-0.16	D	0.997	...	-0.40
BM-280	+0.22	D	0.967	...	+0.01
BM-281	+0.34	D	0.997	...	+0.14
BM-282	+0.46	D	0.995	...	+0.27
BM-284	+0.74	D:	0.659	...	+0.56
BM-285	+1.00	D	0.996	...	+0.84 <sup>a</sup>
BM-286	+0.67	D	0.989	+0.38	+0.49
BM-287	+1.37	D	0.934	...	+1.24 <sup>a</sup>
BM-288	+0.34	D	0.978	...	+0.14
BM-289	+0.39	D	0.999	...	+0.19
BM-290	-0.49	D	0.999	...	-0.75
BM-291	+0.61	D	0.996	...	+0.42
BM-292	+0.28	D	0.938	...	+0.08
BM-293	+0.23	D	0.998	...	+0.03
BM-294	+0.48	D	0.995	...	+0.29
BM-295	+0.24	D	0.999	...	+0.03
BM-297	+0.15	D	0.996	...	-0.07
BM-298	+0.24	D	0.974	...	+0.03

**Table 3** — *Continued*

BM Name (1)	[C/Fe] <sub>S</sub> (2)	DETECT (3)	CC (4)	[C/Fe] <sub>H</sub> (5)	[C/Fe] <sub>C</sub> (6)
BM-299	+0.59	D	0.963	...	+0.41
BM-300	+0.55	D	0.959	...	+0.36
BM-301	-0.05	D	1.000	-0.05	-0.28
BM-302	...	N	...	...	...
BM-303	+0.17	D	0.999	...	-0.04
BM-304	+0.01	D	0.996	...	-0.21
BM-305	+0.00	D	0.998	-0.22	-0.23
BM-306	-0.24	D	0.991	...	-0.48
BM-307	+0.68	D	0.962	...	+0.51
BM-308	+0.12	D	1.000	...	-0.10
BM-309	+0.90	D	0.979	...	+0.74 <sup>a</sup>
BM-310	+0.46	D	0.789	-1.05	+0.26
BM-311	-0.69	D	0.925	...	-0.96
BM-313	+0.50	D	0.927	...	+0.31
BM-314	+0.38	D	0.832	...	+0.18
BM-315	+0.56	D	0.904	...	+0.38
BM-316	+0.47	D	0.921	...	+0.28
BM-317	+0.09	D	0.999	...	-0.13
BM-318	+0.12	D	0.995	...	-0.10
BM-319	+0.58	D	0.977	...	+0.40
BM-320	+0.39	D	1.000	-0.01	+0.19
BM-321	+0.42	D	0.995	...	+0.22
BM-322	+0.64	D	0.969	...	+0.46
BM-323	+0.19	D	0.998	...	-0.02
BM-325	+0.37	D	0.966	...	+0.17
BM-326	+0.18	D	1.000	...	-0.03

<sup>a</sup> CEMP star ( $[\text{C}/\text{Fe}]_C \geq +0.7$ , DETECT = “D”, and CC  $\geq 0.7$ )

**Table 4**  
Parallaxes, Distance Estimates, and Proper Motions

BM Name (1)	$\pi_{\text{HIP}}$ (mas) (2)	$\sigma_{\pi_{\text{HIP}}}$ (mas) (3)	$D_{\text{pho}}$ (kpc) (4)	$D_{\text{HIP}}$ (kpc) (5)	$\sigma_{\pi_{\text{HIP}}} / \pi_{\text{HIP}}$ (6)	$D_{\text{ado}}$ (kpc) (7)	$\sigma_{D_{\text{ado}}}$ (kpc) (8)	$\mu_\alpha$ (mas yr $^{-1}$ ) (9)	$\mu_\delta$ (mas yr $^{-1}$ ) (10)	$\sigma_{\mu_\alpha}$ (mas yr $^{-1}$ ) (11)	$\sigma_{\mu_\delta}$ (mas yr $^{-1}$ ) (12)	HIP/TYCHO ID (13)
BM-001	6.71	1.40	0.097	0.149	0.21	0.097	0.015	8.82	23.43	1.50	0.80	921
BM-002	0.88	0.81	0.530	1.136	0.92	0.530	0.080	-1.25	-51.79	0.90	0.59	2463
BM-003	9.51	1.11	0.096	0.105	0.12	0.105	0.012	20.94	-546.76	1.31	0.79	3026
BM-004	4.24	1.14	0.133	0.236	0.27	0.133	0.020	61.47	-22.35	1.23	0.69	3134
BM-005	5.01	1.32	0.547	0.200	0.26	0.547	0.082	60.61	21.00	1.35	0.94	3554
BM-006	3.19	0.79	0.115	0.314	0.25	0.115	0.017	63.61	49.81	0.92	0.50	5104
BM-007	7.23	0.86	0.133	0.138	0.12	0.138	0.016	134.10	12.53	0.70	0.97	5455
BM-008	10.56	1.01	0.072	0.095	0.10	0.095	0.009	284.85	-8.13	0.93	0.72	5489
BM-009	15.35	1.17	0.042	0.065	0.08	0.065	0.005	-230.98	-459.24	1.14	0.87	6159
BM-010	7.61	1.38	0.125	0.131	0.18	0.131	0.024	55.01	-16.16	1.43	0.91	6164
BM-011	9.72	1.39	0.095	0.103	0.14	0.103	0.015	97.07	52.91	1.33	1.04	8383
BM-012	4.07	1.74	0.241	0.246	0.43	0.241	0.036	257.39	95.69	1.69	1.78	8572
BM-013	9.37	0.58	0.139	0.107	0.06	0.107	0.007	268.79	-30.03	0.58	0.79	8558
BM-014	2.77	1.29	0.185	0.361	0.47	0.185	0.028	24.23	-209.84	1.18	0.84	8786
BM-015	13.24	1.30	0.048	0.076	0.10	0.076	0.007	224.21	222.02	1.21	0.97	9056
BM-016	2.78	1.43	0.242	0.360	0.51	0.242	0.036	-1.21	-14.91	1.48	1.02	10114
BM-017	12.98	1.29	0.066	0.077	0.10	0.077	0.008	44.76	-172.67	1.31	1.10	10413
BM-018	4.26	1.14	0.116	0.235	0.27	0.116	0.017	-3.02	13.69	1.15	1.32	10583
BM-019	12.57	0.85	0.065	0.080	0.07	0.080	0.005	50.18	-114.85	0.88	0.92	11387
BM-021	5.75	1.56	0.197	0.174	0.27	0.197	0.030	400.23	-57.65	1.31	1.33	11729
BM-022	8.93	1.44	0.105	0.112	0.16	0.112	0.018	57.27	-187.74	1.85	1.48	11952
BM-023	9.89	1.86	0.089	0.101	0.19	0.101	0.019	29.86	25.68	1.99	1.47	12041
BM-024	2.33	1.20	0.519	0.429	0.52	0.519	0.078	81.07	1.47	1.06	1.13	12353
BM-025	4.73	0.78	0.092	0.211	0.17	0.211	0.035	22.88	11.64	0.87	0.97	11957
BM-026	6.18	0.72	0.175	0.162	0.12	0.162	0.019	65.62	92.88	0.67	0.83	12748
BM-028	0.17	1.45	0.178	5.882	8.53	0.178	0.027	3.63	10.41	1.03	1.19	13044
BM-029	2.70	2.04	0.549	0.370	0.76	0.549	0.082	0.20	20.18	2.20	2.02	13876
BM-030	2.60	0.74	0.180	0.385	0.28	0.180	0.027	-24.44	-8.74	0.68	0.83	14747
BM-032	5.56	1.40	0.160	0.180	0.25	0.160	0.024	-11.16	-7.28	1.39	1.18	15592
BM-033	0.50	1.03	1.200	2.000	2.06	1.200	0.180	31.66	-33.34	0.67	0.98	15709
BM-034	4.03	1.00	0.331	0.248	0.25	0.331	0.050	67.09	-78.56	1.41	0.91	16214
BM-035	3.93	1.53	0.302	0.255	0.39	0.302	0.045	79.54	-124.73	0.96	1.20	17001
BM-036	39.12	0.56	0.019	0.026	0.01	0.026	0.001	689.15	-213.18	0.83	0.61	17147
BM-037	2.84	0.64	0.167	0.352	0.23	0.167	0.025	3.22	22.40	0.62	0.73	17246
BM-038	2.19	0.95	0.203	0.457	0.43	0.203	0.030	13.97	26.10	0.96	0.99	17419
BM-039	1.83	0.74	0.996	0.546	0.40	0.996	0.149	19.94	-2.46	0.56	0.60	17639
BM-040	2.55	0.70	0.350	0.392	0.28	0.350	0.053	137.17	74.09	0.76	0.98	18742
BM-041	1.59	0.78	0.634	0.629	0.49	0.634	0.095	44.21	-4.40	0.81	0.63	19378
BM-042	7.11	0.71	0.109	0.141	0.10	0.141	0.014	20.04	175.40	0.72	0.72	19383
BM-043	2.88	1.08	0.197	0.347	0.38	0.197	0.030	27.33	-39.15	1.25	1.10	19701
BM-044	1.19	1.10	0.497	0.840	0.92	0.497	0.075	27.27	-68.31	0.80	1.10	20454
BM-045	1.40	0.88	1.377	0.714	0.63	1.377	0.207	-13.18	-56.20	0.81	0.80	21648
BM-046	1.23	0.65	0.255	0.813	0.53	0.255	0.038	32.00	12.36	0.78	1.03	21473
BM-047	13.80	10.93	0.144	0.072	0.79	0.144	0.022	36.38	-3.35	12.02	9.08	21906
BM-048	2.28	1.03	0.204	0.439	0.45	0.204	0.031	27.66	-41.72	1.04	1.36	21814
BM-049	1.63	1.53	0.176	0.614	0.94	0.176	0.026	-4.22	-2.20	1.33	1.18	22173
BM-050	6.62	1.79	0.176	0.151	0.27	0.176	0.026	-8.72	2.97	1.09	1.24	22436
BM-051	15.00	1.13	0.063	0.067	0.07	0.067	0.005	165.55	-27.75	0.81	1.25	22632
BM-052	-1.28	0.87	1.280	-0.781	-0.68	1.280	0.192	40.47	6.40	0.94	1.15	22629
BM-053	0.04	1.27	0.285	25.000	31.75	0.285	0.043	24.76	-13.74	0.99	1.60	23771

**Table 4** — *Continued*

BM Name	$\pi_{\text{HIP}}$ (mas)	$\sigma_{\pi_{\text{HIP}}}$ (mas)	$D_{\text{pho}}$ (kpc)	$D_{\text{HIP}}$ (kpc)	$\sigma_{\pi_{\text{HIP}}} / \pi_{\text{HIP}}$	$D_{\text{ado}}$ (kpc)	$\sigma_{D_{\text{ado}}}$ (kpc)	$\mu_\alpha$ (mas yr $^{-1}$ )	$\mu_\delta$ (mas yr $^{-1}$ )	$\sigma_{\mu_\alpha}$ (mas yr $^{-1}$ )	$\sigma_{\mu_\delta}$ (mas yr $^{-1}$ )	HIP/TYCHO ID
(1)	(2)	(3)	(4)	(5)	(6)	(7)	(8)	(9)	(10)	(11)	(12)	(13)
BM-054	2.65	0.99	0.704	0.377	0.37	0.704	0.106	30.36	130.52	1.07	1.28	23397
BM-055	3.16	1.28	0.201	0.317	0.41	0.201	0.030	1.75	-13.80	1.49	1.59	23696
BM-056	1.26	0.98	0.915	0.794	0.78	0.915	0.137	78.53	-29.96	0.91	1.07	24120
BM-057	4.65	1.21	0.239	0.215	0.26	0.239	0.036	-28.26	-1.45	1.50	1.60	24061
BM-058	1.98	0.96	0.738	0.505	0.48	0.738	0.111	49.07	-42.45	1.04	1.45	24074
BM-059	14.72	0.86	0.074	0.068	0.06	0.068	0.004	936.93	515.24	0.85	0.78	24316
BM-060	6.57	1.50	0.112	0.152	0.23	0.112	0.017	185.17	-239.08	1.48	1.82	24742
BM-061	1.37	1.28	0.280	0.730	0.93	0.280	0.042	-8.69	-19.25	1.15	0.99	25096
BM-062	13.97	0.97	0.063	0.072	0.07	0.072	0.005	-90.46	-77.52	0.85	1.18	25183
BM-063	0.46	0.58	1.243	2.174	1.26	1.243	0.186	2.98	-17.16	0.56	0.66	25916
BM-064	2.99	0.86	0.334	0.334	0.29	0.334	0.050	10.55	-122.65	1.04	1.01	26040
BM-065	3.82	1.33	0.115	0.262	0.35	0.115	0.017	20.59	-34.90	1.36	1.48	26242
BM-067	2.50	0.47	0.467	0.400	0.19	0.400	0.075	37.49	-47.90	0.37	0.35	26740
BM-068	2.72	0.82	0.226	0.368	0.30	0.226	0.076	2.48	1.56	0.88	1.07	26489
BM-069	15.49	0.78	0.039	0.065	0.05	0.065	0.003	-82.13	288.35	0.55	0.74	27128
BM-070	1.69	0.86	0.304	0.592	0.51	0.304	0.046	-0.54	18.46	0.79	0.83	27047
BM-071	10.34	0.69	0.080	0.097	0.07	0.097	0.006	-19.04	34.55	0.71	0.38	28224
BM-072	2.73	0.72	0.269	0.366	0.26	0.269	0.040	-16.82	21.43	0.74	0.65	28055
BM-073	4.02	1.56	0.105	0.249	0.39	0.105	0.016	-26.25	-44.41	1.64	1.14	28627
BM-074	6.84	1.11	0.070	0.146	0.16	0.146	0.024	-13.65	3.20	0.88	0.91	28733
BM-075	4.30	1.69	0.160	0.233	0.39	0.160	0.024	-10.87	1.52	1.60	1.49	29799
BM-076	4.74	0.98	0.089	0.211	0.21	0.089	0.013	-20.31	58.12	1.02	1.34	28880
BM-077	5.57	0.84	0.396	0.180	0.15	0.180	0.027	81.72	-40.71	0.86	0.81	29992
BM-078	5.38	0.34	0.128	0.186	0.06	0.186	0.012	-11.35	19.62	0.42	0.46	29427
BM-079	0.56	1.13	0.831	1.786	2.02	0.831	0.125	14.89	-24.42	0.84	0.92	30196
BM-080	1.65	0.78	0.285	0.606	0.47	0.285	0.043	0.20	0.26	0.81	0.66	30269
BM-081	6.72	0.70	0.138	0.149	0.10	0.149	0.016	8.07	-90.36	0.76	0.63	30668
BM-082	5.50	0.54	0.179	0.182	0.10	0.182	0.018	81.31	-89.33	0.46	0.52	30705
BM-083	2.10	0.86	0.586	0.476	0.41	0.586	0.088	71.62	-45.06	0.92	0.94	31400
BM-084	3.24	1.12	0.166	0.309	0.35	0.166	0.025	12.08	-17.34	0.95	1.27	32154
BM-085	4.58	1.37	0.366	0.218	0.30	0.366	0.055	15.72	33.68	1.50	1.11	32445
BM-086	10.42	0.88	0.124	0.096	0.08	0.096	0.008	-177.53	-148.36	0.82	0.89	33221
BM-087	3.92	1.28	0.132	0.255	0.33	0.132	0.020	23.67	-22.01	1.23	0.97	34309
BM-088	6.67	1.25	0.123	0.150	0.19	0.150	0.028	-21.06	28.22	1.38	1.18	34625
BM-089	7.09	1.17	0.163	0.141	0.17	0.141	0.023	159.67	-270.31	1.11	1.14	36269
BM-090	9.03	0.97	0.095	0.111	0.11	0.111	0.012	-18.07	-8.63	0.83	1.10	36686
BM-091	22.50	0.59	0.029	0.044	0.03	0.044	0.001	-35.07	95.55	0.46	0.43	36836
BM-092	18.57	0.64	0.026	0.054	0.03	0.054	0.002	228.91	-123.02	0.73	0.42	37233
BM-093	13.61	0.98	0.031	0.073	0.07	0.074	0.005	-44.35	-156.21	0.80	0.54	37327
BM-095	8.22	1.51	0.118	0.122	0.18	0.122	0.022	30.93	57.90	1.27	1.02	37964
BM-096	...	...	0.324	...	...	0.324	0.049	49.00	-45.60	1.50	1.50	5986-1000-1
BM-097	6.95	0.78	0.070	0.144	0.11	0.144	0.016	-11.68	-49.35	0.74	0.84	39188
BM-099	2.33	1.19	0.406	0.429	0.51	0.406	0.061	-11.37	-0.05	1.11	1.24	40886
BM-100	2.30	1.72	0.711	0.435	0.75	0.711	0.107	26.20	-14.20	1.36	1.20	41869
BM-101	7.86	1.31	0.110	0.127	0.17	0.127	0.021	351.36	-484.58	1.16	1.01	42592
BM-102	4.97	1.12	0.135	0.201	0.23	0.135	0.020	-41.68	17.05	0.89	0.71	42668
BM-103	4.53	1.60	0.266	0.221	0.35	0.266	0.040	-331.75	-161.08	1.65	1.04	43099
BM-104	6.57	1.05	0.107	0.152	0.16	0.152	0.024	70.05	-12.70	0.77	0.52	44919
BM-105	24.53	0.56	0.029	0.041	0.02	0.041	0.001	-64.66	-132.61	0.60	0.57	44811
BM-106	3.13	0.60	0.426	0.320	0.19	0.320	0.061	-102.15	85.16	0.75	0.59	45845

Table 4 — *Continued*

BM Name (1)	$\pi_{\text{HIP}}$ (mas) (2)	$\sigma_{\pi_{\text{HIP}}}$ (mas) (3)	$D_{\text{pho}}$ (kpc) (4)	$D_{\text{HIP}}$ (kpc) (5)	$\sigma_{\pi_{\text{HIP}}} / \pi_{\text{HIP}}$ (6)	$D_{\text{ado}}$ (kpc) (7)	$\sigma_{D_{\text{ado}}}$ (kpc) (8)	$\mu_{\alpha}$ (mas yr <sup>-1</sup> ) (9)	$\mu_{\delta}$ (mas yr <sup>-1</sup> ) (10)	$\sigma_{\mu_{\alpha}}$ (mas yr <sup>-1</sup> ) (11)	$\sigma_{\mu_{\delta}}$ (mas yr <sup>-1</sup> ) (12)	HIP/TYCHO ID (13)
BM-107	4.22	0.92	0.108	0.237	0.22	0.108	0.074	-10.51	-12.44	0.93	0.85	46011
BM-108	3.01	0.93	0.083	0.332	0.31	0.083	0.012	-38.29	9.91	1.10	0.91	46132
BM-109	1.14	0.89	0.126	0.877	0.78	0.126	0.019	-7.30	23.78	0.69	0.64	46332
BM-110	-1.25	1.57	0.388	-0.800	-1.26	0.388	0.058	-12.03	-15.02	0.96	1.26	46508
BM-111	2.86	1.05	0.549	0.350	0.37	0.549	0.082	37.33	-126.15	1.43	0.76	46822
BM-112	4.50	0.89	0.101	0.222	0.20	0.222	0.044	-24.93	3.01	0.89	0.83	
BM-113	3.16	0.78	0.071	0.317	0.25	0.071	0.060	-16.36	20.53	0.68	0.73	47021
BM-114	0.96	0.77	0.830	1.042	0.80	0.830	0.125	-17.06	-20.12	0.67	0.54	47139
BM-115	10.26	0.95	0.088	0.098	0.09	0.098	0.009	27.99	18.14	0.85	0.85	47048
BM-117	5.65	0.71	0.114	0.177	0.13	0.177	0.022	-41.93	29.93	0.54	0.57	47155
BM-118	10.92	0.87	0.078	0.092	0.08	0.092	0.007	-126.62	90.13	0.75	0.82	47643
BM-119	33.90	14.14	0.047	0.029	0.42	0.047	0.007	-19.38	86.91	12.41	13.16	47836
BM-120	0.12	0.65	1.183	8.333	5.42	1.183	0.177	-19.58	-3.25	0.52	0.54	48019
BM-121	3.41	1.20	1.992	0.293	0.35	1.992	0.299	-16.61	-22.27	1.28	0.96	48516
BM-122	0.96	1.26	0.417	1.042	1.31	0.417	0.063	4.29	-5.05	1.22	1.02	48979
BM-123	5.69	0.91	0.106	0.176	0.16	0.176	0.028	-1.73	6.28	0.73	0.82	49009
BM-125	2.65	1.00	0.142	0.377	0.38	0.142	0.087	-21.18	9.66	0.79	0.86	49918
BM-126	8.09	1.12	0.115	0.124	0.14	0.124	0.017	-20.38	2.69	0.98	0.97	50834
BM-127	16.23	0.63	0.046	0.062	0.04	0.062	0.002	-148.68	56.72	0.50	0.45	50883
BM-128	4.81	2.26	0.105	0.208	0.47	0.105	0.016	-1.35	-15.50	2.02	1.93	51144
BM-129	15.19	0.67	0.037	0.066	0.04	0.066	0.003	-219.24	119.81	0.69	0.68	51216
BM-130	16.71	0.89	0.048	0.060	0.05	0.060	0.003	-130.94	50.56	0.89	0.90	51415
BM-131	4.94	1.17	0.087	0.202	0.24	0.087	0.073	3.77	-7.85	1.17	1.18	51545
BM-132	5.45	1.04	0.108	0.184	0.19	0.184	0.035	-55.27	31.64	1.01	0.84	52090
BM-133	1.96	1.24	0.549	0.510	0.63	0.549	0.082	-12.61	-41.29	0.91	1.08	52297
BM-134	1.49	1.04	0.591	0.671	0.70	0.591	0.089	-20.91	-46.90	0.89	0.88	52781
BM-135	3.43	1.72	0.129	0.291	0.50	0.129	0.019	-2.96	22.26	1.93	1.31	53235
BM-136	...	...	0.119	...	...	0.119	0.018	30.30	-28.30	2.30	0.00	7212-1089-1
BM-138	18.36	0.58	0.042	0.054	0.03	0.055	0.002	160.06	-201.30	0.61	0.54	54641
BM-139	10.29	1.30	0.128	0.097	0.13	0.097	0.012	-124.38	174.73	1.22	0.83	55790
BM-140	9.32	1.05	0.063	0.107	0.11	0.107	0.012	-172.66	25.03	1.10	0.97	55909
BM-141	2.87	0.91	0.623	0.348	0.32	0.623	0.093	10.94	-25.94	0.88	0.87	56074
BM-142	1.10	1.19	0.225	0.909	1.08	0.225	0.034	-14.85	8.30	0.90	0.72	56635
BM-143	9.45	1.07	0.117	0.106	0.11	0.106	0.012	32.08	-107.09	0.93	0.75	56664
BM-144	0.90	1.03	0.195	1.111	1.14	0.195	0.029	-315.13	-14.50	1.09	0.65	56713
BM-146	13.00	0.98	0.076	0.077	0.07	0.077	0.006	60.32	-109.88	0.62	0.72	57360
BM-147	1.77	1.03	1.319	0.565	0.58	1.319	0.198	-114.11	12.49	1.09	0.90	57787
BM-148	1.10	1.19	0.322	0.909	1.08	0.322	0.048	-55.41	14.85	1.06	0.71	57982
BM-149	-0.34	1.41	0.710	-2.941	-4.15	0.710	0.107	-51.55	-6.86	1.55	1.00	58378
BM-150	6.85	1.09	0.130	0.146	0.16	0.146	0.023	-99.22	-65.88	0.83	0.68	58435
BM-151	4.23	1.71	0.115	0.236	0.40	0.115	0.017	-1.79	-7.40	1.45	1.01	58532
BM-152	3.99	2.05	0.245	0.251	0.51	0.245	0.037	-32.13	-7.78	1.85	1.15	58611
BM-153	-0.72	1.23	1.690	-1.389	-1.71	1.690	0.254	-33.41	-6.55	1.18	0.67	58896
BM-155	-0.53	1.37	1.006	-1.887	-2.58	1.006	0.151	-6.62	-28.59	1.19	1.01	59158
BM-157	10.31	1.17	0.134	0.097	0.11	0.097	0.011	-5.46	-207.89	0.86	0.72	59699
BM-158	5.96	1.75	0.224	0.168	0.29	0.224	0.034	-24.16	-120.96	1.94	0.84	59696
BM-159	3.97	1.19	0.585	0.252	0.30	0.585	0.088	-67.69	-10.97	0.88	0.72	59837
BM-160	19.96	0.66	0.035	0.050	0.03	0.050	0.002	48.45	-34.70	0.53	0.45	60497
BM-161	12.52	1.20	0.056	0.080	0.10	0.080	0.008	-321.38	-214.65	0.85	1.05	60779
BM-164	9.94	0.96	0.118	0.101	0.10	0.101	0.010	-19.25	-18.49	1.05	0.65	61646

Table 4 — *Continued*

BM Name (1)	$\pi_{\text{HIP}}$ (mas) (2)	$\sigma_{\pi_{\text{HIP}}}$ (mas) (3)	$D_{\text{pho}}$ (kpc) (4)	$D_{\text{HIP}}$ (kpc) (5)	$\sigma_{\pi_{\text{HIP}}} / \pi_{\text{HIP}}$ (6)	$D_{\text{ado}}$ (kpc) (7)	$\sigma_{D_{\text{ado}}}$ (kpc) (8)	$\mu_{\alpha}$ (mas yr $^{-1}$ ) (9)	$\mu_{\delta}$ (mas yr $^{-1}$ ) (10)	$\sigma_{\mu_{\alpha}}$ (mas yr $^{-1}$ ) (11)	$\sigma_{\mu_{\delta}}$ (mas yr $^{-1}$ ) (12)	HIP/TYCHO ID (13)
BM-165	2.69	1.62	0.262	0.372	0.60	0.262	0.109	13.09	-3.63	1.63	0.98	62020
BM-166	8.17	1.43	0.146	0.122	0.17	0.122	0.021	-222.01	-17.66	0.84	0.78	62108
BM-167	9.48	0.86	0.081	0.106	0.09	0.106	0.010	-23.11	58.32	0.62	0.55	62538
BM-168	5.18	1.77	0.168	0.193	0.34	0.168	0.025	-66.20	-18.80	1.30	0.84	62525
BM-169	3.92	1.36	0.183	0.255	0.35	0.183	0.080	-11.85	-19.55	1.13	0.73	62649
BM-170	4.33	0.86	0.197	0.231	0.20	0.231	0.046	-274.59	-321.90	0.80	0.49	62747
BM-171	14.53	1.04	0.034	0.069	0.07	0.069	0.005	-43.89	79.65	0.85	0.68	62923
BM-172	10.50	1.26	0.087	0.095	0.12	0.095	0.011	299.64	-794.83	0.96	0.63	62882
BM-173	0.11	2.12	0.219	9.091	19.27	0.219	0.121	-16.78	3.78	2.55	1.18	63067
BM-174	18.03	0.84	0.034	0.056	0.05	0.056	0.003	-476.58	-203.12	0.90	0.48	63559
BM-175	8.74	0.90	0.072	0.114	0.10	0.114	0.012	4.68	11.46	0.79	0.96	63689
BM-176	7.41	1.69	0.127	0.135	0.23	0.127	0.019	9.35	-28.62	1.38	0.83	63719
BM-177	4.91	1.11	0.347	0.204	0.23	0.347	0.052	10.05	-18.83	0.84	0.70	64462
BM-178	5.40	1.76	0.137	0.185	0.33	0.137	0.021	-46.07	-15.90	1.46	1.18	64479
BM-179	3.05	1.56	0.260	0.328	0.51	0.260	0.039	-1.15	-24.89	1.53	1.09	65047
BM-180	14.66	1.37	0.077	0.068	0.09	0.068	0.006	-753.37	104.52	1.31	1.15	65201
BM-181	4.38	1.06	0.293	0.228	0.24	0.293	0.044	-58.11	-22.89	0.91	0.64	65819
BM-182	0.37	1.19	1.519	2.703	3.22	1.519	0.228	-24.52	-12.87	1.70	0.94	66246
BM-183	3.38	1.75	0.444	0.296	0.52	0.444	0.067	21.89	-58.43	1.72	1.23	67181
BM-185	5.31	1.29	0.075	0.188	0.24	0.075	0.011	47.48	-19.99	1.19	1.22	67791
BM-186	1.46	1.20	1.496	0.685	0.82	1.496	0.224	-35.28	-10.88	1.47	1.10	67964
BM-187	8.62	0.91	0.079	0.116	0.11	0.116	0.012	-114.13	-35.55	0.82	0.84	68246
BM-188	10.46	1.07	0.098	0.096	0.10	0.096	0.010	-453.33	-81.62	0.89	0.83	68464
BM-189	9.45	1.12	0.106	0.106	0.12	0.106	0.013	-2.37	-4.08	1.10	0.97	68565
BM-190	3.16	0.59	0.447	0.317	0.19	0.317	0.059	-93.92	-43.86	0.57	0.49	68807
BM-191	0.01	1.34	0.811	100.00	134.0	0.811	0.122	-93.57	-29.73	1.80	1.12	69470
BM-192	4.44	2.16	0.063	0.225	0.49	0.063	0.009	-34.51	-25.68	1.38	1.95	69909
BM-193	5.76	1.38	0.118	0.174	0.24	0.118	0.018	4.24	-7.73	1.23	1.50	70312
BM-194	1.44	1.29	2.228	0.694	0.90	2.228	0.334	-24.11	-13.15	1.14	1.09	70199
BM-195	3.82	0.77	0.299	0.262	0.20	0.262	0.045	25.31	-105.69	0.58	0.53	70519
BM-196	0.89	1.23	0.724	1.124	1.38	0.724	0.109	-15.97	-53.09	1.08	0.95	70647
BM-197	7.51	1.30	0.118	0.133	0.17	0.133	0.023	23.75	-6.51	1.09	1.03	70925
BM-198	8.72	1.06	0.091	0.115	0.12	0.115	0.014	-19.14	-38.80	0.71	0.87	71341
BM-199	2.24	1.51	1.510	0.446	0.67	1.510	0.227	-9.27	-9.50	1.64	1.13	71375
BM-200	4.04	1.30	0.162	0.247	0.32	0.162	0.093	-51.14	13.99	1.44	1.07	71414
BM-201	6.09	1.08	0.111	0.164	0.18	0.164	0.029	62.11	-342.60	1.71	0.83	71458
BM-202	12.80	0.94	0.052	0.078	0.07	0.078	0.006	49.35	23.46	0.85	0.96	71693
BM-203	5.42	1.49	0.123	0.184	0.28	0.123	0.018	-52.28	29.76	1.80	1.34	71761
BM-204	6.15	1.50	0.109	0.163	0.24	0.109	0.016	-61.20	76.57	1.88	1.43	71844
BM-205	6.97	1.82	0.153	0.143	0.26	0.153	0.023	15.62	4.01	1.99	1.97	72038
BM-206	20.06	0.71	0.037	0.050	0.04	0.050	0.002	54.00	112.43	0.69	0.60	72673
BM-207	6.64	1.14	0.057	0.151	0.17	0.151	0.026	21.76	-40.71	1.03	0.82	72960
BM-208	10.23	0.84	0.037	0.098	0.08	0.098	0.008	-558.49	-500.37	0.85	0.68	73385
BM-209	3.59	2.26	0.220	0.279	0.63	0.220	0.033	-149.31	-37.21	2.39	1.45	73444
BM-210	7.07	1.33	0.139	0.141	0.19	0.141	0.027	-0.09	1.91	1.52	1.10	73505
BM-211	4.40	1.51	0.070	0.227	0.34	0.070	0.011	-60.38	-36.66	1.43	1.43	73780
BM-212	2.53	1.42	0.829	0.395	0.56	0.829	0.124	-30.01	-3.78	1.91	1.50	73781
BM-213	5.86	1.29	0.102	0.171	0.22	0.102	0.082	-130.95	-42.39	1.21	1.15	74717
BM-214	9.34	0.83	0.071	0.107	0.09	0.107	0.010	86.52	-44.27	0.83	0.78	75781
BM-215	6.85	1.58	0.099	0.146	0.23	0.099	0.015	-48.32	58.06	1.45	1.29	76226

**Table 4** — *Continued*

BM Name (1)	$\pi_{\text{HIP}}$ (mas) (2)	$\sigma_{\pi_{\text{HIP}}}$ (mas) (3)	$D_{\text{pho}}$ (kpc) (4)	$D_{\text{HIP}}$ (kpc) (5)	$\sigma_{\pi_{\text{HIP}}} / \pi_{\text{HIP}}$ (6)	$D_{\text{ado}}$ (kpc) (7)	$\sigma_{D_{\text{ado}}}$ (kpc) (8)	$\mu_\alpha$ (mas yr <sup>-1</sup> ) (9)	$\mu_\delta$ (mas yr <sup>-1</sup> ) (10)	$\sigma_{\mu_\alpha}$ (mas yr <sup>-1</sup> ) (11)	$\sigma_{\mu_\delta}$ (mas yr <sup>-1</sup> ) (12)	HIP/TYCHO ID (13)
BM-216	11.22	1.94	0.073	0.089	0.17	0.089	0.015	-17.07	-44.98	2.35	1.71	76657
BM-217	17.44	0.97	0.071	0.057	0.06	0.057	0.003	-1115.54	-302.77	0.93	0.83	76976
BM-218	4.85	1.08	0.418	0.206	0.22	0.418	0.063	19.43	-10.99	1.14	1.16	77383
BM-219	15.06	0.78	0.062	0.066	0.05	0.066	0.003	-39.18	-27.01	0.97	0.87	77427
BM-220	6.42	1.04	0.048	0.156	0.16	0.156	0.025	-67.89	-11.23	0.90	0.83	77727
BM-221	4.50	1.62	0.331	0.222	0.36	0.331	0.050	-42.98	-78.72	1.79	1.57	77735
BM-222	1.06	0.91	0.189	0.943	0.86	0.189	0.028	0.83	-5.46	0.66	0.83	78289
BM-223	10.93	1.23	0.075	0.092	0.11	0.092	0.010	-9.40	48.95	1.24	1.14	77944
BM-224	6.35	0.78	0.222	0.158	0.12	0.158	0.019	-23.38	-36.47	0.79	0.77	78378
BM-225	4.91	2.13	0.785	0.204	0.43	0.785	0.118	-47.91	-59.81	2.13	1.69	79271
BM-226	4.47	1.10	0.158	0.224	0.25	0.158	0.078	19.93	-1.64	0.97	0.97	81329
BM-227	12.93	1.23	0.070	0.077	0.10	0.077	0.007	-1.28	-48.17	1.42	1.32	81166
BM-228	6.08	1.69	0.069	0.165	0.28	0.069	0.010	-10.51	-5.06	1.71	1.57	81789
BM-229	8.53	0.93	0.318	0.117	0.11	0.117	0.013	-7.30	0.56	1.23	0.65	81920
BM-230	14.42	0.79	0.053	0.069	0.06	0.069	0.004	-64.42	18.83	0.56	0.56	83243
BM-231	11.11	0.83	0.102	0.090	0.07	0.090	0.007	2.22	-44.36	1.16	0.68	84895
BM-232	2.30	1.27	0.568	0.435	0.55	0.568	0.085	7.81	-6.04	1.40	0.56	85990
BM-233	9.09	1.31	0.100	0.110	0.14	0.110	0.016	-61.77	-395.70	1.55	1.10	86694
BM-234	8.67	0.95	0.084	0.115	0.11	0.115	0.013	31.39	26.25	0.50	0.76	87285
BM-235	-1.35	1.60	1.347	-0.741	-1.19	1.347	0.202	28.99	-24.81	1.07	1.39	87492
BM-236	9.09	1.27	0.215	0.110	0.14	0.110	0.015	-145.04	-209.55	1.65	0.90	87101
BM-237	...	...	0.076	...	...	0.076	0.056	-8.70	-0.70	1.40	1.50	7385-1410-1
BM-238	...	...	0.146	...	...	0.146	0.084	-14.60	-44.50	1.60	1.80	7378-947-1
BM-239	9.38	1.41	0.096	0.107	0.15	0.107	0.016	-44.23	-53.74	1.93	1.09	87731
BM-240	4.56	0.84	0.616	0.219	0.18	0.219	0.040	-98.98	-190.05	0.86	0.52	88977
BM-241	15.80	0.91	0.075	0.063	0.06	0.063	0.004	-260.62	-125.75	0.93	0.68	89554
BM-242	8.97	1.24	0.052	0.112	0.14	0.112	0.015	30.62	-24.75	1.15	1.04	89733
BM-243	0.91	1.29	0.274	1.099	1.42	0.274	0.041	-15.11	-14.68	1.30	0.94	89987
BM-244	4.47	1.12	0.584	0.224	0.25	0.584	0.088	-8.33	1.73	1.35	0.97	91182
BM-245	1.73	1.38	1.105	0.578	0.80	1.105	0.166	-5.08	27.46	1.66	1.06	92610
BM-246	3.54	1.60	0.133	0.282	0.45	0.133	0.020	20.53	-160.71	1.75	1.30	93186
BM-247	3.39	1.19	0.288	0.295	0.35	0.288	0.043	12.17	-131.09	1.22	0.84	93288
BM-248	13.92	0.74	0.054	0.072	0.05	0.072	0.004	-29.45	-34.24	0.92	0.70	93444
BM-249	1.15	1.76	...	0.870	1.53	...	-9.999	-2.40	-2.10	1.79	1.55	93550
BM-251	-0.26	3.62	0.324	-3.846	-13.9	0.324	0.049	-6.69	-56.16	3.76	2.70	94196
BM-252	2.87	1.17	0.704	0.348	0.41	0.704	0.106	-38.37	-169.80	1.16	0.80	94964
BM-253	10.86	1.77	0.094	0.092	0.16	0.092	0.015	-67.64	-816.50	2.37	1.54	95333
BM-254	9.62	1.07	0.114	0.104	0.11	0.104	0.012	57.27	-54.03	0.56	0.93	95800
BM-256	4.97	0.71	0.254	0.201	0.14	0.201	0.029	131.12	-198.13	0.68	0.44	96248
BM-257	2.31	1.01	1.289	0.433	0.44	1.289	0.193	3.67	-52.70	1.49	1.02	96508
BM-258	1.59	1.14	1.240	0.629	0.72	1.240	0.186	-20.79	-83.30	1.30	0.77	97192
BM-259	9.43	0.61	0.058	0.106	0.07	0.106	0.007	-7.56	13.64	0.55	0.49	97591
BM-260	1.45	0.82	0.730	0.690	0.57	0.730	0.110	37.00	-57.87	0.77	0.35	97468
BM-261	6.33	1.91	0.173	0.158	0.30	0.173	0.026	8.93	-436.12	2.75	2.08	98002
BM-262	6.96	1.33	0.093	0.144	0.19	0.144	0.027	57.81	-14.82	1.50	1.18	97981
BM-264	0.92	1.14	1.470	1.087	1.24	1.470	0.221	12.93	-90.92	1.37	0.68	98339
BM-265	5.46	1.32	0.094	0.183	0.24	0.094	0.014	0.15	45.05	1.48	1.17	98883
BM-266	4.78	0.98	0.220	0.209	0.20	0.209	0.033	-36.25	-166.24	1.26	0.85	98974
BM-267	5.46	1.11	0.064	0.183	0.20	0.064	0.010	0.68	44.57	0.73	0.81	99496
BM-268	17.64	0.82	0.038	0.057	0.05	0.057	0.003	314.39	-129.51	0.90	0.61	99938

Table 4 — *Continued*

BM Name (1)	$\pi_{\text{HIP}}$ (mas) (2)	$\sigma_{\pi_{\text{HIP}}}$ (mas) (3)	$D_{\text{pho}}$ (kpc) (4)	$D_{\text{HIP}}$ (kpc) (5)	$\sigma_{\pi_{\text{HIP}}} / \pi_{\text{HIP}}$ (6)	$D_{\text{ado}}$ (kpc) (7)	$\sigma_{D_{\text{ado}}}$ (kpc) (8)	$\mu_{\alpha}$ (mas yr $^{-1}$ ) (9)	$\mu_{\delta}$ (mas yr $^{-1}$ ) (10)	$\sigma_{\mu_{\alpha}}$ (mas yr $^{-1}$ ) (11)	$\sigma_{\mu_{\delta}}$ (mas yr $^{-1}$ ) (12)	HIP/TYCHO ID (13)
BM-269	0.92	1.08	0.346	1.087	1.17	0.346	0.052	-20.71	-97.94	1.34	1.07	100248
BM-270	5.24	1.75	0.067	0.191	0.33	0.067	0.010	70.12	10.36	2.28	1.49	100257
BM-271	9.24	0.85	0.063	0.108	0.09	0.108	0.010	-149.30	-122.04	0.99	0.80	100394
BM-272	8.51	1.35	0.147	0.118	0.16	0.118	0.019	-25.40	75.14	1.13	0.82	101103
BM-273	3.21	1.63	0.150	0.311	0.51	0.150	0.023	-26.00	-46.80	2.32	1.33	101176
BM-274	-1.21	1.55	0.876	-0.826	-1.28	0.876	0.131	17.84	-16.57	1.84	1.27	101306
BM-276	16.15	0.93	0.048	0.062	0.06	0.062	0.004	44.61	-429.58	0.89	0.74	102046
BM-277	7.58	1.94	0.110	0.132	0.26	0.110	0.017	15.12	31.16	2.46	1.37	102204
BM-279	-0.03	1.62	1.352	-33.33	-54.0	1.352	0.203	-17.44	-6.18	1.88	1.51	102225
BM-280	7.16	1.45	0.134	0.140	0.20	0.134	0.020	-60.68	-319.04	1.80	1.11	102337
BM-281	4.23	2.16	0.170	0.236	0.51	0.170	0.026	44.90	-153.56	3.00	1.56	103161
BM-282	4.44	1.59	0.155	0.225	0.36	0.155	0.023	37.60	4.43	2.44	1.45	103479
BM-284	2.71	1.42	0.430	0.369	0.52	0.430	0.065	-8.54	-0.22	1.54	1.07	103663
BM-285	5.47	1.72	0.560	0.183	0.31	0.560	0.084	-15.18	-102.96	0.89	1.25	104151
BM-286	2.54	1.15	0.376	0.394	0.45	0.376	0.056	192.53	-274.00	1.38	0.92	104191
BM-287	6.49	0.93	0.333	0.154	0.14	0.154	0.022	16.38	-4.45	0.84	0.59	104408
BM-288	8.01	1.57	0.161	0.125	0.20	0.125	0.024	62.00	-16.13	1.54	0.91	104437
BM-289	24.26	0.97	0.028	0.041	0.04	0.041	0.002	-579.48	-117.82	1.00	0.64	106560
BM-290	2.03	1.30	1.184	0.493	0.64	1.184	0.178	-30.89	-41.42	1.46	0.75	106724
BM-291	5.28	1.51	0.176	0.189	0.29	0.176	0.026	60.90	-6.72	1.50	1.08	107052
BM-292	1.99	1.64	0.228	0.502	0.82	0.228	0.105	14.60	10.23	1.68	0.84	107719
BM-293	24.91	0.56	0.039	0.040	0.02	0.040	0.001	341.57	-85.34	0.53	0.38	107877
BM-294	5.04	1.46	0.120	0.198	0.29	0.120	0.018	-106.64	-101.73	1.20	0.85	108168
BM-295	2.51	1.06	0.270	0.398	0.42	0.270	0.041	131.61	-198.77	0.98	0.53	108132
BM-297	3.30	0.65	0.111	0.303	0.20	0.303	0.060	34.95	-254.12	0.55	0.39	108361
BM-298	10.82	0.76	0.098	0.092	0.07	0.092	0.006	16.60	-1.97	0.76	0.52	108475
BM-299	4.51	1.33	0.216	0.222	0.29	0.216	0.032	18.14	-22.97	1.18	0.89	108702
BM-300	7.71	1.17	0.129	0.130	0.15	0.130	0.020	43.83	8.68	1.09	0.69	108730
BM-301	4.18	1.30	0.477	0.239	0.31	0.477	0.072	-43.62	-85.40	1.44	0.73	109390
BM-302	10.65	0.53	0.112	0.094	0.05	0.094	0.005	20.63	15.73	0.64	0.34	109952
BM-303	0.76	1.47	0.256	1.316	1.93	0.256	0.038	50.61	-36.45	1.92	1.00	110271
BM-304	33.73	1.36	0.022	0.030	0.04	0.030	0.001	166.61	-1057.88	1.37	0.83	110468
BM-305	4.04	1.01	0.176	0.247	0.25	0.176	0.026	289.81	-156.64	0.83	0.69	111228
BM-306	3.88	1.59	0.183	0.258	0.41	0.183	0.027	4.15	-3.90	1.64	0.98	111225
BM-307	6.35	1.51	0.146	0.158	0.24	0.146	0.022	-60.47	-250.97	1.47	0.83	111372
BM-308	-0.80	0.99	0.576	-1.250	-1.24	0.576	0.086	50.54	-25.38	1.03	0.67	111655
BM-309	5.97	1.03	0.077	0.168	0.17	0.168	0.029	23.11	-5.61	0.56	0.61	111722
BM-310	2.79	1.42	0.499	0.358	0.51	0.499	0.075	173.39	-55.61	1.65	0.89	111730
BM-311	1.49	1.39	2.379	0.671	0.93	2.379	0.357	15.67	-40.43	1.48	1.03	112070
BM-313	5.49	1.65	0.212	0.182	0.30	0.212	0.032	32.82	-305.19	2.23	1.26	112613
BM-314	0.20	1.80	0.846	5.000	9.00	0.846	0.127	38.56	-119.45	1.78	1.44	112766
BM-315	1.55	1.36	0.176	0.645	0.88	0.176	0.026	15.76	16.25	1.10	1.16	113573
BM-316	6.25	1.16	0.166	0.160	0.19	0.160	0.030	15.07	14.84	1.20	1.02	113678
BM-317	-0.45	1.19	0.658	-2.222	-2.64	0.658	0.099	69.94	-67.13	0.99	0.84	113841
BM-318	2.54	1.33	0.637	0.394	0.52	0.637	0.096	25.37	-25.80	1.31	1.21	113888
BM-319	12.87	1.13	0.093	0.078	0.09	0.078	0.007	71.26	13.88	1.24	0.99	114487
BM-320	3.21	1.09	0.306	0.311	0.34	0.306	0.046	-48.36	-95.00	1.79	0.88	114502
BM-321	10.48	1.38	0.113	0.095	0.13	0.095	0.013	-18.03	7.91	1.07	0.78	114710
BM-322	6.49	0.94	0.085	0.154	0.14	0.154	0.022	-36.09	3.87	0.91	0.72	114761
BM-323	5.24	1.75	0.311	0.191	0.33	0.311	0.047	210.01	-287.48	1.36	1.11	115340

**Table 4** — *Continued*

BM Name (1)	$\pi_{\text{HIP}}$ (mas) (2)	$\sigma_{\pi_{\text{HIP}}}$ (mas) (3)	$D_{\text{pho}}$ (kpc) (4)	$D_{\text{HIP}}$ (kpc) (5)	$\sigma_{\pi_{\text{HIP}}} / \pi_{\text{HIP}}$ (6)	$D_{\text{ado}}$ (kpc) (7)	$\sigma_{D_{\text{ado}}}$ (kpc) (8)	$\mu_{\alpha}$ (mas yr $^{-1}$ ) (9)	$\mu_{\delta}$ (mas yr $^{-1}$ ) (10)	$\sigma_{\mu_{\alpha}}$ (mas yr $^{-1}$ ) (11)	$\sigma_{\mu_{\delta}}$ (mas yr $^{-1}$ ) (12)	HIP/TYCHO ID (13)
BM-325	2.48	0.74	0.483	0.403	0.30	0.483	0.072	155.80	-98.43	0.81	0.84	117168
BM-326	1.75	1.26	0.259	0.571	0.72	0.259	0.039	67.60	-8.66	0.88	0.99	117369

**Table 5**  
Space Motions and Orbital Parameters

BM Name (1)	R (kpc) (2)	Z (kpc) (3)	U (km s <sup>-1</sup> ) (4)	V (km s <sup>-1</sup> ) (5)	W (km s <sup>-1</sup> ) (6)	$\sigma(U)$ (km s <sup>-1</sup> ) (7)	$\sigma(V)$ (km s <sup>-1</sup> ) (8)	$\sigma(W)$ (km s <sup>-1</sup> ) (9)	$V_R$ (km s <sup>-1</sup> ) (10)	$V_\phi$ (km s <sup>-1</sup> ) (11)	$r_{\text{peri}}$ (kpc) (12)	$r_{\text{apo}}$ (kpc) (13)	$Z_{\max}$ (kpc) (14)	e (15)	INOUT (16)
BM-001	8.503	-0.091	1	34	-32	2	2	5	2	254	8.50	11.41	0.55	0.15	1/1/1
BM-002	8.514	-0.520	-80	-107	43	11	16	4	-78	113	3.05	9.35	1.01	0.51	1/1/0
BM-003	8.514	-0.099	-144	-225	-36	15	25	10	-144	-4	0.10	10.54	0.69	0.98	1/0/0
BM-004	8.511	-0.130	19	-13	-26	4	5	5	19	206	7.30	8.74	0.37	0.09	1/1/0
BM-005	8.579	-0.521	143	-45	82	24	7	2	145	171	4.88	13.03	3.33	0.46	1/0/0
BM-006	8.521	-0.111	36	15	7	6	1	1	36	235	7.98	10.29	0.17	0.13	1/1/2
BM-007	8.469	-0.120	40	-84	-93	9	5	1	38	136	4.44	8.81	2.40	0.33	1/1/0
BM-008	8.521	-0.091	104	-55	-29	10	7	5	104	164	4.53	10.45	0.46	0.40	1/1/0
BM-009	8.517	-0.061	-143	-58	-40	10	5	4	-142	161	4.16	11.96	0.82	0.48	1/0/0
BM-010	8.528	-0.127	18	-13	-13	4	5	1	18	206	7.30	8.72	0.21	0.09	1/1/1
BM-011	8.524	-0.100	44	2	11	8	1	2	44	222	7.48	9.86	0.20	0.14	1/1/0
BM-012	8.589	-0.222	284	-82	74	42	15	15	284	136	2.81	23.92	4.64	0.79	1/0/0
BM-013	8.466	-0.075	84	-80	47	6	7	4	82	140	3.90	9.48	0.86	0.42	1/1/1
BM-014	8.520	-0.179	-112	-143	10	16	23	4	-112	76	1.80	9.83	0.24	0.69	1/0/0
BM-015	8.526	-0.071	94	23	53	10	1	4	94	243	7.13	13.53	1.31	0.31	1/1/1
BM-016	8.575	-0.229	-11	-3	-24	2	2	1	-11	216	8.10	8.78	0.42	0.04	1/1/2
BM-017	8.506	-0.071	-37	-69	-44	4	5	2	-37	150	4.53	8.74	0.73	0.32	1/1/2
BM-018	8.489	-0.098	-4	24	14	1	1	1	-5	244	8.48	10.28	0.23	0.10	1/1/0
BM-019	8.495	-0.067	-32	-52	-14	1	4	4	-32	167	5.11	8.71	0.19	0.26	1/1/1
BM-021	8.581	-0.178	299	-297	-75	32	43	20	299	-77	1.50	23.31	3.77	0.88	1/0/0
BM-022	8.553	-0.099	-38	-84	-29	6	15	3	-37	135	3.86	8.75	0.43	0.39	1/1/2
BM-023	8.551	-0.087	20	11	-5	4	1	5	20	231	8.26	9.59	0.12	0.08	1/1/0
BM-024	8.516	-0.448	121	-131	62	20	20	13	118	92	2.42	10.17	1.92	0.62	1/0/0
BM-025	8.419	-0.120	14	0	7	4	4	3	9	220	8.10	8.63	0.15	0.03	1/1/0
BM-026	8.494	-0.134	78	17	5	10	1	1	75	238	7.24	11.89	0.21	0.24	1/1/0
BM-028	8.539	-0.160	66	-101	-265	2	1	1	65	119	7.82	16.24	14.23	0.35	1/0/0
BM-029	8.542	-0.462	32	50	11	8	7	6	23	271	8.47	13.43	0.74	0.23	1/1/0
BM-030	8.490	-0.138	-29	-1	-29	3	4	4	-31	218	7.64	9.32	0.46	0.10	1/1/0
BM-032	8.607	-0.118	-38	16	24	4	1	4	-38	236	8.03	10.59	0.39	0.14	1/1/0
BM-033	8.913	-1.006	-26	-276	2	10	36	15	-23	-57	1.52	9.02	1.01	0.71	1/0/0
BM-034	8.738	-0.229	92	-158	-93	3	25	2	91	62	1.77	9.83	3.01	0.69	1/0/0
BM-035	8.646	-0.239	-41	-217	-31	12	29	6	-40	2	0.05	8.80	0.59	0.99	1/0/0
BM-036	8.519	-0.018	102	-78	-35	1	3	2	102	141	3.79	10.04	0.56	0.45	1/1/0
BM-037	8.505	-0.125	8	17	4	3	1	1	4	237	8.49	9.73	0.15	0.07	1/1/0
BM-038	8.518	-0.154	17	32	32	4	3	4	12	253	8.48	11.35	0.61	0.14	1/1/0
BM-039	8.915	-0.782	59	-98	-5	5	11	9	52	124	3.58	9.32	0.81	0.44	1/1/0
BM-040	8.409	-0.207	196	-106	116	30	21	14	191	119	3.17	14.59	5.61	0.64	1/0/0
BM-041	8.906	-0.432	38	-87	83	6	14	13	34	133	4.51	9.14	2.46	0.34	1/1/2
BM-042	8.589	-0.096	128	51	-7	9	7	5	126	272	7.08	17.88	0.24	0.43	1/0/0
BM-043	8.669	-0.101	-136	-19	78	1	7	1	-136	200	5.62	13.83	2.40	0.42	1/0/0
BM-044	8.684	-0.350	-116	-129	17	19	18	7	-119	86	2.09	10.27	0.47	0.66	1/0/0
BM-045	9.486	-0.797	-259	-189	-191	40	29	28	-260	14	2.66	25.92	25.67	0.81	1/0/0
BM-046	8.512	-0.166	17	-33	12	4	5	5	12	187	6.23	8.56	0.23	0.16	1/1/0
BM-047	8.602	-0.082	15	-16	9	6	7	8	13	203	7.26	8.69	0.14	0.09	1/1/0
BM-048	8.483	-0.125	-69	-248	-151	5	4	5	-68	-29	1.39	9.58	7.34	0.75	1/0/0
BM-049	8.633	-0.093	-17	15	7	4	2	3	-18	235	8.43	9.94	0.14	0.08	1/1/1
BM-050	8.607	-0.104	0	9	-6	3	3	3	-2	229	8.60	9.18	0.14	0.03	1/1/0
BM-051	8.536	-0.040	54	-90	-21	1	3	3	53	129	3.57	8.92	0.27	0.43	1/1/0
BM-052	8.522	-0.781	73	-273	80	15	22	28	79	-44	1.27	9.22	3.08	0.76	1/0/0

Table 5 — *Continued*

BM Name	$R$ (kpc)	$Z$ (kpc)	$U$ (km s $^{-1}$ )	$V$ (km s $^{-1}$ )	$W$ (km s $^{-1}$ )	$\sigma(U)$ (km s $^{-1}$ )	$\sigma(V)$ (km s $^{-1}$ )	$\sigma(W)$ (km s $^{-1}$ )	$V_R$ (km s $^{-1}$ )	$V_\phi$ (km s $^{-1}$ )	$r_{\text{peri}}$ (kpc)	$r_{\text{apo}}$ (kpc)	$Z_{\text{max}}$ (kpc)	$e$	INOUT
(1)	(2)	(3)	(4)	(5)	(6)	(7)	(8)	(9)	(10)	(11)	(12)	(13)	(14)	(15)	(16)
BM-053	8.652	-0.161	27	-73	-20	4	6	5	24	146	4.36	8.75	0.31	0.34	1/1/2
BM-054	8.405	-0.400	404	-201	-111	66	12	4	401	45	0.77	49.43	12.74	0.97	0/0/0
BM-055	8.528	-0.121	-17	-16	-10	3	4	3	-21	202	7.05	8.73	0.18	0.11	1/1/0
BM-056	8.878	-0.529	-88	-224	272	12	37	39	-87	-11	7.03	16.21	16.19	0.40	1/0/0
BM-057	8.515	-0.141	-13	0	-40	2	5	5	-17	220	8.10	9.04	0.65	0.05	1/1/0
BM-058	8.497	-0.428	-142	-317	6	19	17	24	-134	-106	2.58	10.68	0.52	0.61	1/0/0
BM-059	8.502	-0.039	198	-338	100	12	10	14	198	-116	2.90	14.74	4.26	0.67	1/0/0
BM-060	8.524	-0.064	-60	-311	-90	17	13	12	-58	-92	2.72	9.01	2.49	0.54	1/0/0
BM-061	8.704	-0.123	-15	-7	-19	5	3	4	-18	212	7.80	8.97	0.29	0.07	1/1/1
BM-062	8.535	-0.038	-40	24	-18	2	1	2	-41	244	8.05	11.13	0.28	0.16	1/1/0
BM-063	9.024	-0.648	-55	-126	-59	14	7	3	-64	87	2.53	9.52	1.96	0.58	1/0/0
BM-064	8.580	-0.180	-158	-179	-88	28	9	3	-159	35	0.90	11.50	3.29	0.85	1/0/0
BM-065	8.532	-0.061	-28	3	15	3	4	3	-30	223	7.83	9.45	0.21	0.09	1/1/0
BM-067	8.808	-0.141	82	-189	-37	11	18	5	81	32	0.78	9.45	0.64	0.85	1/0/0
BM-068	8.487	-0.120	-7	12	10	1	2	1	-12	232	8.37	9.43	0.19	0.06	1/1/0
BM-069	8.537	-0.028	167	-61	-68	3	3	1	166	159	4.02	13.46	1.95	0.54	1/0/0
BM-070	8.483	-0.159	9	-90	-56	4	4	3	5	129	3.84	8.50	1.07	0.38	1/1/2
BM-071	8.587	-0.018	20	18	2	1	1	1	18	238	8.41	10.09	0.04	0.09	1/1/0
BM-072	8.573	-0.128	23	11	-16	4	5	3	17	232	8.36	9.62	0.26	0.07	1/1/0
BM-073	8.595	-0.016	2	-7	-17	5	3	3	0	212	7.93	8.60	0.21	0.04	0/1/0
BM-074	8.595	-0.048	-5	16	-1	3	4	2	-8	236	8.55	9.73	0.05	0.06	1/1/0
BM-075	8.615	-0.040	-29	36	7	4	3	2	-32	256	8.37	11.95	0.13	0.18	1/1/0
BM-076	8.473	-0.043	17	13	0	4	1	1	14	233	8.32	9.51	0.05	0.07	1/1/0
BM-077	8.629	-0.043	74	-147	15	5	8	7	73	73	1.80	9.16	0.21	0.67	1/1/0
BM-078	8.456	-0.089	23	60	25	2	4	2	17	280	8.41	14.11	0.50	0.25	1/1/0
BM-079	9.065	-0.217	-51	-106	6	12	12	4	-58	109	2.99	9.48	0.24	0.52	1/1/0
BM-080	8.734	-0.045	3	3	5	2	2	1	0	223	8.73	8.82	0.07	0.00	0/1/0
BM-081	8.633	-0.010	234	-178	-38	3	6	3	234	43	0.88	15.27	0.96	0.89	1/0/0
BM-082	8.587	-0.059	-46	-118	15	8	6	4	-47	100	2.61	8.84	0.19	0.54	1/1/2
BM-083	8.667	-0.216	-87	-363	36	24	16	22	-77	-148	4.24	9.65	0.65	0.39	1/0/0
BM-084	8.574	-0.046	-21	0	9	3	4	2	-24	219	7.85	9.19	0.12	0.08	1/1/0
BM-085	8.831	0.014	5	49	57	5	6	8	0	269	8.83	13.82	1.45	0.22	0/1/0
BM-086	8.541	-0.023	-16	-41	-108	3	2	8	-17	178	7.02	8.77	2.79	0.11	1/1/0
BM-087	8.609	0.008	6	-21	15	4	4	1	4	198	6.99	8.62	0.19	0.10	0/1/0
BM-088	8.629	0.017	15	26	4	2	4	1	13	246	8.56	10.68	0.06	0.11	1/1/0
BM-089	8.547	-0.024	-119	-308	-25	32	12	2	-117	-90	2.19	10.07	0.38	0.64	1/0/0
BM-090	8.544	-0.013	2	-11	-6	2	4	1	0	208	7.56	8.55	0.07	0.06	1/1/0
BM-091	8.528	0.002	14	16	10	1	1	1	13	236	8.42	9.79	0.14	0.08	1/1/0
BM-092	8.539	0.007	-14	-59	50	2	1	1	-14	160	5.08	8.59	0.83	0.26	1/1/0
BM-093	8.548	0.006	0	-60	-28	2	2	3	0	159	4.90	8.55	0.37	0.27	1/1/0
BM-095	8.587	0.021	6	26	39	2	3	6	3	246	8.58	10.83	0.67	0.12	1/1/0
BM-096	8.683	0.025	-26	-140	45	13	9	5	-28	78	2.07	8.77	0.77	0.62	0/1/0
BM-097	8.576	0.014	-35	7	-18	2	2	3	-38	226	7.79	9.95	0.25	0.12	1/1/0
BM-099	8.566	-0.035	0	38	-9	3	5	4	-12	258	8.53	11.74	0.14	0.16	0/1/0
BM-100	8.835	0.137	27	-259	103	13	7	8	29	-37	1.18	9.07	3.62	0.77	1/0/0
BM-101	8.560	0.034	-228	-335	67	52	29	1	-226	-117	2.62	16.32	2.42	0.72	0/0/0
BM-102	8.549	0.023	20	6	-5	4	5	2	16	226	8.26	9.20	0.07	0.05	0/1/0
BM-103	8.632	0.083	147	-107	-416	20	13	66	143	116	7.93	67.56	64.60	0.79	0/0/0
BM-104	8.543	0.037	-57	33	31	6	1	5	-61	252	7.83	12.59	0.58	0.23	1/1/0

Table 5 — *Continued*

BM Name	$R$ (kpc)	$Z$ (kpc)	$U$ (km s $^{-1}$ )	$V$ (km s $^{-1}$ )	$W$ (km s $^{-1}$ )	$\sigma(U)$ (km s $^{-1}$ )	$\sigma(V)$ (km s $^{-1}$ )	$\sigma(W)$ (km s $^{-1}$ )	$V_R$ (km s $^{-1}$ )	$V_\phi$ (km s $^{-1}$ )	$r_{\text{peri}}$ (kpc)	$r_{\text{apo}}$ (kpc)	$Z_{\text{max}}$ (kpc)	$e$	INOUT
(1)	(2)	(3)	(4)	(5)	(6)	(7)	(8)	(9)	(10)	(11)	(12)	(13)	(14)	(15)	(16)
BM-105	8.499	-0.001	-19	14	-19	1	1	1	-20	234	8.25	9.75	0.26	0.08	1/1/0
BM-106	8.423	-0.071	184	-42	-17	37	10	5	177	184	4.37	14.49	0.32	0.54	1/0/0
BM-107	8.497	0.001	-10	-11	0	1	3	6	-13	208	7.42	8.60	0.01	0.07	0/1/0
BM-108	8.498	0.002	3	-23	0	2	1	1	1	196	...	...	...	...	0/1/0
BM-109	8.538	0.046	20	-32	33	2	5	2	17	187	6.32	8.64	0.47	0.16	1/1/0
BM-110	8.545	0.066	20	-324	29	2	5	6	24	-103	2.76	8.62	0.41	0.51	0/0/0
BM-111	8.685	0.226	-212	-334	-37	40	24	20	-205	-125	2.84	14.87	0.92	0.68	1/0/0
BM-112	8.431	-0.060	9	0	-11	4	3	3	3	219	8.20	8.47	0.14	0.02	1/1/0
BM-113	8.494	0.000	-1	1	8	7	1	1	-3	221	8.36	8.54	0.09	0.01	0/1/0
BM-114	8.750	0.320	21	-125	-46	2	6	15	12	95	2.65	8.78	0.97	0.54	1/1/2
BM-115	8.495	0.004	-12	35	21	1	1	1	-14	255	8.44	11.44	0.32	0.15	1/1/0
BM-117	8.535	0.054	39	-12	10	5	5	2	35	208	7.10	9.15	0.14	0.13	1/1/2
BM-118	8.491	0.001	59	8	0	5	1	1	56	229	7.39	10.56	0.01	0.18	1/1/0
BM-119	8.496	0.002	7	13	18	4	1	3	5	233	8.47	9.44	0.24	0.05	0/1/0
BM-120	8.584	0.191	63	-84	-63	11	5	13	44	142	4.40	8.91	1.36	0.34	0/1/0
BM-121	9.056	0.814	14	-232	-169	11	18	37	15	-9	2.64	9.91	9.84	0.58	1/0/0
BM-122	8.571	0.166	-3	-103	55	3	5	3	-7	115	3.33	8.59	1.06	0.44	1/1/2
BM-123	8.481	0.013	-2	36	8	1	1	1	-7	256	8.47	11.34	0.12	0.14	1/1/0
BM-125	8.482	0.015	4	-7	5	9	5	2	0	212	7.80	8.48	0.07	0.04	0/1/0
BM-126	8.485	0.021	0	-6	4	2	1	1	-3	213	7.84	8.50	0.05	0.04	1/1/0
BM-127	8.489	0.006	41	28	-5	1	1	1	38	249	8.09	11.31	0.07	0.17	1/1/0
BM-128	8.478	0.006	-9	26	0	1	3	1	-12	246	8.42	10.49	0.01	0.11	0/1/0
BM-129	8.478	-0.009	60	-25	0	3	1	1	58	194	6.08	9.46	0.01	0.22	1/1/0
BM-130	8.478	-0.012	14	-34	-7	2	1	1	13	185	6.07	8.52	0.09	0.17	1/1/0
BM-131	8.468	-0.018	-19	-4	0	2	2	2	-21	214	7.61	8.83	0.02	0.07	1/1/0
BM-132	8.454	0.008	44	-4	7	10	3	1	39	216	7.30	9.39	0.09	0.13	1/1/0
BM-133	8.493	0.226	-50	-273	17	5	7	15	-46	-56	1.37	8.70	0.34	0.73	1/0/0
BM-134	8.510	0.291	-31	-185	-44	4	11	19	-32	32	0.81	8.63	0.87	0.83	1/0/0
BM-135	8.484	0.045	1	28	12	2	1	2	-2	248	8.48	10.65	0.17	0.11	1/1/0
BM-136	8.482	0.044	-35	-6	8	4	1	1	-37	212	7.22	9.26	0.12	0.12	1/1/0
BM-138	8.479	-0.004	-82	-11	-29	2	1	1	-83	207	6.25	10.73	0.47	0.26	1/1/0
BM-139	8.477	0.035	19	-196	140	10	1	6	18	23	0.98	8.91	6.12	0.80	1/0/0
BM-140	8.462	0.009	75	-12	-9	9	4	2	72	208	6.42	10.27	0.13	0.23	1/1/0
BM-141	8.292	0.056	-86	-35	-49	8	5	10	-99	178	5.02	10.34	0.90	0.35	0/1/0
BM-142	8.474	0.146	11	22	-1	3	4	3	6	242	8.46	10.12	0.17	0.09	1/1/0
BM-143	8.471	0.038	-48	-5	-31	4	1	5	-50	214	7.08	9.75	0.46	0.16	1/1/0
BM-144	8.461	0.101	202	-260	9	37	18	14	202	-36	0.75	12.88	0.19	0.89	1/0/0
BM-146	8.473	0.020	-98	-129	17	3	1	2	-98	90	2.19	9.50	0.23	0.63	1/1/0
BM-147	7.972	-0.196	474	-596	-132	96	49	15	523	-303	...	...	...	...	0/0/0
BM-148	8.421	0.173	73	-17	8	13	4	1	67	204	6.33	9.91	0.22	0.22	1/1/2
BM-149	8.291	0.305	96	-171	2	22	14	9	91	54	1.28	9.09	0.33	0.75	1/0/0
BM-150	8.447	0.046	31	-41	-44	7	6	9	27	178	5.82	8.65	0.68	0.19	1/1/0
BM-151	8.475	0.075	-8	14	0	1	1	1	-10	234	8.39	9.47	0.08	0.06	1/1/0
BM-152	8.435	0.138	24	4	-16	5	3	2	19	224	8.05	9.10	0.26	0.06	1/1/0
BM-153	8.104	0.910	197	-150	-71	33	22	15	182	101	2.52	12.49	3.79	0.67	1/0/0
BM-155	8.173	0.400	-99	-207	-44	6	10	20	-100	2	0.06	9.13	0.91	0.99	1/0/0
BM-157	8.460	0.030	-62	-69	-61	3	3	10	-63	149	4.45	9.16	1.18	0.35	1/1/0
BM-158	8.427	0.121	-44	-77	-86	4	10	17	-47	141	4.48	8.87	2.09	0.33	1/1/0
BM-159	8.255	0.127	160	-55	-54	24	14	9	149	173	4.40	12.44	1.34	0.48	1/0/0

Table 5 — *Continued*

BM Name	$R$ (kpc)	$Z$ (kpc)	$U$ (km s $^{-1}$ )	$V$ (km s $^{-1}$ )	$W$ (km s $^{-1}$ )	$\sigma(U)$ (km s $^{-1}$ )	$\sigma(V)$ (km s $^{-1}$ )	$\sigma(W)$ (km s $^{-1}$ )	$V_R$ (km s $^{-1}$ )	$V_\phi$ (km s $^{-1}$ )	$r_{\text{peri}}$ (kpc)	$r_{\text{apo}}$ (kpc)	$Z_{\text{max}}$ (kpc)	$e$	INOUT
(1)	(2)	(3)	(4)	(5)	(6)	(7)	(8)	(9)	(10)	(11)	(12)	(13)	(14)	(15)	(16)
BM-160	8.476	0.004	-44	-24	4	1	1	1	-44	194	6.28	9.10	0.05	0.18	1/1/0
BM-161	8.463	0.020	79	-63	-82	9	8	9	78	157	4.88	9.70	2.04	0.33	1/1/0
BM-164	8.448	-0.005	-7	0	-2	3	4	1	-8	219	8.08	8.59	0.03	0.03	1/1/0
BM-165	8.392	0.149	-33	4	15	7	5	3	-37	223	7.56	9.56	0.27	0.12	1/1/0
BM-166	8.440	0.038	-12	-238	62	18	12	2	-12	-18	0.47	8.47	1.26	0.89	1/0/0
BM-167	8.444	0.011	8	16	34	1	1	3	5	236	8.43	9.74	0.52	0.07	1/1/0
BM-168	8.415	0.048	71	39	-29	7	6	3	66	261	7.72	13.32	0.55	0.27	1/1/0
BM-169	8.407	0.053	-3	1	-9	3	4	7	-7	221	8.19	8.58	0.11	0.02	1/1/0
BM-170	8.419	0.175	90	-387	-206	21	77	46	92	-166	7.09	14.39	9.85	0.34	0/0/0
BM-171	8.463	0.006	7	11	32	1	1	2	5	231	8.43	9.31	0.45	0.05	1/1/0
BM-172	8.463	0.066	-317	-215	-143	29	16	30	-317	2	0.06	28.00	14.17	1.00	1/0/0
BM-173	8.409	0.145	-13	-24	40	9	4	2	-15	195	6.79	8.51	0.63	0.11	1/1/0
BM-174	8.473	0.032	-29	-236	100	5	5	2	-28	-17	0.50	8.66	3.12	0.89	1/0/0
BM-175	8.437	-0.012	-25	-6	10	1	1	1	-27	213	7.39	8.93	0.12	0.09	1/1/0
BM-176	8.441	0.079	-15	12	-12	2	1	2	-16	232	8.24	9.44	0.18	0.07	1/1/2
BM-177	8.303	0.053	-34	0	-21	2	1	5	-41	219	7.26	9.44	0.28	0.13	0/1/0
BM-178	8.429	0.075	52	39	-40	4	5	3	49	260	8.00	12.78	0.81	0.23	1/1/0
BM-179	8.351	0.100	5	21	-32	3	4	5	0	241	8.35	10.00	0.50	0.09	1/1/2
BM-180	8.461	0.027	106	-221	123	18	12	5	105	0	0.02	9.98	5.10	1.00	1/0/0
BM-181	8.327	0.122	56	-42	-13	9	9	3	51	178	5.42	8.92	0.22	0.24	1/1/0
BM-182	7.742	1.080	148	-106	-98	19	26	7	137	126	3.68	10.60	4.45	0.48	1/0/0
BM-183	8.223	0.206	-322	-271	80	9	5	18	-319	-62	1.16	25.17	5.46	0.91	1/0/0
BM-185	8.451	0.007	-39	0	-1	2	1	2	-40	220	7.41	9.54	0.02	0.13	0/1/0
BM-186	7.564	0.632	101	-243	42	27	30	7	103	-10	0.24	8.56	1.00	0.95	1/0/0
BM-187	8.430	-0.020	63	-2	10	5	4	1	61	218	6.93	10.18	0.14	0.19	1/1/0
BM-188	8.435	0.037	156	-119	18	15	15	2	155	101	2.33	11.26	0.28	0.66	1/0/0
BM-189	8.429	0.010	3	22	3	1	1	1	0	242	8.43	10.00	0.05	0.09	1/1/0
BM-190	8.308	0.222	-31	-184	119	15	25	1	-31	34	1.15	8.61	4.29	0.76	1/0/0
BM-191	8.005	0.583	1	-403	281	32	47	7	7	-183	7.98	21.06	16.75	0.45	1/0/0
BM-192	8.457	-0.002	-6	-2	2	3	3	1	-7	217	8.00	8.53	0.03	0.03	0/1/0
BM-193	8.415	0.018		21	0	1	1	1	-2	241	8.41	9.90	0.02	0.08	0/1/0
BM-194	7.293	1.845	102	-255	22	19	42	8	103	-31	0.73	8.56	2.05	0.84	1/0/0
BM-195	8.306	0.072	-209	-179	-53	3	7	22	-210	37	0.78	13.25	1.29	0.89	1/0/0
BM-196	7.993	0.420	-121	-200	-19	3	23	17	-121	14	0.32	9.33	0.54	0.93	1/0/0
BM-197	8.407	-0.001	-31	7	-2	2	2	2	-33	227	7.75	9.58	0.03	0.11	1/1/0
BM-198	8.424	-0.015	8	3	-7	2	1	2	5	224	8.32	8.65	0.09	0.02	1/1/0
BM-199	7.489	1.047	21	-75	-19	9	17	8	13	145	4.11	7.59	1.14	0.30	1/1/0
BM-200	8.380	0.086	43	6	12	16	11	14	41	227	7.55	9.82	0.19	0.13	1/1/0
BM-201	8.377	0.078	-19	-83	-257	12	23	40	-20	136	8.29	14.54	12.20	0.27	1/0/0
BM-202	8.442	0.009	-47	6	11	1	1	1	-47	225	7.43	10.04	0.14	0.15	1/1/0
BM-203	8.407	0.062	-6	-7	45	3	2	4	-7	212	7.89	8.48	0.68	0.04	1/1/2
BM-204	8.416	0.027	25	22	49	3	1	7	23	243	8.24	10.69	0.89	0.13	1/1/0
BM-205	8.381	0.060	-3	29	-1	1	2	1	-5	248	8.37	10.54	0.08	0.12	1/1/1
BM-206	8.464	-0.001	-49	6	24	1	1	1	-50	226	7.43	10.21	0.34	0.16	1/1/0
BM-207	8.383	0.018	-26	0	-23	1	1	6	-28	218	7.60	9.09	0.30	0.09	1/1/0
BM-208	8.423	0.052	-45	-373	58	8	27	3	-44	-153	4.69	8.78	1.09	0.30	1/0/0
BM-209	8.336	0.140	59	-121	64	12	20	8	58	98	2.66	8.77	1.31	0.54	1/1/2
BM-210	8.385	0.054	-12	11	9	4	2	2	-13	230	8.23	9.22	0.13	0.06	1/1/0
BM-211	8.445	0.005	22	6	4	15	12	2	20	226	8.05	9.20	0.05	0.07	0/1/0

Table 5 — *Continued*

BM Name	<i>R</i> (kpc)	<i>Z</i> (kpc)	<i>U</i> (km s <sup>-1</sup> )	<i>V</i> (km s <sup>-1</sup> )	<i>W</i> (km s <sup>-1</sup> )	$\sigma(U)$ (km s <sup>-1</sup> )	$\sigma(V)$ (km s <sup>-1</sup> )	$\sigma(W)$ (km s <sup>-1</sup> )	$V_R$ (km s <sup>-1</sup> )	$V_\phi$ (km s <sup>-1</sup> )	$r_{\text{peri}}$ (kpc)	$r_{\text{apo}}$ (kpc)	$Z_{\text{max}}$ (kpc)	<i>e</i>	INOUT
(1)	(2)	(3)	(4)	(5)	(6)	(7)	(8)	(9)	(10)	(11)	(12)	(13)	(14)	(15)	(16)
BM-212	7.892	0.551	132	-62	-15	10	15	9	129	159	3.95	10.52	0.85	0.45	1/1/2
BM-213	8.414	0.036	60	-26	9	27	44	14	59	194	6.02	9.41	0.12	0.22	1/1/0
BM-214	8.413	0.005	-19	33	-36	1	2	4	-21	253	8.30	11.36	0.62	0.16	1/1/0
BM-215	8.413	0.030	-31	1	52	2	1	5	-32	221	7.75	9.51	0.90	0.10	1/1/0
BM-216	8.423	0.040	-56	-17	22	1	3	2	-56	202	6.47	9.52	0.31	0.19	1/1/0
BM-217	8.453	0.032	240	-238	48	6	14	7	239	-18	0.38	15.30	1.33	0.95	1/0/0
BM-218	8.163	-0.019	-12	30	-33	2	3	7	-19	250	8.06	10.69	0.51	0.14	0/1/0
BM-219	8.440	0.022	11	2	3	1	1	1	10	222	8.18	8.71	0.04	0.03	1/1/0
BM-220	8.361	0.024	12	-26	32	4	6	4	10	193	6.58	8.41	0.42	0.12	1/1/0
BM-221	8.200	0.096	-11	-127	-29	6	20	8	-12	92	2.33	8.22	0.39	0.56	1/1/0
BM-222	8.378	-0.057	-213	-209	-92	3	4	2	-212	7	0.17	13.91	3.85	0.98	1/0/0
BM-223	8.422	0.001	-33	9	26	1	1	2	-34	229	7.80	9.81	0.36	0.11	1/1/0
BM-224	8.366	-0.002	-17	-29	-2	5	4	1	-19	190	6.24	8.48	0.03	0.15	1/1/0
BM-225	7.800	0.355	-79	-273	35	3	43	7	-79	-54	1.25	8.36	0.73	0.74	1/0/0
BM-226	8.372	-0.028	-22	13	-6	4	5	6	-24	233	8.05	9.65	0.09	0.09	1/1/0
BM-227	8.427	0.007	18	6	-6	1	1	1	17	226	8.12	9.10	0.08	0.06	1/1/0
BM-228	8.433	0.011	29	15	2	1	1	1	28	235	8.05	9.97	0.04	0.11	0/1/0
BM-229	8.399	0.052	6	6	2	1	1	1	6	226	8.31	8.76	0.06	0.03	1/1/0
BM-230	8.444	-0.016	-34	-13	19	1	1	1	-34	206	6.96	9.01	0.24	0.13	1/1/0
BM-231	8.414	0.021	-6	-4	-5	5	1	1	-5	215	7.90	8.45	0.06	0.03	1/1/0
BM-232	8.001	0.161	-11	8	-20	5	3	5	-5	228	7.97	8.59	0.30	0.04	1/1/0
BM-233	8.392	-0.010	-66	-194	-81	6	27	12	-66	25	0.67	8.87	2.10	0.86	1/0/0
BM-234	8.415	-0.041	-51	4	-18	4	4	2	-52	224	7.28	10.13	0.25	0.16	1/1/0
BM-235	7.506	-0.465	1	-68	-255	17	8	34	-14	150	7.52	13.80	11.18	0.29	1/0/0
BM-236	8.396	0.018	76	-152	-3	5	17	2	76	67	1.60	8.96	0.04	0.70	1/1/0
BM-237	8.424	-0.005	-71	4	5	1	1	2	-71	224	6.92	10.82	0.07	0.22	0/1/0
BM-238	8.354	-0.006	-4	-19	0	5	18	4	-4	200	6.89	8.36	0.01	0.10	0/1/0
BM-239	8.395	-0.013	4	-21	14	1	5	1	3	198	6.84	8.40	0.16	0.10	1/1/0
BM-240	8.296	0.020	-150	-172	9	14	38	1	-149	48	1.05	10.49	0.13	0.82	1/0/0
BM-241	8.446	-0.020	42	-34	78	1	4	4	41	185	6.42	9.07	1.68	0.17	1/1/0
BM-242	8.407	-0.038	-6	6	-14	1	1	3	-7	226	8.31	8.80	0.17	0.03	1/1/0
BM-243	8.254	-0.083	-27	-21	9	5	4	3	-29	198	6.52	8.57	0.14	0.14	1/1/1
BM-244	7.930	-0.079	25	0	34	1	3	5	28	219	7.30	8.69	0.46	0.09	0/1/0
BM-245	7.436	-0.219	-4	132	89	5	19	15	4	352	7.44	25.01	3.94	0.54	1/0/0
BM-246	8.381	-0.050	-118	-113	-92	6	13	6	-118	105	2.92	10.31	2.78	0.56	1/0/0
BM-247	8.226	-0.060	-91	-128	-94	3	23	13	-90	91	2.57	9.29	2.65	0.57	1/0/0
BM-248	8.433	-0.013	-41	7	5	3	1	1	-40	227	7.61	9.85	0.07	0.13	1/1/0
BM-249	17.765	0.661	21	158	-52	6	17	6	-92	367	...	...	...	...	0/1/0
BM-251	8.200	-0.119	-310	-104	-133	6	13	6	-310	114	2.40	28.56	11.77	0.85	1/0/0
BM-252	7.854	-0.184	-150	-541	-100	22	83	17	-158	-317	6.73	28.11	5.61	0.61	0/0/0
BM-253	8.417	-0.038	43	-336	-57	12	56	9	43	-115	3.24	8.67	1.05	0.46	0/0/0
BM-254	8.425	-0.050	51	21	4	5	3	4	49	242	7.75	11.05	0.09	0.18	1/1/0
BM-256	8.323	-0.058	302	-250	-76	1	19	26	302	-33	0.62	22.00	3.71	0.94	1/0/0
BM-257	7.335	-0.551	-52	-293	-132	8	46	17	-52	-73	2.44	7.87	4.32	0.53	1/0/0
BM-258	7.436	-0.415	-203	-446	-79	25	71	13	-216	-213	4.42	18.59	3.74	0.62	0/0/0
BM-259	8.417	-0.054	-13	17	10	1	1	1	-14	237	8.31	9.73	0.14	0.08	1/1/0
BM-260	7.896	-0.227	141	-214	-125	2	21	29	141	0	0.00	10.43	4.79	1.00	1/0/0
BM-261	8.349	-0.084	168	-328	7	9	52	11	167	-108	2.44	11.74	0.18	0.66	0/0/0
BM-262	8.375	-0.058	49	-2	-11	5	2	7	49	217	7.07	9.68	0.15	0.16	1/1/0

Table 5 — *Continued*

BM Name	$R$ (kpc)	$Z$ (kpc)	$U$ (km s $^{-1}$ )	$V$ (km s $^{-1}$ )	$W$ (km s $^{-1}$ )	$\sigma(U)$ (km s $^{-1}$ )	$\sigma(V)$ (km s $^{-1}$ )	$\sigma(W)$ (km s $^{-1}$ )	$V_R$ (km s $^{-1}$ )	$V_\phi$ (km s $^{-1}$ )	$r_{\text{peri}}$ (kpc)	$r_{\text{apo}}$ (kpc)	$Z_{\text{max}}$ (kpc)	$e$	INOUT
(1)	(2)	(3)	(4)	(5)	(6)	(7)	(8)	(9)	(10)	(11)	(12)	(13)	(14)	(15)	(16)
BM-264	7.276	-0.570	-5	-589	-244	16	84	46	-32	-368	7.28	51.60	25.78	0.75	0/0/0
BM-265	8.419	-0.043	-24	35	3	1	3	1	-23	255	8.28	11.40	0.07	0.16	1/1/0
BM-266	8.310	-0.109	-150	-151	-68	3	27	1	-149	69	1.88	10.83	1.79	0.71	1/0/0
BM-267	8.453	-0.035	-30	16	-5	1	2	1	-30	235	8.01	12.06	0.18	0.20	1/1/1
BM-268	8.457	-0.022	105	-62	-36	3	2	5	105	156	4.24	10.29	0.59	0.42	1/1/0
BM-269	8.221	-0.163	41	-186	44	8	23	4	41	32	0.78	8.37	0.76	0.83	1/0/0
BM-270	8.445	-0.032	68	-6	27	2	1	3	68	213	6.68	10.30	0.41	0.21	1/1/0
BM-271	8.413	-0.052	-40	-67	65	5	6	4	-39	153	4.75	8.71	1.26	0.29	1/1/1
BM-272	8.409	-0.069	-54	42	-2	5	6	3	-54	262	7.90	12.89	0.11	0.24	1/1/1
BM-273	8.379	-0.088	-11	-22	23	4	5	4	-11	197	6.75	8.44	0.29	0.11	1/1/0
BM-274	7.810	-0.463	91	-70	-25	8	10	14	95	146	3.72	9.14	0.63	0.42	1/1/0
BM-276	8.453	-0.033	-7	-116	-22	2	7	3	-7	103	2.74	8.46	0.29	0.51	1/1/0
BM-277	8.413	-0.067	1	28	6	4	3	3	0	248	8.41	10.56	0.12	0.11	1/1/0
BM-279	7.497	-0.739	-104	-26	71	14	11	15	-90	200	5.49	10.22	1.86	0.30	1/1/0
BM-280	8.395	-0.079	-64	-186	-7	8	30	3	-63	33	0.57	8.77	0.13	0.88	1/0/0
BM-281	8.371	-0.109	8	-112	-34	7	19	5	8	107	2.88	8.38	0.49	0.49	1/1/2
BM-282	8.383	-0.100	57	10	27	5	1	5	57	230	7.35	10.62	0.44	0.18	1/1/1
BM-284	8.208	-0.248	-23	12	17	3	2	3	-17	233	8.02	9.36	0.37	0.08	1/1/2
BM-285	8.114	-0.356	-52	-288	15	7	39	14	-50	-70	1.69	8.37	0.41	0.66	1/0/0
BM-286	8.226	-0.251	312	-459	-175	43	71	32	313	-237	4.65	52.08	21.74	0.84	0/0/0
BM-287	8.390	-0.102	7	11	5	2	1	2	5	231	8.36	9.11	0.13	0.04	1/1/2
BM-288	8.408	-0.085	27	3	-10	5	2	5	26	223	7.79	9.21	0.15	0.08	1/1/0
BM-289	8.472	-0.030	-153	-16	19	4	1	4	-153	203	5.15	13.97	0.34	0.46	1/0/0
BM-290	7.709	-0.881	-193	-206	86	23	33	20	-193	14	0.30	12.11	2.79	0.95	1/0/0
BM-291	8.394	-0.128	29	1	-25	6	2	6	30	221	7.65	9.29	0.37	0.10	1/1/1
BM-292	8.358	-0.176	4	21	-4	7	4	6	4	241	8.35	9.89	0.21	0.09	1/1/0
BM-293	8.477	-0.030	61	-23	-3	1	1	1	61	196	6.11	9.57	0.05	0.22	1/1/0
BM-294	8.424	-0.092	-112	-47	-12	8	7	8	-112	172	4.64	10.73	0.22	0.40	1/1/1
BM-295	8.339	-0.211	167	-287	13	12	41	19	166	-68	1.51	11.26	0.40	0.76	1/0/0
BM-297	8.310	-0.232	-21	-363	-10	7	72	8	-20	-143	4.09	8.37	0.27	0.34	0/0/0
BM-298	8.443	-0.072	1	10	8	3	1	4	1	230	8.44	9.07	0.12	0.04	1/1/0
BM-299	8.381	-0.170	34	-30	42	3	4	5	35	189	6.25	8.76	0.69	0.17	1/1/1
BM-300	8.423	-0.104	7	14	-17	3	1	3	7	234	8.38	9.43	0.24	0.06	1/1/0
BM-301	8.284	-0.365	-155	-148	21	23	23	2	-153	75	1.69	10.81	0.55	0.73	1/0/0
BM-302	8.453	-0.077	3	15	6	1	1	1	3	235	8.45	9.49	0.11	0.06	1/1/0
BM-303	8.355	-0.210	40	-42	-13	7	8	6	39	177	5.48	8.71	0.27	0.23	1/1/2
BM-304	8.483	-0.024	1	-137	33	1	5	1	0	82	2.12	8.48	0.48	0.60	1/1/0
BM-305	8.414	-0.152	191	-179	-55	24	27	18	191	39	0.87	12.48	1.34	0.87	1/0/0
BM-306	8.421	-0.155	-9	9	1	1	1	1	-7	229	8.36	9.03	0.17	0.04	1/1/0
BM-307	8.423	-0.124	-99	-148	15	10	24	7	-98	71	1.68	9.40	0.24	0.70	1/0/0
BM-308	8.206	-0.495	280	-83	264	16	15	10	280	136	4.89	43.01	35.88	0.80	1/0/0
BM-309	8.408	-0.129	8	4	2	4	2	4	6	224	8.31	8.69	0.14	0.02	1/1/2
BM-310	8.291	-0.430	327	-236	-132	45	33	33	327	-21	0.43	28.91	11.04	0.97	1/0/0
BM-311	7.594	-2.057	102	-552	133	15	70	25	69	-340	7.74	30.85	12.60	0.60	0/0/0
BM-313	8.394	-0.182	7	-279	137	5	46	10	6	-59	2.34	8.71	5.34	0.58	1/0/0
BM-314	8.098	-0.744	-98	-498	-191	7	76	6	-97	-278	7.72	25.28	12.77	0.53	0/0/0
BM-315	8.427	-0.160	-2	22	-18	3	2	5	-2	242	8.43	10.07	0.32	0.09	1/1/1
BM-316	8.450	-0.143	7	16	10	3	1	1	8	236	8.40	9.62	0.21	0.07	1/1/1
BM-317	8.173	-0.505	94	-290	-80	26	38	5	96	-67	1.73	9.31	2.17	0.69	1/0/0

**Table 5** — *Continued*

BM Name	$R$ (kpc)	$Z$ (kpc)	$U$ (km s $^{-1}$ )	$V$ (km s $^{-1}$ )	$W$ (km s $^{-1}$ )	$\sigma(U)$ (km s $^{-1}$ )	$\sigma(V)$ (km s $^{-1}$ )	$\sigma(W)$ (km s $^{-1}$ )	$V_R$ (km s $^{-1}$ )	$V_\phi$ (km s $^{-1}$ )	$r_{\text{peri}}$ (kpc)	$r_{\text{apo}}$ (kpc)	$Z_{\text{max}}$ (kpc)	$e$	INOUT
(1)	(2)	(3)	(4)	(5)	(6)	(7)	(8)	(9)	(10)	(11)	(12)	(13)	(14)	(15)	(16)
BM-318	8.212	-0.564	-30	-101	-139	8	15	5	-30	118	4.83	8.60	4.80	0.28	1/0/0
BM-319	8.472	-0.072	13	8	-8	3	1	5	13	228	8.28	9.18	0.13	0.05	1/1/1
BM-320	8.421	-0.276	-85	-144	157	18	15	1	-83	76	3.20	10.09	6.85	0.52	1/0/0
BM-321	8.457	-0.081	-33	8	-23	2	2	4	-33	228	7.85	9.76	0.34	0.11	1/1/0
BM-322	8.432	-0.135	-42	19	-5	3	2	1	-42	238	7.83	10.61	0.18	0.15	1/1/1
BM-323	8.367	-0.274	121	-501	-32	25	75	7	122	-281	7.09	18.47	0.99	0.45	0/0/0
BM-325	8.296	-0.388	267	-303	65	39	49	6	268	-77	1.58	18.61	3.62	0.84	1/0/0
BM-326	8.399	-0.223	35	-52	-64	11	7	5	33	167	5.45	8.69	1.28	0.23	1/1/2

**Note.** — INOUT indicates membership in various subsamples considered in this paper (see text). The first digit takes on a value of “1” if the star is accepted for the kinematic analysis, “0” if not. The second digit takes on a value of “1” if the star is likely to be a member of the disk system, according to the Lindblad diagram shown in Figure 12, “0” if not. The third digit takes on a value of “1” if the star is a likely disk member with metallicity in the range  $-0.8 < [\text{Fe}/\text{H}] \leq -0.5$ , “2” if it is a likely disk member in the metallicity range  $-1.8 < [\text{Fe}/\text{H}] \leq -0.8$ , “0” if not.